Issues in Diversity and Adaptive Error Control Coding for Wireless Communications

by
Arndt Joseph Mueller
Bachelor of Applied Science in Electrical Engineering, University of Alberta, 1992

A Thesis Submitted in Partial Fulfillment of the
Requirements for the Degree of

Master of Applied Science in Electrical Engineering

in the Department of
Electrical and Computer Engineering

We accept this thesis as conforming
to the required standard

[redacted]
Dr. Vijay K. Bhargava, Supervisor

[redacted]
Dr. Qiang Wang, Departmental Member

[redacted]
Dr. Panajotis Agathoklis, Graduate Advisor

[redacted]
Dr. Ron Podhorodeski, Outside Member

[redacted]
Dr. Jon C. Muzio, External Examiner

Supervisor: Dr. Vijay K. Bhargava

ABSTRACT

One of the most challenging aspects of mobile cellular communications is the non-stationary nature of the channel. Due to user mobility, the channel conditions vary widely. Thus, to achieve efficient and reliable data transmission, techniques for combating these fluctuations are required. This thesis addresses two such techniques: diversity and adaptive error control coding.

Two channel models are considered: the land mobile satellite channel and the land mobile terrestrial channel. Following previous empirical studies, the terrestrial channel is modelled as a lognormally shadowed Rician distribution and the satellite channel is modelled as a weighted sum of Rice and Suzuki distributions. Where analysis is performed, the channel model parameters are obtained from actual channel measurements.

For systems employing diversity, an analytical technique well suited to numerical analysis is presented for computing the average bit error rate (BER) and outage probability for several common modulation schemes including both M-ary coherent PSK (M-PSK) and differential PSK (M-DPSK). Both micro- and macro-diversity reception are considered where either maximal ratio or selection diversity combining techniques are employed. A numerical example is provided illustrating the achievable performance of both M-PSK and M-DPSK with micro-diversity in the satellite channel.

Classically, adaptive error control coding has been used to compensate for time varying channel conditions. Therefore, the cellular channel — where the propagation channel is continuously changing and fades greater than 20 dB are not uncommon — is an ideal candidate. A more recent motivation for adaptive coding is presented by the need to transmit multi-media data, where each data source may possess unique bit error rate and delay requirements. In light of these motivations, a rate adaptive error control code using a hybrid

type-II automatic repeat request / forward error correction (ARQ/FEC) scheme is proposed. For forward error correction, a concatenated code composed of a punctured rate $(N-1)/N$ convolutional code and a punctured Reed-Solomon code is used. Type-II hybrid ARQ is then employed through the decomposition of the Reed-Solomon code into two or more smaller code words and by soft-decision combining of repeated unreliable packets. Examples of the BER performance are provided for the fading channel through simulation.

Examiners

[redacted]

Dr. Vijay K. Bhargava (Electrical and Computer Engineering)

[redacted]

Dr. Qiang Wang (Electrical and Computer Engineering)

[redacted]

Dr. Panajotis Agathoklis (Electrical and Computer Engineering)

[redacted]

Dr. Ron Podhorodeski (Mechanical Engineering)

[redacted]

Dr. Jon C. Muzio (Computer Science)

Table of Contents

List of Figures

List of Tables

Acknowledgments

First and foremost, I would like to thank my supervisor and mentor, Dr. Vijay K. Bhargava. I appreciated the freedom and flexibility with which you entrusted me, the generous personal and financial support you provided and for offering the best lab on campus from which I could perform my research.

I also wish to thank my fellow graduate students for their camaraderie, helpful suggestions and for answering (and tolerating) my many questions. I would especially like to thank Dr. Chintha Tellambura for providing the research topic on diversity and for his support and assistance in researching this topic.

I would also like to thank my parents. You encouraged me to choose my own course, while still providing the support I needed when I made mistakes. Thanks Dad for proofreading this thesis - I am sure it was not easy!

Finally, I wish to thank my beautiful wife, Sandra without whose support, encouragement and spag-a-chili, I would have never made it. Regardless of how often I disappeared into the lab, you where always there when I returned. Thanks for always being there. Our life is turning a page — here's to places never burned before!

To
Life's rich pageant

List of Acronyms

ACK	Positive acknowledgment (ARQ feedback message)
AECC	Adaptive error control code (or coding)
ARQ	Automatic repeat request
ASK	Amplitude shift keying
ATM	Asynchronous transfer mode
AWGN	Additive white Gaussian noise
BER	Bit error rate
BPSK	Binary phase shift keying
CDF	Cumulative distribution function
ECC	Error control code (or coding)
FEC	Forward error correction
FSK	Frequency shift keying
GBN	Go back N (ARQ protocol)
HARQ	Hybrid automatic repeat request
IWAN	Integrated wireless access network
LOS	Line of sight (with respect to transmission path)
MGF	Moment generating function
MLD	Maximum likelihood decoding
MDS	Maximum distance separable
MRC	Maximal ratio combining
M-DPSK	M-ary differential phase shift keying
M-PSK	M-ary coherent phase shift keying

NACK	Negative acknowledgment (ARQ feedback message)
PCS	Personal communications systems (or service)
PDF	Probability density function
PSK	Phase shift keying
QPSK	Quadrature phase shift keying
SDC	Selection diversity combining
SNR	Signal to noise ratio

Chapter 1

Introduction

Over the past decade, the demand for wireless communication services has grown phenomenally. Historically, communication has been restricted primarily to voice traffic between two fixed points rather than between two people. Now, with the advance of wireless communications, a transition from point to point communication towards person to person communication - independent of location - has begun. Testimony to this is the rapidly increasing penetration of cordless and cellular phones not just in North America but all across the world. In anticipation of growing consumer demands, the next generation of wireless communications, namely personal communications services (PCS), endeavors to provide person to person wireless communication of packetized multi-media data. This provides many new challenges to designers, one of which is ensuring the integrity of the data is maintained during transmission.

The largest obstacle facing designers of wireless communications systems is the nature of the channel. The wireless channel is non-stationary and typically very noisy. Noise arises from sources such as thermal noise in the receiver, power lines, machinery and other transmitters using the same frequency band. Furthermore, these noise sources change with time. In addition, for the mobile user, the effects of moving through areas of strong reception to areas where the transmission path is blocked by obstacles provides an additional challenge to designers.

In this thesis, two effective techniques for combating the non-stationary, noisy nature of the channel are investigated. These are diversity reception and adaptive error control coding. Other methods, such as power control, exist but are not considered here. It is not intended that diversity reception or error control coding replace these other methods since, in many cases, these may all be employed simultaneously.

An additional motivation for the application of error control coding arises from the need to reliably communicate multi-media data. Multi-media data, as the name suggests, is the union of several different data types. In many cases these data types have unique bit error rate and delay requirements. An example of these requirements for several common data types is given in Table 1.1. Adaptive error control coding provides an efficient method of achieving these requirements. Present wired networks transporting this mixed traffic favor a fixed packet structure in light of its ambiguity towards the traffic type. Thus, the emphasis is placed on a packet based, rather than continuous error control coding scheme.

Data Type	**BER**	**Delay**	**Delay Jitter**
Voice	10^{-3}	Critical	Critical
Facsimile	10^{-4}	Non-Critical	Non-Critical
Low Resolution Video	10^{-5}	Non-Critical	Critical
Asynchronous Packet Data	10^{-9}	Non-Critical	Non-Critical
Synchronous Packet Data	10^{-9}	Non-Critical	Critical

Table 1.1. Bit error rate and delay requirements of various data types.

1.1 Significance of Research

With the growing interest in mobile communications to provide PCS, the importance of exact theoretical analysis for such systems cannot be understated. Particularly important are exact analytical expressions for the bit error rate and outage probability required to design effective signalling and error control coding schemes. Furthermore, a consequence of the exploding demand for mobile communications services is the need to provide a large number of users with such services despite the limited radio spectrum. This warrants a consideration of modulation methods with larger constellation sizes (greater than or equal to four bits per symbol), leading to systems with higher bandwidth efficiency. In light of these considerations, this paper takes an analytical approach to studying the performance of such communications systems employing both microscopic and macroscopic diversity in both the terrestrial and satellite mobile channels. This analysis is performed for several common modulation schemes, including M-ary PSK and DPSK and for maximal ratio and selection diversity combining techniques.

For error control coding, a very powerful, flexible and highly adaptive error control

code is proposed. The proposed code combines two commonly implemented error correction codes (the convolutional and Reed-Solomon codes — both optimal in their own sense) and exploits several of their properties to further enhance the performance of the overall error correction code. Packet structure and delay requirements are accounted for and consideration is given to implementation complexity. Examples of bit error rate performance over the fading channel are obtained through simulation.

1.2 Thesis Outline

This thesis consists of seven chapters. In Chapter 2, statistical channel models are developed for the land mobile terrestrial channel and the land mobile satellite channel. The statistics of interest are the moment generating function and the cumulative probability distribution. A digital channel simulator incorporating the effects of time correlation is provided.

The channel statistics derived in Chapter 2 are extended to channels with diversity in Chapter 3. Both selection diversity and maximal ratio combining are considered for microscopic diversity, and selection diversity combining is considered for macroscopic diversity.

Using the moment generating functions and cumulative distribution functions derived for the channel, expressions for the average bit error rate and outage probability are derived in Chapter 4. A numerical analysis of the land mobile satellite channel with microscopic diversity is provided as an example.

In Chapter 5 the proposed adaptive error control code is presented. Where necessary, background theory is provided.

Some simulated results indicating the performance of the proposed code are presented in Chapter 6. This includes analysis in the Gaussian channel as well as in several fading channel environments.

Finally, in Chapter 7, conclusions and suggestions for future work are provided.

Chapter 2

Cellular Channel Model

To meet cellular subscribers' increasing demands for ubiquitous service, both terrestrial and satellite base stations are proposed for future cellular service. In order to design effective signalling and error control coding schemes, models for both the terrestrial channel and the satellite channel are required. In this chapter, the models for both are presented.

As actual samples for the various channels of interest are not readily available, statistical representations of the channels are required. Where available, the parameters for the statistical models are taken from the measured data of others. Due to the diverse nature of the cellular environment (i.e., from dense downtown cores to flat open rural areas), selecting a single channel model for either the terrestrial or satellite channel, which is representative of all cellular environments, is impossible.

Historically, a combined Rayleigh lognormal distribution has been used to model the terrestrial channel [1], [2], [3]. Although applicable for macrocellular channels, recent studies indicate a combined lognormal Rice distribution is more accurate for microcellular channels [4], [5], [6], [7], [8]. Other studies show that this model is also reasonable for the indoor environment [4]. The Nakagami-m distribution, popular for modelling the indoor channel, is not considered here [9]. Since the lognormal Rice distribution reverts to the lognormal Rayleigh distribution in the limiting case, it is a natural choice for the terrestrial channel.

Several statistical models for the satellite channel have been proposed in literature. Standard models include the Rayleigh, Rice and Rice lognormal distributions. From these standard distributions, new models have evolved based on actual channel measurements. One such model, developed by Loo, is suitable for low elevation angle satellites

and was based on data for the MSAT program in Canada [5], [10], [11]. Lutz et al. proposed a model incorporating the effects of varying elevation angles based on channel measurements in Europe [12], [13]. To maintain a generalized approach, the Lutz channel model is considered here.

In this chapter, the statistical representations for the two channel models are introduced and statistical functions developed. Based on these statistical representations, a fading channel simulator for digital computer simulation is designed.

2.1 Statistical Representation of the Fading Channel

To evaluate and simulate the channel based on the statistical models chosen, the probability density function (PDF), the cumulative distribution function (CDF) and the moment generating function (MGF) for each model is required. These functions are described here[1].

Given a random variable $x(k)$ and any fixed value of x, the CDF of x is defined as

$$F(x) = \text{Prob}[x(k) \leq x] . \tag{2.1}$$

Differentiating $F(x)$ with respect to x, the PDF $p(x)$ is obtained

$$p(x) = \frac{d}{dx}F(x) . \tag{2.2}$$

The PDF indicates the relative frequency of occurrence of any fixed value of x. Finally, the MGF is defined as

$$m(z) = \text{E}[e^{-zx}] = \int_{-\infty}^{\infty} e^{-zx}p(x)\,dx \tag{2.3}$$

where $\text{E}[x]$ is the expected value (also called mean or average value) of $x(k)$. (Note, the MGF is closely related to another statistical function, the characteristic function and is easily translated by the variable substitution $z = -j\nu$.) By definition, Eq. (2.3) is the Laplace transform of the PDF $p(x)$. Thus, using the Laplace transform of a derivative property[2], the MGF may alternatively be written in terms of the CDF:

$$m(z) = \int_{-\infty}^{\infty} e^{-zx}F'(x)\,dx = z\int_{-\infty}^{\infty} e^{-zx}F(x)\,dx - F(0) . \tag{2.4}$$

1. For a more thorough discussion of these functions, refer to [3], [14].

where $F'(x)$ is the first derivative of $F(x)$.

The random variable of interest here is the power in the fading envelope of the received signal. Assuming the channel conditions remain near constant over the duration of any one symbol period (this slow fading assumption is valid for non-frequency selective fading channels [2]), the received signal corresponding to the k-th transmitted symbol may be expressed as

$$y_k = s_k x_k + n_k \tag{2.5}$$

where x_k is the transmitted signal corresponding to the k-th information symbol, n_k is additive Gaussian noise with a single-sided spectral density $N_0/2$ and s_k is the complex channel gain (equal to unity in the absence of fading). In complex notation, $s_k = s_{k,I} + j s_{k,Q}$ where $s_{k,I}$ and $s_{k,Q}$ are the in-phase and quadrature components of the fading envelope respectively. The received power in the faded envelope is then $S = |s|^2 = s_I^2 + s_Q^2$ (where k can be omitted since S is independent of k due to the slow fading assumption) [26], [27]. Thus, it is the statistical characterization of S that is developed here.

The effects of thermal noise, atmospheric noise and co-channel interference (interference from other transmitters sharing the same frequencies) is grouped together as additive white Gaussian noise (AWGN) with power N_0 in the frequency band of interest. The signal to noise ratio γ in the *unfaded* link is then defined as [26]

$$\gamma = \mathrm{E}[|x_k|^2]/N_0 = E_s/N_0 \tag{2.6}$$

where E_s is the energy per symbol at the receiver in the absence of fading (i.e., $S = 1$).

2.1.1 Rician Distribution

The Rician fading channel is characterized by a direct or line of sight (LOS) signal component summed with a multipath (or specular) component consisting of multiple reflected, refracted and diffused copies of the same signal [4], [15]. The multipath signals may either sum constructively or destructively depending on the topographical features surrounding the mobile terminal (see Figure 2.2). Destructive addition of signals results

---

2. Given an original function $F(t)$ and it's Laplace transform $f(s)$, then [18]

$$\frac{dF(t)}{dt} \Leftrightarrow sf(s) - F(0).$$

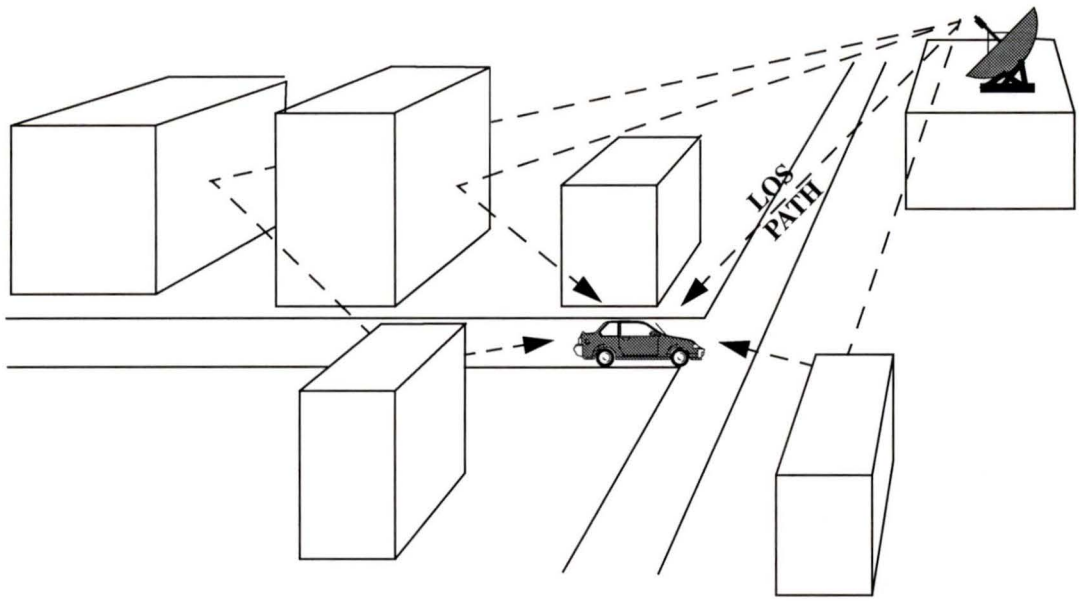

Figure 2.1 Example of the Rician channel illustrating multipath fading.

in fading.

For the Rician channel, s_I and s_Q are independent Gaussian random processes, where s_I has a mean equal to the signal strength in the LOS path, s_Q has zero mean and both have variances equal to the power in the multipath component [3]. The received, faded power therefore obeys the non-central Chi-squared distribution with two degrees of freedom [3], [14]. Since the expressions for the CDF and MGF for the Chi-squared distribution are well known, they are repeated here without explanation.

The CDF is given as [3],

$$F_{\text{Rice}}(S) = 1 - Q(\sqrt{2K}, \sqrt{2(1+K)S}) \tag{2.7}$$

where K is the Rice factor, defined as the ratio of the power in the LOS path to the power in the multipaths, and $Q(\alpha, \beta)$ is Marcum's Q function[3] (see Appendix C in [16]).

3. Marcum's Q function is defined as [16]

$$Q(\alpha, \beta) = 1 - e^{-(\alpha^2+\beta^2)/2}\sum_{n=1}^{\infty}\left(\frac{\beta}{\alpha}\right)^n I_n(\alpha\beta)$$

where $I_n(x)$ is the n th order modified Bessel function of the first kind.

Note that Eq. (2.7) is obtained by setting the expected value of the power to unity (i.e. $\mathrm{E}[S] \equiv 1$). Similarly, the MGF is given as [3]

$$m_{\text{Rice}}(z) = \frac{1+K}{1+K+z} e^{-\left[\frac{zK}{1+K+z}\right]}. \tag{2.8}$$

Two limiting cases exist. The first occurs when the power in the LOS path approaches zero (i.e. a LOS path no longer exists), then $K \to 0$ and the channel reverts to the Rayleigh fading channel. Thus the non-centralized Chi-squared distribution for the general case becomes a centralized Chi-squared distribution for the Rayleigh case. If S_0 represents the power of the multipath component, the Rayleigh CDF is [3]

$$F_{\text{Rayleigh}}(S) = 1 - e^{-S/S_0} \tag{2.9}$$

and the corresponding MGF is [3]

$$m_{\text{Rayleigh}}(z) = \frac{1}{1+zS_0}. \tag{2.10}$$

For the second limiting case, the power in the multipath component becomes negligible compared to the power in the LOS path (i.e. $K \to \infty$). In this case, the Rician distribution reverts to the Gaussian distribution. This becomes a valid approximation for the Rician channel when $K > 30$ [3].

The Rician distribution assumes a constant K. In reality, this is not the case since as the mobile terminal (or simply mobile) moves through the cell, various different topographical surroundings are encountered. This is particularly evident in the terrestrial environment where shadowing (physical obstruction of the signal path) is more severe.

2.1.2 Lognormal Rice Distribution

The lognormal Rice distribution is a combined distribution incorporating the effects of shadowing into the Rician distribution. Over local areas, the channel is Rice distributed (as described in Section 2.1.1) while over larger areas, the local area mean is lognormally distributed [4], [8].

Define two mutually independent random processes: ρ, which is Rice distributed and S_0, which is lognormally distributed. The received power in the fading envelope can then be expressed as the product $S = \rho S_0$ where S is now a lognormally distributed Rician random variable.

Using the definition in Eq. (2.3), the MGF of S is [8]

$$m_{\text{lnRice}}(z) = \int_0^\infty e^{-z\rho S_0} p(\rho S_0)\, d(\rho S_0) = \int_0^\infty \int_0^\infty e^{-z\rho S_0} p(\rho)\, p(S_0)\, d\rho\, dS_0 \tag{2.11}$$

where $p(x)$ denotes the PDF of x and $p(\rho S_0) = p(\rho)\, p(S_0)$ since ρ and S_0 are independent. The inner integral of Eq. (2.11) with respect to ρ can be evaluated to obtain $m_{\text{Rice}}(zS_0)$ as defined in Eq. (2.8). The lognormal PDF $p(S_0)$ is defined as [15], [17]

$$p_{\ln}(S_0) = \frac{1}{\sqrt{2\pi}\sigma S_0} \exp\left[-\frac{1}{2\sigma^2} \ln^2\left(\frac{S_0}{\mu}\right)\right] \tag{2.12}$$

where σ is the logarithmic standard deviation of shadowing in natural units and μ is the local mean power. Thus substituting Eq. (2.8) and Eq. (2.12) into Eq. (2.11) yields

$$\begin{aligned} m_{\text{lnRice}}(z) &= \int_0^\infty m_{\text{Rice}}(zS_0)\, p_{\ln}(S_0)\, dS_0 \\ &= \int_0^\infty \frac{1+K}{1+K+zS_0} e^{-\left[\frac{zK}{1+K+zS_0}\right]} \frac{1}{\sqrt{2\pi}\sigma S_0} \exp\left[-\frac{1}{2\sigma^2} \ln^2\left(\frac{S_0}{\mu}\right)\right] dS_0 \end{aligned} \tag{2.13}$$

Introducing the same notation as in [8], namely

$$\phi(x, k) \equiv \frac{1+k}{1+k+x} e^{-\frac{kx}{1+k+x}} \tag{2.14}$$

and making the variable substitution $x = [\ln(S_0/\mu)] / (\sqrt{2}\sigma)$ presented in [17], Eq. (2.13) can be rewritten as

$$m_{\text{lnRice}}(z) = \frac{1}{\sqrt{\pi}} \int_0^\infty \phi(z\mu e^{\sqrt{2}\sigma x}, K)\, e^{-x^2} dx. \tag{2.15}$$

Applying Hermitian integration[4], a closed form expression for Eq. (2.15) is obtained [8]

---

4. Given the Hermite polynomial $H_n(x)$, then [18]

$$\int_{-\infty}^{\infty} e^{-x^2} f(x)\, dx = \sum_{i=1}^{n} w_i f(x_i) + R_n$$

where x_i and w_i are the i th abscissa and weight respectively of the n th order Hermite polynomial and R_n is a remainder term.

$$m_{\text{lnRice}}(z) = \frac{1}{\sqrt{\pi}} \sum_{i=1}^{n} w_i \phi\left(z\mu e^{\sqrt{2}\sigma x_i}, K \right) + R_n \tag{2.16}$$

where x_i and w_i are tabulated in [18] for $n \leq 20$ and R_n is a remainder term. Appendix A provides an analysis of the remainder term.

The CDF for the lognormal Rician distribution can be obtained directly from the MGF given by Eq. (2.16) by recognizing that $\phi(x, k) = m_{\text{Rice}}(z|K = k)$ and by using the Laplace transform pair defined by Eq. (2.4). Thus, using the linearity[5] and s-domain scaling[6] properties of the Laplace transform, the lognormal Rice CDF is

$$F_{\text{lnRice}}(S) = \frac{1}{\sqrt{\pi}} \sum_{i=1}^{n} \frac{w_i}{a_i} \left[1 - Q\left(\sqrt{2K}, \sqrt{2(1+K)(S/a_i)} \right) \right] + R_n . \tag{2.17}$$

2.1.3 Suzuki Distribution

Suzuki fading characterizes the joint effects of Rayleigh fading and lognormal shadowing and models a shadowed multipath channel without a LOS path. Over a local area, the fading envelope obeys a Rayleigh distribution with a local area mean power S_0. Due to changing topographical features, S_0 varies over larger areas following a lognormal distribution [1], [2], [4]. The Suzuki distribution is a special case of the lognormal Rician distribution presented in the previous section for which the Rician factor K is zero.

Thus by setting $K = 0$ in Eq. (2.16) and Eq. (2.17), the MGF and CDF of the Suzuki channel is obtained. After simplification, the Suzuki MGF is

$$m_{\text{Suzuki}}(z) = \frac{1}{\sqrt{\pi}} \sum_{i=1}^{n} \frac{w_i}{1 + z a_i} + R_n \tag{2.18}$$

where a_i is equal to $\mu \exp\left[\sqrt{2}\sigma x_i\right]$. Similarly, the Suzuki CDF is

---

5. Given the Laplace transform pairs, $F_1(t) \Leftrightarrow f_1(s)$ and $F_2(t) \Leftrightarrow f_2(s)$ then [18]
$$AF_1(t) + BF_2(t) \Leftrightarrow Af_1(s) + Bf_2(s)$$
where A and B are constants.

6. Given the Laplace transform pair $F(t) \Leftrightarrow f(s)$ and some constant $c > 0$, then
$$\frac{1}{c} F\left(\frac{t}{c} \right) \Leftrightarrow f(cs) .$$

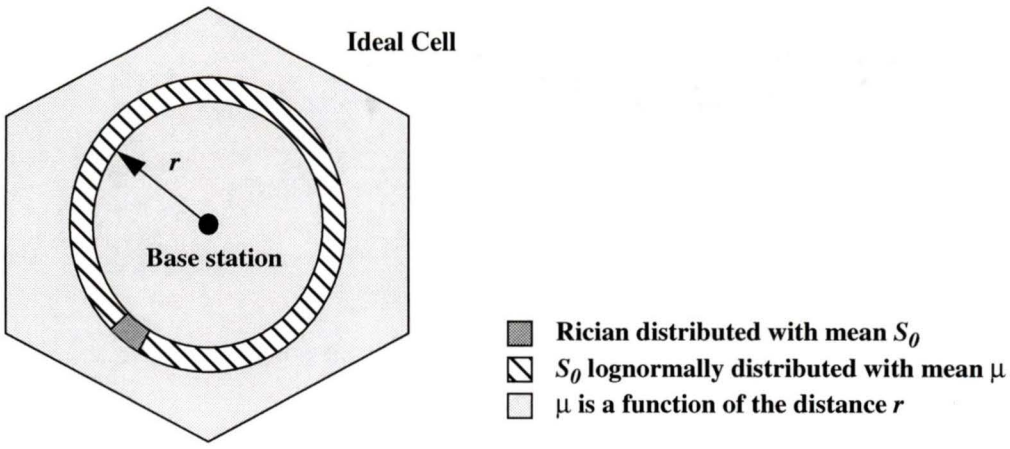

Figure 2.2 Physical representation of the terrestrial cellular channel.

$$F_{\text{Suzuki}}(S) = \frac{1}{\sqrt{\pi}} \sum_{i=1}^{n} w_i [1 - e^{-S/a_i}] + R_n . \tag{2.19}$$

These results are in agreement with those derived directly from the Rayleigh and lognormal distributions in [19].

2.2 Land Mobile Terrestrial Channel Model

The land mobile terrestrial channel refers to the channel between a land based mobile and a land based (or terrestrial) base station. One base station typically services the calls of several surrounding mobiles.

Figure 2.2, shows an ideal hexagonal cell serviced by a single base station and illustrates the scope of the fading channel effects. It is generally accepted that over a spacial dimension of a few hundred wavelengths, the received signal is Rician (or Rayleigh) distributed and is lognormally shadowed over areas equidistant from the base station whose dimension is much greater [1], [4]. The CDF and MGF for the power in the envelope of the received signal corresponding to this fading environment was derived in Section 2.1.2. The large area average path strength is a deterministic function of the distance between the mobile and base station (referred to as path loss or propagation attenuation) [4], [7].

Consider the local area Rician fading. For a mobile with velocity v, each of the

multipath signals is frequency shifted due to the Doppler effect and results in frequency spreading of the fading spectrum [15]. Thus, the fading spectrum has a low pass frequency response with frequency cutoff equal to the maximum Doppler frequency [15]

$$f_D = \frac{v}{\lambda}. \tag{2.20}$$

where λ is the wavelength of the carrier. This frequency spreading results in time-selective fading (i.e. the channel changes with time). As channel samples taken $\lambda/2$ apart are uncorrelated, Rician fading is a fast fading process [4]. At 800 MHz, this fading is typically one fade per second per mile per hour of vehicle speed [20].

The severity of fading is a function of the Rician factor K. For macrocells with a diameter greater than several kilometers, K is typically zero. For cells with diameter less than two kilometers, K is usually small, in the range of 1 to 2. For picocells, K varies widely and may often exceed 5 and values above 30 are not uncommon [7].

The variation in K is a function of shadowing. Unfortunately, shadowing is highly dependent on environmental factors including building heights, roof shape, construction materials, gaps between buildings and cross streets, foliage and terrain. A signal may drop 20 dB by simply turning a corner [4]. Shadowing is a slow fading process whose behavior is obtained by averaging over 10-20 meters [2], [4]. The standard deviation of shadowing, σ, is typically 6 to 9 dB but may be as high as 12 dB or as low as 3 dB [7].

The local mean power μ is a function of the distance r between the mobile and base station, and is typically given as [7]

$$\mu = \frac{D}{r^{\alpha}} \tag{2.21}$$

where D is the propagation constant (dependent on the transmitter and receiver hardware design) and α is the propagation exponent. α is typically in the range of 3.5 to 4.5 but may be less than 2 (the free-space index) when the mobile is close to the base station or in a narrow corridor.

2.3 Land Mobile Satellite Channel Model

The land mobile satellite channel refers to the channel between a land based mobile and a satellite base station. The model presented here assumes a geostationary satellite.

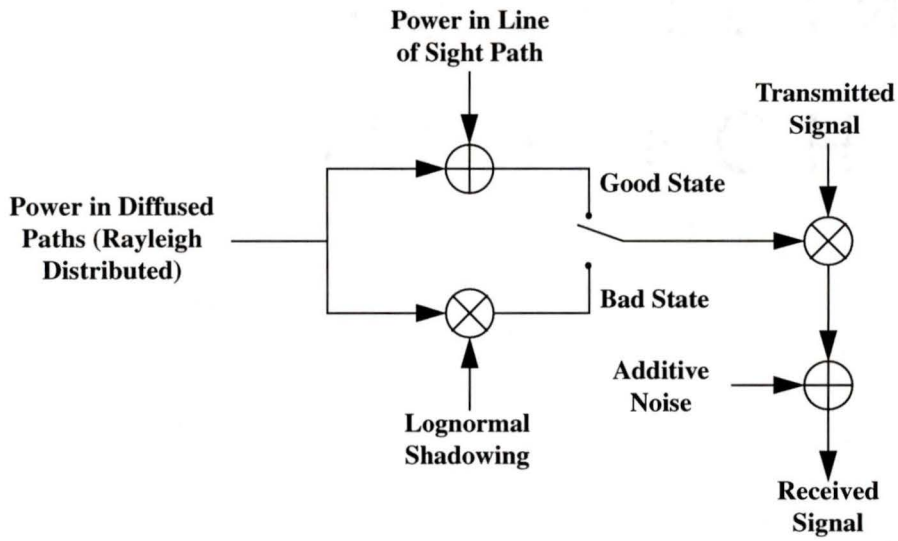

Figure 2.3 Functional diagram of the satellite channel model.

In [12], [13], a two-state land mobile satellite channel model based on channel measurements is presented (see Figure 2.3). For a fraction of the time $1-A$, the channel is in the good state modelled as a Rician random process. For the remaining fraction of the time A, the channel is in the bad state modelled as a lognormally shadowed Rayleigh random process, or equivalently, a Suzuki random process. The net PDF of the received power is thus the weighted sum of the Rician and Suzuki PDFs, $p_{\text{Rice}}(S)$ and $p_{\text{Suzuki}}(S)$ respectively,

$$p(S) = (1-A)\,p_{\text{Rice}}(S) + A p_{\text{Suzuki}}(S)\,. \tag{2.22}$$

Similarly, using the definition of the MGF from Eq. (2.3), the net MGF is

$$m(z) = \int_0^\infty e^{-zS} p(S)\,dS = (1-A)\,m_{\text{Rice}}(z) + A m_{\text{Suzuki}}(z) \tag{2.23}$$

where $m_{\text{Rice}}(z)$ and $m_{\text{Suzuki}}(z)$ are the MGFs for the Rician and Suzuki fading states given in Eq. (2.8) and Eq. (2.18). Finally, integrating Eq. (2.22), the net CDF is obtained,

$$F(S) = \int_0^S p(\xi)\,d\xi = (1-A)\,F_{\text{Rice}}(S) + A F_{\text{Suzuki}}(S) \tag{2.24}$$

where $F_{\text{Rice}}(S)$ and $F_{\text{Suzuki}}(S)$ are given in Eq. (2.7) and Eq. (2.19).

The parameters used to represent the fading channel are taken from [13]. These are repeated in Table 2.1. Note that conversion from dB to linear units is required for K and

μ, and conversion from dB to nepers for σ. The angle immediately following the location specifies the elevation angle between the earth and geostationary satellite for which the measurements were performed. As the typical orbit for a geostationary satellite is at 36 000 km above the equator, the effect of mobile movement on the path loss is negligible and thus not considered here.

Parameter set	A	K, **dB**	μ, **dB**	σ, **dB**
Munich city (24°)	0.70	8.7	-8.5	3.0
Munich wood (24°)	0.54	10.7	-5.3	1.3
Munich highway (24°)	0.16	11.7	-7.0	4.5
Hamburg city (21°)	0.75	9.4	-8.7	3.2
Copenhagen city (18°)	0.80	5.5	-9.4	3.0
Stockholm city (13°)	0.87	7.0	-9.5	3.0

Table 2.1. Parameter sets for the analog channel model [13].

2.4 Fading Channel Simulator

To perform the computer simulations required to evaluate the error control codes, a digital fading simulator is required. It must be capable of simulating the Rice, lognormal Rice and lognormal Rayleigh channels. Here, the Rayleigh channel is simulated as Rice with $K = 0$. Following [21], a single sample per symbol is used to represent the signal fading process. A block diagram of the fading simulator is shown in Figure 2.4.

The Rician channel section of the simulator follows directly from the fact that the received power in the faded envelope is a non-central Chi-squared random variable with two degrees of freedom [3], [22]. The time correlation between samples in the Rician channel is introduced through low pass filtering. Although there is no general consensus on the exact filter to employ, a third-order Butterworth filter with normalized gain and 3 dB cut-off equal to f_D (as employed in [11], [22]) is selected as a compromise between simulation speed and complexity. The digital implementation of this filter is shown in Figure 2.5 where the filter weights are calculated in terms of the following

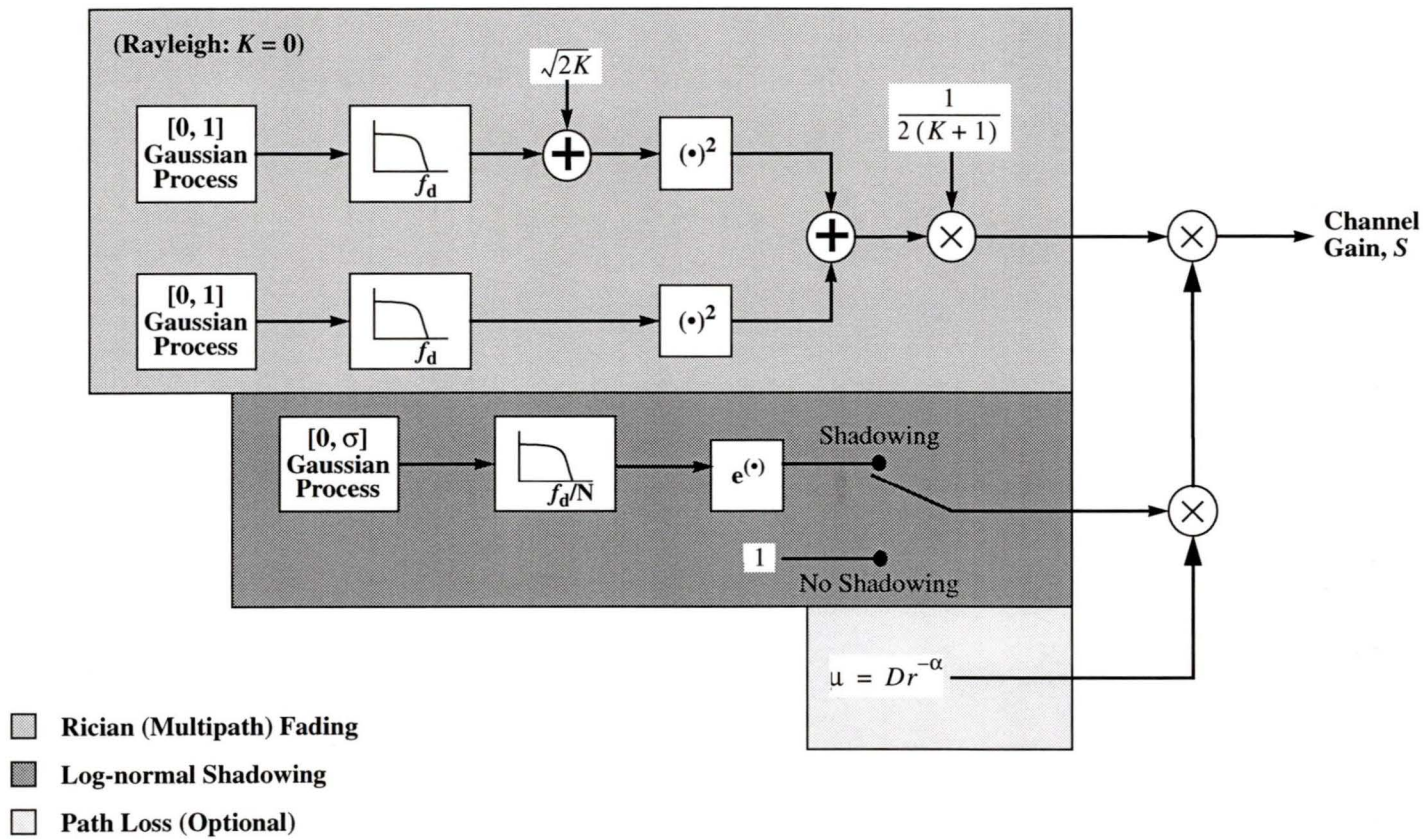

Figure 2.4 Fading channel simulator.

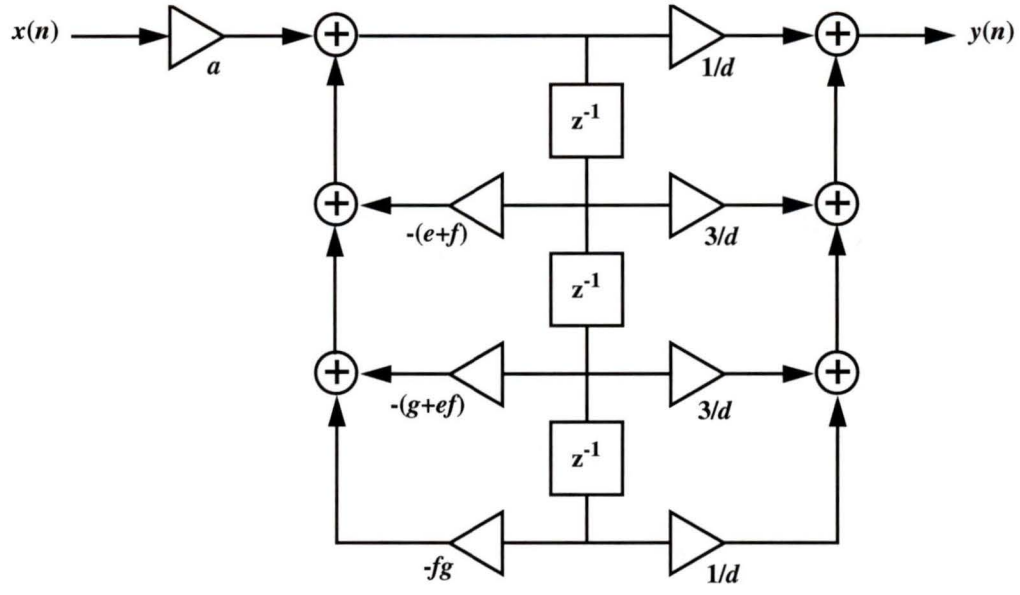

Figure 2.5 Digital implementation of a third-order digital Butterworth filter.

$$
\begin{aligned}
a &= \sqrt{\frac{3\,(c^6-1)}{2c^5-c^3+2c-3}} \\
d &= (1+c)\,(1+c+c^2) \\
e &= \frac{2\,(1-c^2)}{1+c+c^2} \\
f &= \frac{1-c}{1+c} \\
g &= \frac{1-c+c^2}{1+c+c^2}
\end{aligned}
\tag{2.25}
$$

In Eq. (2.25), $c = [\tan(\pi f_D T)]^{-1}$ where T^{-1} is the symbol rate and $f_D T$ is referred to as the normalized fading bandwidth. (Refer to [23] for more information on Butterworth filter design.)

The lognormal shadowing section of the simulator is implemented directly from the definition of the lognormal distribution [17]. Correlation in the shadowing is introduced through low pass filtering using the same Butterworth filter as for the Rician case [22]. As shadowing is a much slower fading process compared to multipath fading, a 3 dB cutoff frequency of f_D/N is used where $N > 1$ and is dependent on the topographical

features of the terrain surrounding the mobile. In [22], the suggested value for N is 10.

The local mean area μ represents the path loss and is implemented directly from Eq. (2.21) for the terrestrial channel and is read from Table 2.1 for the satellite channel.

Figure 2.6 shows the simulated channel gain for a 900 MHz signal given several different channel conditions and mobile velocities. The effects of mobile speed are obvious. At 80 km/hr, deep fades occur much more frequently and the variation in shadowing is evident. At 20 km/hr, deep fades are less common and the time variations in shadowing are not evident over this short a sample period. The severity of fading is seen to increase significantly for the Rayleigh channel ($K = 0$) in comparison to the Rician channel with $K = 2.$. Finally, the effect of increasing the standard deviation of shadowing is seen to produce more rapid and severe variations in the short term signal mean.

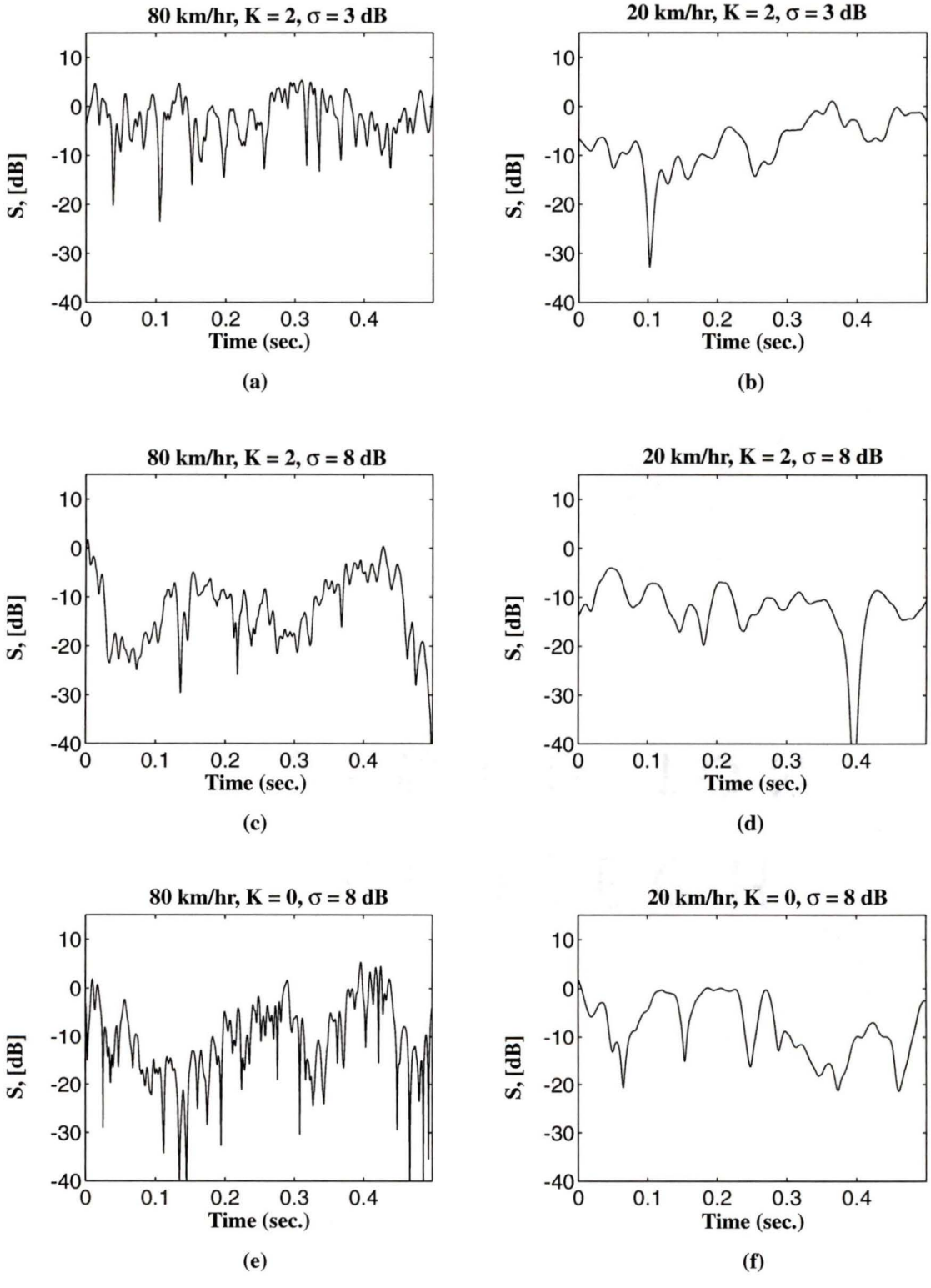

Figure 2.6 Examples of the channel gain simulated using the channel simulator for various channel fading parameters.

Chapter 3

Diversity Techniques

Diversity reception is employed to mitigate the effects of short-term fading. The underlying premise is that if two or more signals are taken from "sufficiently" spaced receiving antennas[1,2], it is improbable that these signals will experience simultaneous deep fades [2]. Diversity reception can be used either at the base station (macroscopic diversity or macro-diversity) or at the mobile (microscopic diversity or micro-diversity), although the antenna separation required differs for each case. In practice, micro-diversity reception combats the fast fading variations in the received signal strength caused by multipath fading, whereas macro-diversity combats the slower fading variations caused by shadowing [2]. A composite macro- and micro-diversity system combats both multipath and shadowing [25].

To capitalize on the improvement in signal statistics due to diversity, several combining techniques have been proposed. Two such techniques are considered here: selection diversity combining (SDC — perhaps the simplest combining method), and maximal ratio combining (MRC — the best known linear combining method). The performance of other techniques generally fall between these two.

In this chapter, the effects of composite macro- and micro-diversity on the power in the received envelope after combining are evaluated. Both the terrestrial and satellite channel models presented in Chapter 2 are considered. The CDF and MGF are derived

---

1. Although space diversity (i.e. multiple sufficiently spaced antennas) is assumed, the expressions derived here are also valid for polarization diversity. Other diversity techniques, such as time or frequency diversity, achieve independent fading by multiple transmissions which requires more transmission power and thus are not as efficient as space diversity [2].

2. Due to the reciprocity of the channel, the effects on the signal strength are equivalent regardless of whether the signal is being received with multiple antennas or transmitted with multiple antennas.

assuming either SDC or MRC micro-diversity and SDC macro-diversity.

3.1 Diversity Combining Techniques

In systems employing diversity, a method of combining the multiple received signals into a single improved signal is required. Two methods, selection diversity combining (SDC) and maximal ratio combining (MRC) are described here.

SDC measures the signal to noise ratio (SNR) at each branch (i.e. antenna) and selects the branch with the highest SNR value. Thus, if L branch diversity is employed and the mean noise power per branch is the same for all branches, the decision criteria reduces to $\max [S_i]$, $i = 1, \ldots, L$, where S_i is the channel gain from the ith branch. For MRC, rather than selecting the single strongest signal, MRC weights each signal proportionately to their current SNR and then sums all the signals. It is shown in [2] that for L branch diversity, the total channel gain S is the sum of the individual channel gains S_i, $i = 1, \ldots, L$, from each antenna (assuming the mean noise power per branch is the same for all branches).

Figure 3.1 illustrates the effects of two branch micro-diversity on the power S in the fading envelope for both SDC and MRC. This was obtained through simulation (refer to channel simulator in Section 2.4) with the following parameters: 900 MHz carrier frequency, a mobile speed of 15 kilometers per hour and a Rician factor $K = 2$. As micro-diversity has no effect on shadowing, shadowing was not simulated. This figure clearly illustrates the performance improvements obtained from diversity, especially with MRC. Note that for SDC, the combined signal strength will never exceed the strength of the best branch. However, for MRC, the combined signal strength will always exceed that of the best branch. Furthermore, since the channel gain of any branch may occasionally exceed unity in the multipath fading environment, with sufficient diversity branches (either MRC or SDC), the average signal strength in the multipath channel may actually exceed that of the non-fading channel.

To evaluate the performance of SDC and MRC diversity, their effects on the channel statistics must be ascertained. Considering SDC, the probability that S_i, $i = 1, \ldots, L$ are all simultaneously less than or equal to some S is $\text{Prob}\,[S_i \leq S]$, $i = 1, \ldots, L$. Since sufficient antenna separation is assumed, S_i, $i = 1, \ldots, L$, are uncorrelated and identically distributed. Thus using the definition of the CDF given in Eq. (2.1)

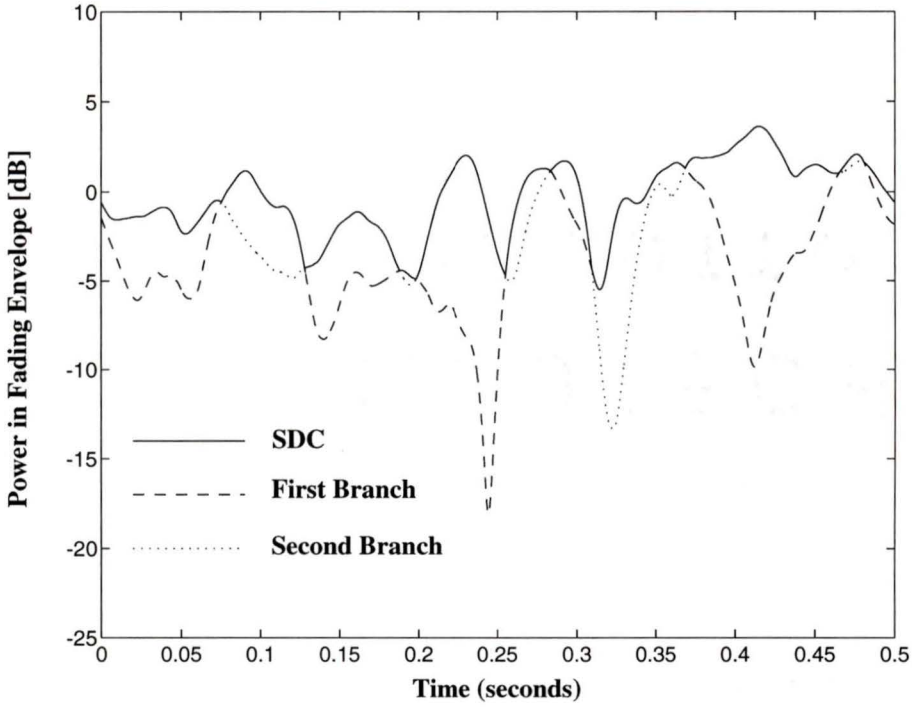

(a) Selection Diversity Combining

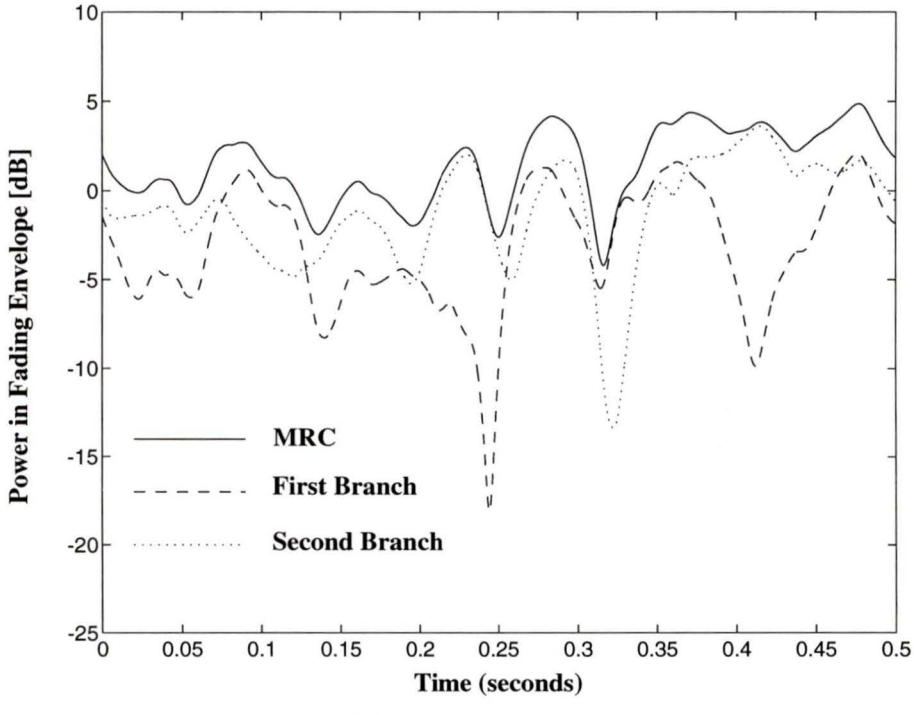

(b) Maximal Ratio Combining

Figure 3.1 Effects of diversity on the received power in the Rician fading channel.

$$F^{(\mathrm{SDC})}(S) = \prod_{i=1}^{L} \mathrm{Prob}[S_i \le S] = (\mathrm{Prob}[S_i \le S])^L = [F(S_i)]^L \tag{3.1}$$

where $F(x)$ is the CDF for the received power in one branch and $F(S_i) = F(S_j)$ for $i = 1, \ldots, L$ and $j = 1, \ldots, L$.

Similarly for MRC, from the definition of the MGF given by Eq. (2.3), the MGF of the combined signal power S is

$$\begin{aligned} m^{(\mathrm{MRC})}(z) &= \mathrm{E}[e^{-z(S_1 + S_2 + \ldots + S_L)}] \\ &= \int_0^\infty \int_0^\infty \ldots \int_0^\infty e^{-z(S_1 + S_2 + \ldots + S_L)} p(S_1) p(S_2) \ldots p(S_L) \, dS_1 dS_2 \ldots dS_L \end{aligned} \tag{3.2}$$

Assuming S_i, $i = 1, \ldots, L$, are independent and identically distributed (achieved through sufficient antenna separation), Eq. (3.2) can be written in the desired form

$$m^{(\mathrm{MRC})}(z) = \left[\int_0^\infty e^{-zS_i} p(S_i) \, dS_i\right]^L = [m(z)]^L \tag{3.3}$$

where $m(z)$ is the MGF for a single diversity branch.

3.2 Terrestrial Channel

At the mobile, an antenna separation of 0.5λ has been found to achieve almost independent multipath fading diversity branches [2], [4]. However, due to the larger area effect of shadowing and the limited antenna separation distance at the mobile, antenna separation cannot decorrelate the effects of shadowing between the antennas. In fact, it is assumed that the shadowing effects at each antenna are identical (a valid assumption for antenna separations less than a few meters [4]). Both SDC and MRC are considered.

As sufficient antenna separation at the mobile is typically not possible (i.e. greater than 20 meters [4]), macro-diversity is implemented using multiple base stations sufficiently separated to obtain independent shadowing. For macro-diversity, SDC is assumed. Thus, given M base stations, each experiencing independent shadowing effects, the base station measuring the strongest received signal services the mobile. A handoff to another base station is initiated only if the mobile's transmitted signal is received more strongly at another base station.

3.2.1 SDC Micro-Diversity with SDC Macro-Diversity

For the terrestrial channel, micro-diversity alleviates the Rician distributed multipath fading. The resulting CDF for the local area power is obtained from Eq. (3.1) using the non-diversity Rician CDF given by Eq. (2.7)

$$F_{\text{Rice}}^{(\text{SDC})}(S) = [1 - Q(\sqrt{2K}, \sqrt{2(1+K)S})]^L. \tag{3.4}$$

Applying the definition of the MGF given by Eq. (2.4), the MGF for SDC in Rician fading is

$$m_{\text{Rice}}^{(\text{SDC})}(z) = z\int_0^\infty e^{-zS}[1 - Q(\sqrt{2K}, \sqrt{2(1+K)S})]^L dS. \tag{3.5}$$

Making the variable substitution, $x = zS$, and applying Gauss-Laguerre integration[3], a closed form expression for Eq. (3.5) is obtained

$$m_{\text{Rice}}^{(\text{SDC})}(z) = \sum_{i=1}^{n} \omega_i \left[1 - Q\left(\sqrt{2K}, \sqrt{2(1+K)(\chi_i/z)}\right)\right]^L + R_n \tag{3.6}$$

where ω_i and χ_i are tabulated in [18] for $n \leq 15$. The remainder term R_n is examined in Appendix A.

Consider now M independently shadowed base stations, all monitoring the received signal strength from the mobile and employing SDC macro-diversity. From Eq. (3.1), the CDF for the shadowing is simply $F_{\ln}^{(\text{SDC})}(S_0) = [F_{\ln}(S_0)]^M$ where $F_{\ln}(S_0)$ is the non-diversity CDF for the lognormally distributed shadowing given as [3]

$$F_{\ln}(S_0) = 1 - Q\left(\frac{\ln(S_0/\mu)}{\sigma}\right) \tag{3.7}$$

where $Q(x)$ is the area in the upper tail of the normalized Gaussian distribution[4]. Thus,

---

3. Given the Laguerre polynomial $L_n(x)$, then [18]

$$\int_0^\infty e^{-x} f(x)\,dx = \sum_{i=1}^{n} \omega_i f(\chi_i) + R_n$$

where χ_i and ω_i are the i th abscissa and weight respectively of the n th order Laguerre polynomial and R_n is a remainder term.

4. Mathematically, $Q(x)$ is expressed as [26]

$$Q(x) = \frac{1}{\sqrt{2\pi}}\int_x^\infty e^{-z^2/2} dz.$$

using the definition of the PDF given by Eq. (2.2)

$$p_{\ln}^{(\mathrm{SDC})}(S_0) = \frac{d}{dS_0}[F_{\ln}(S_0)]^M = M\left[1 - Q\left(\frac{\ln(S_0/\mu)}{\sigma}\right)\right]^{M-1} p_{\ln}(S_0) \tag{3.8}$$

where $p_{\ln}(S_0)$ is given in Eq. (2.12).

Following the same methodology used to derive Eq. (2.13), but replacing $m_{\mathrm{Rice}}(zS_0)$ with $m_{\mathrm{Rice}}^{(\mathrm{SDC})}(zS_0)$ and $p_{\ln}(S_0)$ with $p_{\ln}^{(\mathrm{SDC})}(S_0)$, the MGF for the combined lognormal Rice channel is obtained

$$\begin{aligned} m_{\mathrm{lnRice}}^{(\mathrm{SDC!})}(z) &= \int_0^\infty m_{\mathrm{Rice}}^{(\mathrm{SDC})}(zS_0)\, p_{\ln}^{(\mathrm{SDC})}(S_0)\, dS_0 \\ &= \int_0^\infty m_{\mathrm{Rice}}^{(\mathrm{SDC})}(zS_0)\, M\left[1 - Q\left(\frac{\ln(S_0/\mu)}{\sigma}\right)\right]^{M-1} \frac{1}{\sqrt{2\pi}\sigma S_0} \exp\left[-\frac{1}{2\sigma^2}\ln^2\left(\frac{S_0}{\mu}\right)\right] dS_0 \end{aligned} \tag{3.9}$$

The exclamation mark denotes that composite macro- and micro-scopic diversity is being considered. As before, making the variable substitution $x = [\ln(S_0/\mu)] / (\sqrt{2}\sigma)$, appling Hermitian integration and substituting Eq. (3.6) for $m_{\mathrm{lnRice}}^{(\mathrm{SDC})}(z)$, one obtains (ignoring remainder terms)

$$\begin{aligned} m_{\mathrm{lnRice}}^{(\mathrm{SDC!})}(z) \approx \frac{M}{\sqrt{\pi}} \sum_{i=1}^{n_H} w_i \left[1 - Q\left(\sqrt{2}x_i\right)\right]^{M-1} \\ \times \sum_{j=1}^{n_L} \omega_j \left[1 - Q\left(\sqrt{2K}, \sqrt{2(1+K)(\chi_j/(za_i))}\right)\right]^L \end{aligned} \tag{3.10}$$

where x_i and w_i correspond to the Hermitian integration, χ_i and ω_i correspond to the Laguerre integration, and n_H and n_L are the orders of the Hermitian and Laguerre polynomials.

Applying the inverse Laplace transform to Eq. (3.10), the corresponding CDF is obtained. Recognizing that only the second summation is a function of z, the same arguments used to derive the lognormal Rice CDF for the non-diversity case (see Eq. (2.16)) can be applied. Namely, recognizing the similarity between the second summation and the Rician MGF given by Eq. (3.6) and applying the linearity and s-domain scaling properties of the Laplace transform, the CDF can be written directly from Eq. (3.4) and Eq. (3.10)

$$F_{\text{lnRice}}^{(\text{SDC!})}(S) = \frac{M}{\sqrt{\pi}} \sum_{i=1}^{n} \frac{w_i}{a_i} \left[1 - Q\left(\sqrt{2}x_i\right)\right]^{M-1} \left[1 - Q\left(\sqrt{2K}, \sqrt{2(1+K)(S/a_i)}\right)\right]^{L}. \tag{3.11}$$

As expected, Eq. (3.10) and Eq. (3.11) revert to the non-diversity cases when $L = M = 1$ and match those derived in [19] for the micro-diversity case alone (i.e. $M = 1$).

3.2.2 MRC Micro-Diversity with SDC Macro-Diversity

Consider again the Rician component of the terrestrial fading channel. Recall that for one branch, the received power is the sum of an in-phase and quadrature component which are modeled as independent squared Gaussian random processes. This is described by the non-central Chi-squared distribution with two degrees of freedom. Therefore, the sum of L independent branches is now distributed as a non-central Chi-squared random process with $2L$ degrees of freedom [3]. Thus the CDF is [3]

$$F_{\text{Rice}}^{(\text{MRC})}(S) = 1 - Q_L(\sqrt{2LK}, \sqrt{2(1+K)S}) \tag{3.12}$$

where $Q_m(\alpha, \beta)$ is the generalized Marcum's Q function[5]. Note that K is defined as before, but now the expected value of S is L (i.e. each branch is normalized). Similarly, the MGF for S is [3]

$$m_{\text{Rice}}^{(\text{MRC})}(z) = \left(\frac{1+K}{1+K+z}\right)^{L} e^{-\frac{zKL}{1+K+z}} = [\phi(z, K)]^{L}. \tag{3.13}$$

where $\phi(x, k)$ is given by Eq. (2.14). As expected, this corresponds to the definition of the MRC MGF given by Eq. (3.3).

Following the same procedure as in the previous section, the MGF for the combined lognormal Rice channel is

$$m_{\text{lnRice}}^{(\text{MRC!})}(z) = \int_0^{\infty} m_{\text{Rice}}^{(\text{MRC})}(zS_0)\, p_{\text{ln}}^{(\text{SDC})}(S_0)\, dS_0 \tag{3.14}$$

where $m_{\text{Rice}}^{(\text{MRC})}(z)$ is given by Eq. (3.13) and $p_{\text{ln}}^{(\text{SDC})}(S)$ is given by Eq. (3.8). Making

---

5. Marcum's generalized Q function is defined as [16]

$$Q_M(\alpha, \beta) = 1 - e^{-(\alpha^2+\beta^2)/2} \sum_{n=M}^{\infty} \left(\frac{\beta}{\alpha}\right)^n I_n(\alpha\beta).$$

the variable substitution $x = [\ln(S_0/\mu)] / (\sqrt{2}\sigma)$ and applying Hermitian integration the MGF can be written as

$$m_{\text{lnRice}}^{(\text{MRC!})}(z) \approx \frac{M}{\sqrt{\pi}} \sum_{i=1}^{n} w_i \left[\phi\left(\mu e^{\sqrt{2}\sigma x_i}, K \right) \right]^L \left[1 - Q\left(\sqrt{2} x_i \right) \right]^{M-1}. \tag{3.15}$$

This matches the MGF derived in [8]. Here, the work in [8] is extended by deriving the corresponding CDF.

Following the same procedures used to derive the SDC MGF in Eq. (3.11) and taking the inverse Laplace transform of Eq. (3.15) yields the CDF for the received power in the composite MRC micro-diversity, SDC macro-diversity fading channel

$$F_{\text{lnRice}}^{(\text{MRC!})}(S) = \frac{M}{\sqrt{\pi}} \sum_{i=1}^{n} \frac{w_i}{a_i} \left[1 - Q\left(\sqrt{2} x_i \right) \right]^{M-1} \left[1 - Q_L\left(\sqrt{2LK}, \sqrt{2(1+K)(S/a_i)} \right) \right] \tag{3.16}$$

where the error function $Q(x)$ and Marcum's generalized Q function $Q(\alpha, \beta)$ are previously defined.

As expected, when $L = M = 1$, Eq. (3.15) and Eq. (3.16) revert to the non-diversity cases derived in Chapter 2. These also match the expressions derived in [19] for the micro-diversity case alone (i.e. $M = 1$).

3.3 Satellite Channel

As for the terrestrial channel, L antennas (with independent fast fading components) and M base stations (satellites) are assumed. The MGF and CDF for both SDC and MRC micro-diversity with SDC macro-diversity for the satellite channel are derived here. Recall that the satellite channel model is a time shared, two state model, where the good state is modeled as Rician and the bad state as Suzuki.

3.3.1 SDC Micro-Diversity with SDC Macro-Diversity

The CDF and MGF for the Rician channel state are derived previously for the terrestrial channel and are given by Eq. (3.4) and Eq. (3.6), respectively. For the Suzuki channel state, consider first the uncorrelated Rayleigh components with local area mean S_0. Applying Eq. (3.1), the Rayleigh CDF for L branch SDC is equal to the non-diversity CDF Eq. (2.9) raised to the power L

$$F_{\text{Rayl}}^{(\text{SDC})}(S|S_0) = (1 - e^{-S/S_0})^L. \tag{3.17}$$

Taking the inverse Laplace transform of Eq. (3.17), the corresponding MGF can be derived. Using the binomial expansion[6] and the Laplace transform pair $e^{-at} \Leftrightarrow (s+a)^{-1}$ [18], the Rayleigh MGF conditioned on S_0 for SDC is obtained

$$m_{\text{Rayl}}^{(\text{SDC})}(z) = \sum_{j=0}^{L} (-1)^j \binom{L}{j} \frac{zS_0}{j + zS_0}. \tag{3.18}$$

An equally valid solution can be obtained from the Rician MGF by setting $K = 0$, however, this requires Hermitian integration. Thus Eq. (3.18) is a more attractive solution.

Following the same procedure as in the previous section, the MGF for the combined lognormal Rayleigh channel is

$$m_{\text{Suzuki}}^{(\text{SDC!})}(z) = \int_0^\infty m_{\text{Rayl}}^{(\text{SDC})}(zS_0)\, p_{\text{ln}}^{(\text{SDC})}(S_0)\, dS_0 \tag{3.19}$$

where $m_{\text{Rayl}}^{(\text{SDC})}(z)$ is given by Eq. (3.18) and $p_{\text{ln}}^{(\text{SDC})}(S)$ is given by Eq. (3.8). As before, making the variable substitution $x = [\ln(S_0/\mu)] / (\sqrt{2}\sigma)$ and applying Hermitian integration the MGF can be written as

$$m_{\text{Suzuki}}^{(\text{SDC!})}(z) = \frac{M}{\sqrt{\pi}} \sum_{i=1}^{n} w_i \left[1 - Q\left(\sqrt{2}x_i\right)\right]^{M-1} \sum_{j=0}^{L} (-1)^j \binom{L}{j} \frac{za_i}{j + za_i} + R_n. \tag{3.20}$$

where a_i, w_i and R_n correspond to Hermitian integration as previously defined. The corresponding Suzuki CDF can be obtained by performing the inverse Laplace transform on Eq. (3.20) to get the PDF and integrating. However, recognizing that the summation over j in Eq. (3.20) is simply the MGF given in Eq. (3.18) where a_i replaces S_0, the CDF for the Suzuki channel can be written directly as

$$F_{\text{Suzuki}}^{(\text{SDC!})}(S) = \frac{M}{\sqrt{\pi}} \sum_{i=1}^{n} w_i \left[1 - Q\left(\sqrt{2}x_i\right)\right]^{M-1} [1 - e^{-S/a_i}]^L + R_n. \tag{3.21}$$

Setting $L = M = 1$, Eq. (3.20) and Eq. (3.21) revert to the non-diversity expres-

---

6. The binomial expansion is given as [18]

$$(a + bx)^n = \sum_{i=0}^{n} \binom{n}{i} a^{n-i} (bx)^i.$$

sions derived in Chapter 2. For $M = 1$, the micro-diversity case, Eq. (3.20) and Eq. (3.21) match those derived in [19].

3.3.2 MRC Micro-Diversity with SDC Macro-Diversity

As before, the CDF and MGF for the Rician channel state were derived previously for the terrestrial channel and are given by Eq. (3.12) and Eq. (3.13), respectively.

For the Suzuki channel state, the MGF may be obtained directly from the lognormally shadowed Rician MGF derived for the terrestrial channel. Thus setting $K = 0$ (limiting Rayleigh case of the Rician distribution) in Eq. (3.15), the MGF for MRC micro-diversity is

$$m_{\text{Suzuki}}^{(\text{MRC!})} = \frac{M}{\sqrt{\pi}} \sum_{i=1}^{n} w_i \left[\frac{1}{1 + z\mu e^{\sqrt{2}\sigma x_i}} \right]^L \left[1 - Q\left(\sqrt{2} x_i \right) \right]^{M-1} + R_n . \tag{3.22}$$

The corresponding CDF can be obtained by finding the inverse Laplace transform[7] of Eq. (3.22) to obtain the PDF and then integrating[8] to get

$$F_{\text{Suzuki}}^{(\text{MRC!})}(S) = \frac{M}{\sqrt{\pi}} \sum_{i=1}^{n} w_i \left[1 - e^{S/a_i} \sum_{m=0}^{L-1} \frac{(S/a_i)^m}{m!} \right] \left[1 - Q\left(\sqrt{2} x_i \right) \right]^{M-1} + R_n \tag{3.23}$$

where $a_i = \mu e^{\sqrt{2}\sigma x_i}$.

As expected, Eq. (3.22) and Eq. (3.23) revert back to the non-diversity case when $L = M = 1$. For the micro-diversity case, Eq. (3.22) and Eq. (3.23) default to the expressions derived in [19].

---

7. This is performed using the Laplace transform pair [18]

$$\frac{1}{(s+a)^n} \Leftrightarrow \frac{t^{n-1} e^{-at}}{(n-1)!} \qquad (n = 1, 2, \ldots) .$$

8. Using the following integral solved in [28]

$$\int_0^{\beta} x^{n-1} e^{-ax} dx = a^{-n} \gamma(n, a\beta)$$

where for the special case when $n = 1, 2, \ldots$, [28]

$$\gamma(n, x) = (n-1)! \left[1 - e^{-x} \left(\sum_{m=0}^{n-1} \frac{x^n}{m!} \right) \right] .$$

3.4 Concluding Remarks

In this chapter, computationally simple formulas for the moment generating function and cumulative probability function were derived for fading channels employing diversity combining techniques. The resulting equation numbers are organized in Table 3.1.

Macroscopic Combining	Microscopic Combining	Statistic	Terrestrial	Satellite	
			Lognormally Shadowed Rice	Rice	Suzuki
No Diversity		MGF	Eq. (2.16)	Eq. (2.8)	Eq. (2.18)
		CDF	Eq. (2.17)	Eq. (2.7)	Eq. (2.19)
SDC	SDC	MGF	Eq. (3.10)	Eq. (3.6)	Eq. (3.20)
		CDF	Eq. (3.11)	Eq. (3.4)	Eq. (3.21)
	MRC	MGF	Eq. (3.15)	Eq. (3.13)	Eq. (3.22)
		CDF	Eq. (3.16)	Eq. (3.12)	Eq. (3.23)

Table 3.1. Summary of the MGFs and CDFs for diversity channels.

In all diversity cases, the equations are generalized for L branches at the mobile and M base stations. These are also valid for the limiting cases when $L = 1$, $M = 1$ or $L = M = 1$. The corresponding PDFs are not required for this thesis and thus are not derived here. The PDF of any distribution may be obtained by differentiating its CDF with respect to S, the power in the fading envelope.

Chapter 4

Bit Error Rate and Outage Performance of Diversity Systems

The average BER and outage probability are the two most common measures of communication performance. In this chapter "clean" and numerically efficient solutions for calculating both are derived. It is shown that for many modulation schemes, the average BER can be obtained directly from the MGF of the fading channel, and the outage probability directly from the CDF.

Although somewhat general expressions for the BER and outage are derived, emphasis is placed on M-ary PSK due to its constant envelope characteristics which are especially favorable for digital mobile communications and due its higher bandwidth efficiency. Both coherent and non-coherent (differential) M-PSK are investigated.

In the latter part of this chapter, an example is provided illustrating the application of the theory derived for the satellite channel with micro-diversity.

4.1 Average Bit Error Rate

In this section, expressions for the average BER for several common modulation schemes including both coherent and non-coherent M-ary PSK are derived. The average BER is defined as the number of erroneous bits per block of transmitted bits averaged over all time to account for all channel fading variations. Thus, it is the *expected value* of the instantaneous BER that is required. This is obtained by averaging the instantaneous BER $P_b(\gamma|S)$ conditioned on the instantaneous fading channel gain S (or equivalently, power in the fading envelope) over the range $0 < S < \infty$:

$$\bar{P}_b(\gamma) = \int_0^\infty P_b(\gamma|S)\, p(S)\, dS \tag{4.1}$$

where γ is the SNR for the unfaded link given in Eq. (2.6) and $p(S)$ is the PDF of the fading channel power. By expressing Eq. (4.1) in terms of the MGF of the power in the fading envelope, the BER expressions can be written independent of the type of fading or diversity employed.

4.1.1 Common Modulation Schemes

In this section, expressions for the average BER are derived for several common modulation schemes including coherent and non-coherent (differential) binary PSK, coherent and non-coherent FSK, coherent ASK, coherent QPSK and coherent MSK. A description of these schemes is not required for the following developments and thus is not presented here. The interested reader is referred to any introductory communications text (i.e. [3], [26], [27]).

The formulas for the instantaneous BER $P_b(\gamma|S)$ of the aforementioned modulation schemes are summarized in Table 4.1. One immediately recognizes that these expressions can be categorized into one of two general forms, namely those which are functions of the complementary error function[1] and those which are of exponential form.

Modulation Scheme	$P_b(\gamma\|S)$
Coherent binary PSK	$\frac{1}{2}\text{erfc}(\sqrt{S\gamma})$
Coherent binary FSK Coherent binary ASK	$\frac{1}{2}\text{erfc}\left(\sqrt{\frac{S\gamma}{2}}\right)$
Coherent QPSK Coherent MSK	$\text{erfc}(\sqrt{S\gamma})$
Non-coherent binary FSK	$\frac{1}{2}e^{-S\gamma/2}$
Differential PSK	$\frac{1}{2}e^{-S\gamma}$

Table 4.1 Instantaneous BER of several common modulation schemes [27].

Consider the first form, where the instantaneous BER is

$$P_b^{(1)}(\gamma|S) = a\,\mathrm{erfc}\,(\sqrt{bS\gamma}) \tag{4.2}$$

where a and b are selected according to Table 4.1. In order to obtain an expression which is a function of the channel MGF, an alternate exponential form for erfc (x) is required. Consider the definite integral and its solution given in [Eq. 7.4.11, 18]

$$\int_0^\infty \frac{e^{-\alpha^2 t^2}}{t^2+z^2}dt = \frac{\pi}{2z}e^{\alpha^2 z^2}\mathrm{erfc}\,(\alpha z) \qquad \alpha>0, z>0\ . \tag{4.3}$$

Isolating the erfc function, making the variable substitution $x = \alpha z$ and rearranging

$$\mathrm{erfc}\,(x) = \frac{2x\alpha}{\pi}\int_0^\infty \frac{e^{-x^2(1+\alpha^2t^2/x^2)}}{x^2(1+\alpha^2t^2/x^2)}dt\,. \tag{4.4}$$

Making another variable substitution $\tan\theta = \alpha t/x$ and using the trigonometric property $1+\tan^2\theta = \sec^2\theta$, the desired form is obtained:

$$\mathrm{erfc}\,(x) = \frac{2}{\pi}\int_0^{\pi/2} e^{-x^2\sec^2\theta}d\theta\,. \tag{4.5}$$

This form is both easily evaluated and well suited to numerical integration since the integrand is well behaved over the range of the integral. Substituting this alternative form into Eq. (4.2), the average BER becomes

$$P_b^{(1)}(\gamma) = \frac{2a}{\pi}\int_0^\infty\int_0^{\pi/2} e^{-bS\gamma\sec^2\theta}p(S)\,d\theta dS\,. \tag{4.6}$$

By interchanging the order of integration, and recognizing the integral with respect to S is equal to the MGF of the fading channel evaluated at $b\gamma\sec^2\theta$, Eq. (4.6) can be rewritten as

$$P_b^{(1)}(\gamma) = \frac{2a}{\pi}\int_0^{\pi/2} m\,[b\gamma\sec^2\theta]\,d\theta\,. \tag{4.7}$$

In general, a closed form expression for Eq. (4.7) cannot be obtained. However, if the

---

1. The complementary error function is defined as

$$\mathrm{erfc}\,(x) = 1-\mathrm{erf}\,(x) = 1-\frac{2}{\sqrt{\pi}}\int_0^x e^{-t^2}dt\,.$$

channel's MGF is of the form $m(z) = (1+za)^{-1}$, a closed form expression can be derived and if the MGF is of the more general form $m(z) = (1+za)^{-L}$, one can directly solve Eq. (4.1) to obtain a closed form expression. For both cases, closed form expressions are derived in Appendix B.

The second form in Table 4.1 is the exponential form. The general expression for the instantaneous BER is

$$P_b^{(2)}(\gamma|S) = ae^{-bS\gamma} \tag{4.8}$$

where again a and b are obtained from Table 4.1. Substituting Eq. (4.8) into Eq. (4.1) and interchanging the order of integration, the average BER can be written in terms of the MGF

$$\bar{P}_b^{(2)}(\gamma) = am(b\gamma) . \tag{4.9}$$

Thus, the average BER can be obtained for all the modulation schemes listed in Table 4.1 for all channels and diversity combinations by simply evaluating Eq. (4.7) and Eq. (4.9) with the appropriate channel MGF as derived in Chapter 3.

4.1.2 Coherent and Differential M-ary PSK

Coherent M-PSK maps each block of $k = \log_2 M$ bits to one of M unique symbols each separated by a phase offset equal to $2\pi/M$. Demodulation is performed by measuring the phase offset between the received signal and some fixed reference Eq. [26]. Figure 4.1 illustrates the signal constellation for the $M = 8$ case. For the (010) symbol, the transmitted signal has a phase offset (assuming the in-phase axis is the reference) equal to $3\pi/4$ and an amplitude of $\sqrt{E_s}$. If the phase offset of the received signal is within the decision region (independent of amplitude), then correct demodulation will occur.

Commonly, the instantaneous BER of coherent M-ary PSK is approximated by [26]

$$P_b(\gamma|S) \approx \frac{1}{\log_2 M}\text{erfc}\left(\sqrt{S\gamma\sin^2(\pi/M)}\right) \qquad M>2 \tag{4.10}$$

for which the average BER could be determined directly from Eq. (4.7) where $a = (\log_2 M)^{-1}$ and $b = \sin(\pi/M)$. However, this approximation becomes inaccurate for fading channels where the instantaneous SNR is small. Thus, an alternative solution is required.

When the received signal is perturbed by an instantaneous SNR equal to $S\gamma$, the CDF of the phase error θ (i.e. θ is the phase difference between the transmitted and received signal) is [29], [30]

$$\begin{aligned} F_{\text{PSK}}(\psi, \gamma|S) &= \text{Prob}\,[-\pi < \theta \leq \psi] \\ &= \frac{1}{2\pi}\int_{-\pi/2}^{\pi/2+\psi} e^{-S\gamma\sin^2\psi\sec^2\theta}d\theta \qquad \pi < \psi < 0 \end{aligned} \tag{4.11}$$

where S is the fading channel gain and γ is the SNR for the unfaded link. Averaging Eq. (4.11) over the PDF of the fading channel $p(S)$ (see Eq. (4.1)), and interchanging the order of integration, the average CDF of the phase error as a function of the channel MGF is obtained

$$F_{\text{PSK}}(\psi, \gamma) = \frac{1}{2\pi}\int_{-\pi/2}^{\pi/2+\psi} m\,[\gamma\sin^2\psi\sec^2\theta]\,d\theta\,. \tag{4.12}$$

With the possible exception of some channel types, a closed form expression for Eq. (4.12) is difficult or impossible to obtain. It is however well suited for numerical integration.

For non-coherent M-PSK, or simply differential M-PSK (M-DPSK), the *difference* between two successive M-ary symbols is mapped to one of M unique symbols.

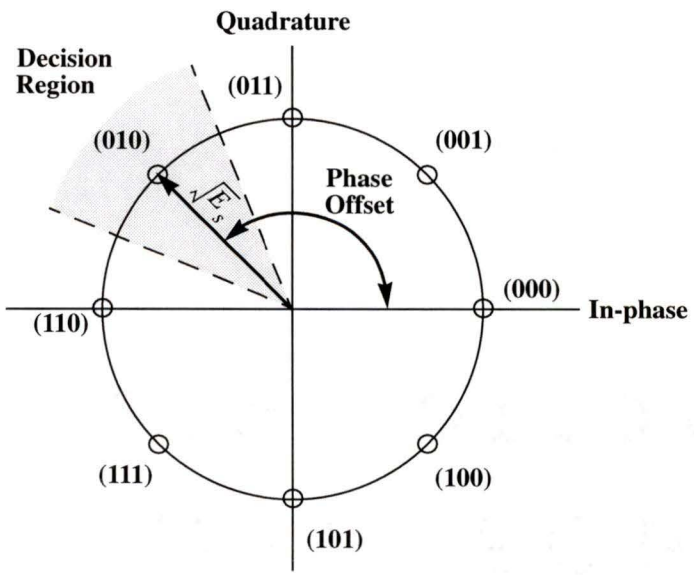

Figure 4.1 Signal constellation for 8-ary PSK with Grey coding.

Demodulation is performed by measuring the phase offset between successively received symbols. For an instantaneous SNR equal to $S\gamma$, the CDF of the phase error θ between the two successively received signals is [29], [30]

$$F_{\text{DPSK}}(\psi, \gamma|S) = \frac{-\sin\psi}{4\pi}\int_{-\pi/2}^{\pi/2} \frac{\exp\left[-S\gamma(1-\cos\psi\cos t)\right]}{1-\cos\psi\cos t}dt. \tag{4.13}$$

Averaging Eq. (4.13) over $p(S)$ and interchanging the integration order, the average CDF of θ in terms of the channel's MGF is

$$F_{\text{DPSK}}(\psi, \gamma) = \frac{-\sin\psi}{4\pi}\int_{-\pi/2}^{\pi/2} \frac{m\left[\gamma(1-\cos\psi\cos t)\right]}{1-\cos\psi\cos t}dt. \tag{4.14}$$

Again, for most channel models, a closed form expression of Eq. (4.14) is difficult or impossible to obtain, however it is well suited to numerical integration.

When demodulating M-PSK and M-DPSK, if the j-th symbol was transmitted, the $(i+j)$-th symbol is demodulated if the phase error θ falls within the range $-(2i+1)\pi/M$ and $-(2i-1)\pi/M$ (see Figure 4.1). The corresponding BER is the Hamming distance between the ith and jth symbol divided by the number of bits per symbol, where the Hamming distance is equal to the number of bit positions in which the two symbols differ. Therefore, assuming all symbols are transmitted with equal probability, the average BER is (exploiting symmetry about the j-th symbol — i.e. the probability of an error in the clockwise direction is equal to that in the counter-clockwise direction)

$$\begin{aligned}\bar{P}_b(\gamma) = \frac{2}{\log_2 M}\Bigg(&\sum_{i=1}^{M/2-1} d_i^{(M)}\,\text{Prob}\left[-\frac{(2i+1)\pi}{M} < \theta \le -\frac{(2i-1)\pi}{M}\right] \\ &+ d_{M/2}^{(M)}\,\text{Prob}\left[-\pi < \theta \le -\frac{(M-1)\pi}{M}\right]\Bigg)\end{aligned} \tag{4.15}$$

where $d_i^{(M)}$ is the Hamming distance between the i-th and j-th symbols averaged over all j. Assuming Grey code symbol mapping[2], the average Hamming distance can be found through simple iteration through all i and j averaged over j. Table 4.2 lists $d_i^{(M)}$ for symbol sizes of 2 to 6 bits long. From the definition of the CDF (see Eq. (2.1)), the

2. Grey code mapping assigns symbols to the signal constellation such that the Hamming distance between any two adjacent symbols is exactly one. Since adjacent symbol errors occur most frequently, this ensures that the number of bit errors is minimized for adjacent symbol errors. See Figure 4.1.

following property is evident: Prob $[\psi_1 < \theta \leq \psi_2] = F(\psi_2) - F(\psi_1)$. Applying this to Eq. (4.15), the desired expression for the average BER becomes

$$\bar{P}_b(\gamma) = \frac{2}{\log_2 M}\left[F\left(-\frac{\pi}{M}, \gamma\right) + \sum_{i=2}^{M/2} (d_i^{(M)} - d_{i-1}^{(M)}) F\left(-\frac{(2i-1)\pi}{M}, \gamma\right)\right] \tag{4.16}$$

where $F(\psi, \gamma)$ is given by Eq. (4.12) for M-PSK and by Eq. (4.14) for M-DPSK.

M	$d_i^{(M)}, i = 1, 2, \ldots, M/2$
4	$1, 2$
8	$1, 2, 2, 2$
16	$1, 2, 2, 2, \frac{5}{2}, 3, \frac{5}{2}, 2$
32	$1, 2, 2, 2, \frac{5}{2}, 3, \frac{5}{2}, 2, \frac{11}{4}, \frac{7}{2}, \frac{13}{4}, 3, \frac{13}{4}, \frac{7}{2}, \frac{11}{4}, 2$
64	$1, 2, 2, 2, \frac{5}{6}, 3, \frac{5}{2}, 2, \frac{11}{4}, \frac{7}{2}, \frac{13}{4}, 3, \frac{13}{4}, \frac{7}{2}, \frac{11}{4}, 2,$ $\frac{23}{8}, \frac{15}{4}, \frac{29}{8}, \frac{7}{2}, \frac{31}{8}, \frac{17}{4}, \frac{29}{8}, 3, \frac{29}{8}, \frac{17}{4}, \frac{31}{8}, \frac{7}{2}, \frac{29}{8}, \frac{15}{4}, \frac{23}{8}, 2$

Table 4.2 Average Hamming distance between symbols for Grey code.

4.2 Outage Probability

Often a more useful measure of transmission quality, the outage probability P_{out} indicates the percentage of the time that the instantaneous BER is above some acceptable threshold, ε. For voice data, the threshold may be as high as 10^{-2} to ensure toll quality speech. For data (uncoded) transmission, the threshold is about 10^{-4}. For video data, BER requirements can be even more stringent. Since the instantaneous BER $P_b(S)$ is a monotonically decreasing function of S, P_{out} can be written as

$$P_{out} = \text{Prob}[S < \hat{S}] = F(\hat{S}) \tag{4.17}$$

where $\hat{S}$ is the solution to $P_b(S) = \varepsilon$ and $F(S)$ is the CDF of the fading channel. Thus, given $\hat{S}$, the outage probability can be expressed in terms of the channel's CDF independent of channel type or diversity scheme employed.

4.2.1 Common Modulation Schemes

Compared to the M-ary PSK cases, the outage probabilities for the modulation schemes listed in Table 4.1 are easily derived. For the erfc (x) form, $\hat{S}$ is obtained by re-arranging Eq. (4.2) to get

$$\hat{S} = \frac{1}{b\gamma}\left[\text{erfc}^{(-1)}\left(\frac{\varepsilon}{a}\right)\right]^2 \tag{4.18}$$

where approximations to the inverse erfc function can be found in many mathematical references (see [18]). The outage probability is obtained by substituting $\hat{S}$ calculated from Eq. (4.18) into Eq. (4.17).

Similarly, for the exponential forms, $\hat{S}$ is obtained by re-arranging Eq. (4.8) to get

$$\hat{S} = -\frac{1}{b\gamma}\ln\left(\frac{\varepsilon}{a}\right). \tag{4.19}$$

Substituting $\hat{S}$ obtained from Eq. (4.19) into Eq. (4.17) results in the outage probability.

4.2.2 Coherent and Differential M-ary PSK

For both M-ary PSK and DPSK, no simple method for obtaining $\hat{S}$ exists. For both M-PSK and M-DPSK, $\hat{S}$ is the solution to

$$\frac{2}{\log_2 M}\left[F\left(-\frac{\pi}{M},\gamma\right) + \sum_{i=2}^{M/2}\left(d_i^{(M)} - d_{i-1}^{(M)}\right)F\left(-\frac{(2i-1)\pi}{M},\gamma\right)\right] = \varepsilon \tag{4.20}$$

where $F(\psi,\gamma)$ for M-PSK is given by Eq. (4.11) with $\hat{S}$ replacing S and $F(\psi,\gamma)$ for M-DPSK is given by Eq. (4.13) where again, $\hat{S}$ replaces S. Since the BER is monotonically decreasing, the solution to Eq. (4.20) is not too difficult to find. Once $\hat{S}$ is found, the outage probability can be obtained directly from Eq. (4.17).

4.3 Numerical Results

In the previous developments, equations for the average BER and outage probability are found for several common modulation schemes as well as for M-ary PSK and DPSK. These equations are general in the sense that they are expressed in terms of either the channel's MGF or CDF. In Chapter 2, the MGFs and CDFs are derived for the lognormally shadowed Rician channel and for the time-shared Rician and lognormally shadowed Rayleigh channel. In Chapter 3, these are extended for the composite micro- and

macro-scopic diversity systems where either SDC or MRC diversity were employed for micro-diversity. Needless to say, a detailed analysis of all these variations is beyond the scope of this thesis. Rather, a detailed analysis of micro-diversity for the satellite channel is provided as an example.

These results are based on a per branch E_b/N_0 (i.e. on average, MRC with L branches has L times more signal energy than a single channel). Where Hermitian or Laguerre approximations to integration are performed, orders of 20 and 15, respectively are used. For other integrations, a routine which successively doubles the number of integration points is used to obtain a relative accuracy greater than 1×10^{-6}. When finding the solution to Eq. (4.20), the bisection root-finding method is employed to obtain $\hat{S}$ with a relative accuracy of 1×10^{-6}. The parameters for the satellite channel model are read from Table 2.1.

4.3.1 Average Bit Error Rate

Figure 4.2 illustrates the average BER of M-ary PSK for $M = \{2, 4, 8, 16, 32\}$ in the shadowed and un-shadowed Munich city environment. At an average BER of 10^{-2}, typical of voice communications, the performance when shadowed (i.e. $A = 1$) is about 16 dB worse than when un-shadowed ($A = 0$). Furthermore, increasing the symbol size beyond two bits (i.e. $M = 4$) degrades the BER performance from 2 to 4 dB. To achieve an average BER of 10^{-2}, a SNR of $\{6.3, 9.0, 13.0, 17.4\}$ dB in the un-shadowed environment and a SNR of $\{23.8, 25.5, 29.4, 32.8\}$ dB in the shadowed environment is required for $M = \{4, 8, 16, 32\}$, respectively. As expected, the performance of DPSK (not shown) was found to be worse than that of PSK. Thus, to achieve a desired BER at a reasonable SNR, some method of improving the performance is required. Micro-diversity is one such method.

For M-ary PSK, the improvement in BER when MRC micro-diversity is employed is shown in Figure 4.3 for the Munich city environment. Note the significant improvement in BER due to micro-diversity. For example, at a BER of 10^{-2}, a SNR gain of $\{7.1, 13.1\}$ dB can be achieved using $L = \{2, 5\}$ branch MRC diversity over no diversity (relatively independent of M). Note that the penalty for increasing the constellation size above that of BPSK or QPSK is about $\{2.3, 5.8\}$ dB (relatively independent of L) for $M = \{8, 16\}$. Thus, by employing two branch MRC, the BER performance of 16-ary PSK surpasses that of BPSK or QPSK without diversity.

Figure 4.4 shows the average BER for differentially detected QPSK (i.e. $M = 4$) with both MRC and SDC micro-diversity in the Munich city fading environment. Comparing the diversity cases to the non-diversity case, we see that a significant increase in BER performance can be achieved through diversity, particularly for MRC. For an average BER of 10^{-2}, a SNR improvement of $\{6.2, 8.3, 9.4\}$ dB for SDC and $\{7.6, 10.7, 12.5\}$ dB for MRC can be achieved over the non-diversity case for $L = \{2, 3, 4\}$, respectively. Note that as the number of branches increases, the incremental savings in SNR decreases. The BER curves for $L = 20$ illustrates this, and further emphasizes the advantage of MRC over SDC.

The average BER for binary DPSK with MRC diversity for 2 and 3 branches is shown in Figure 4.5 for the city and highway environment around Munich. Of interest is the declining dependence on the fading environment as the diversity order increases. At a BER of 10^{-2}, the difference in SNR between the city and highway environments is $\{7.8, 5.5, 4.8\}$ dB for $L = \{1, 2, 3\}$ respectively. This effect is even more pronounced at a BER of 10^{-4} where the difference in SNR between the two environments is $\{6.7, 2.6, 1.3\}$ dB for $L = \{1, 2, 3\}$. For satellite systems where a single transmitter serves multiple environments, increasing the diversity order will reduce the excess signal power when the mobile is in a favorable environment.

Finally, Figure 4.6 illustrates the average BER for DPSK with diversity in the city environment as a function of the elevation angle for a SNR of 20 dB. As anticipated, the BER decreases as the elevation angle increases due to the decrease in shadowing effects. Besides improving the BER performance, the diversity techniques do not mitigate the elevation angle effects. This is anticipated since the elevation angle affects primarily the degree of shadowing which cannot be combatted with micro-diversity techniques. The shallow slope of the curves is advantageous, as it implies a certain degree of elevation independence for the mobile user.

4.3.2 Outage Probability

The outage probability for the Munich city environment for M-ary PSK with and without diversity is shown in Figure 4.7. A fixed SNR of 15 dB is assumed. This figure illustrates the significant improvement in coverage which can be achieved through the use of diversity techniques. For example, at a BER of 10^{-2}, $L = 5$ branch MRC diversity increases the average time that the signal is acceptable by $\{3300, 1200, 300\}$ percent for $M = \{2 \text{ or } 4, 8, 16\}$ PSK. Although not shown, $L = 2$ branch MRC improves the

coverage of $M = \{2 \text{ or } 4, 8, 16\}$ PSK by $\{80, 180, 250\}$ percent, respectively.

Figure 4.8 illustrates the outage probability for DPSK with MRC micro-diversity $L = \{1, 2, 3\}$ for the city and highway environments around Munich. The effect of shadowing in the city environment is readily seen. Again, micro-diversity provides a significant decrease in outage.

Finally, Figure 4.9 shows the outage probability for M-ary PSK in the Munich city environment where $\varepsilon = 10^{-2}$ is fixed and the SNR γ is the variable. The distinct elbow for the 5 branch MRC case is explained as follows. At low SNR, $P_{\text{out}} \to 1$ for both channel states. However as the SNR increases, $P_{\text{out}}^{\text{Rice}} \to 0$ much quicker than $P_{\text{out}}^{\text{Suzuki}}$. For our case $P_{\text{out}}^{\text{Suzuki}}$ is still very close to unity when $P_{\text{out}}^{\text{Rice}}$ approaches zero and thus the elbow occurs at $A = 0.7$ (see Eq. (2.24)). From this figure, we see that if we require the BER to exceed 10^{-2} at least 90% of the time, then for the non-diversity case we require a SNR of about $\{22, 25, 29\}$ dB for $M = \{2 \text{ or } 4, 8, 16\}$ PSK and for the $L = 5$ MRC diversity case we require a SNR of about $\{10, 13, 17\}$ dB for $M = \{2 \text{ or } 4, 8, 16\}$ PSK.

4.3.3 Summary

Using the measured parameters for the satellite channel presented in [13], BER and outage probability curves are plotted for various channel environments. Without diversity reception, the BER performance of M-ary PSK for $M > 4$ is sufficiently poor that the more bandwidth efficient modulation schemes can not be utilized. However, it is shown that diversity reception (especially MRC) provided significant improvements in both the BER and outage probability. In fact, using 2-branch MRC diversity, 16-ary PSK outperforms BPSK without diversity. Furthermore, increasing the number of diversity branches reduces the dependency of the BER and outage probability on the fading environment. Finally, the elevation angle is found to have little effect on the BER performance.

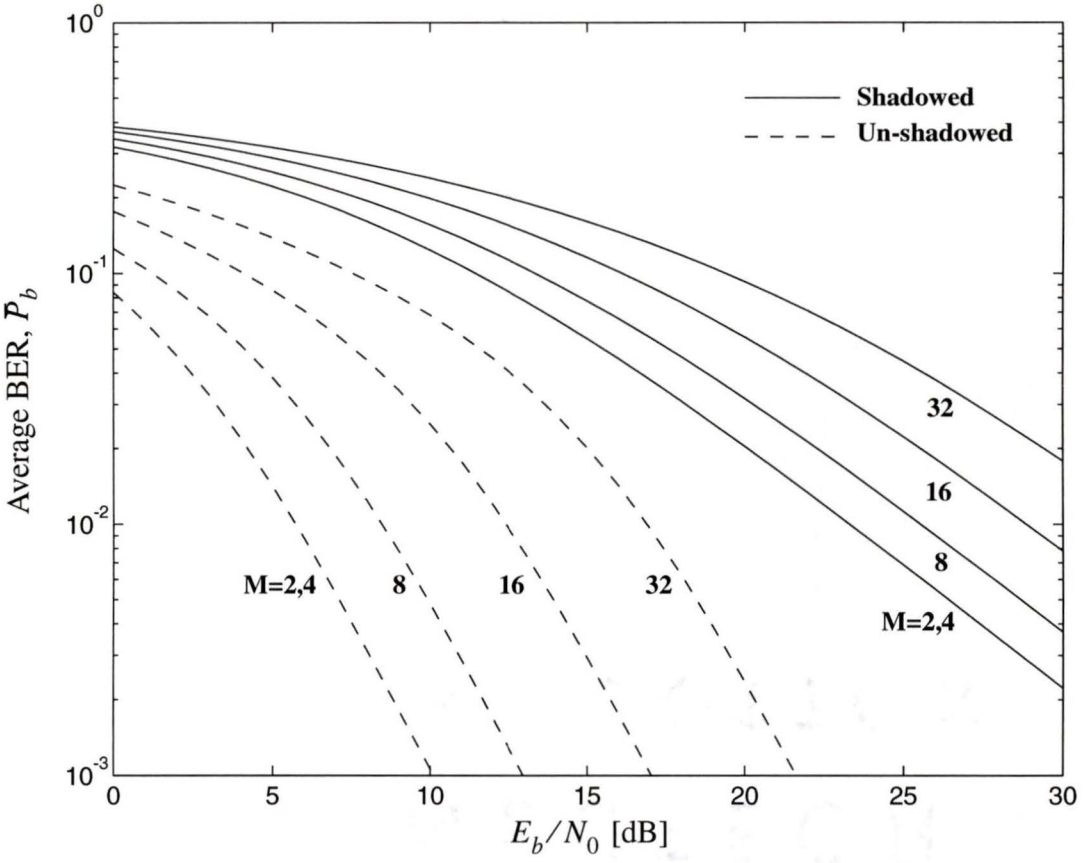

Figure 4.2 Average bit error rate of M-ary PSK ($M = \{2, 4, 8, 16, 32\}$) in the shadowed and un-shadowed Munich city environment.

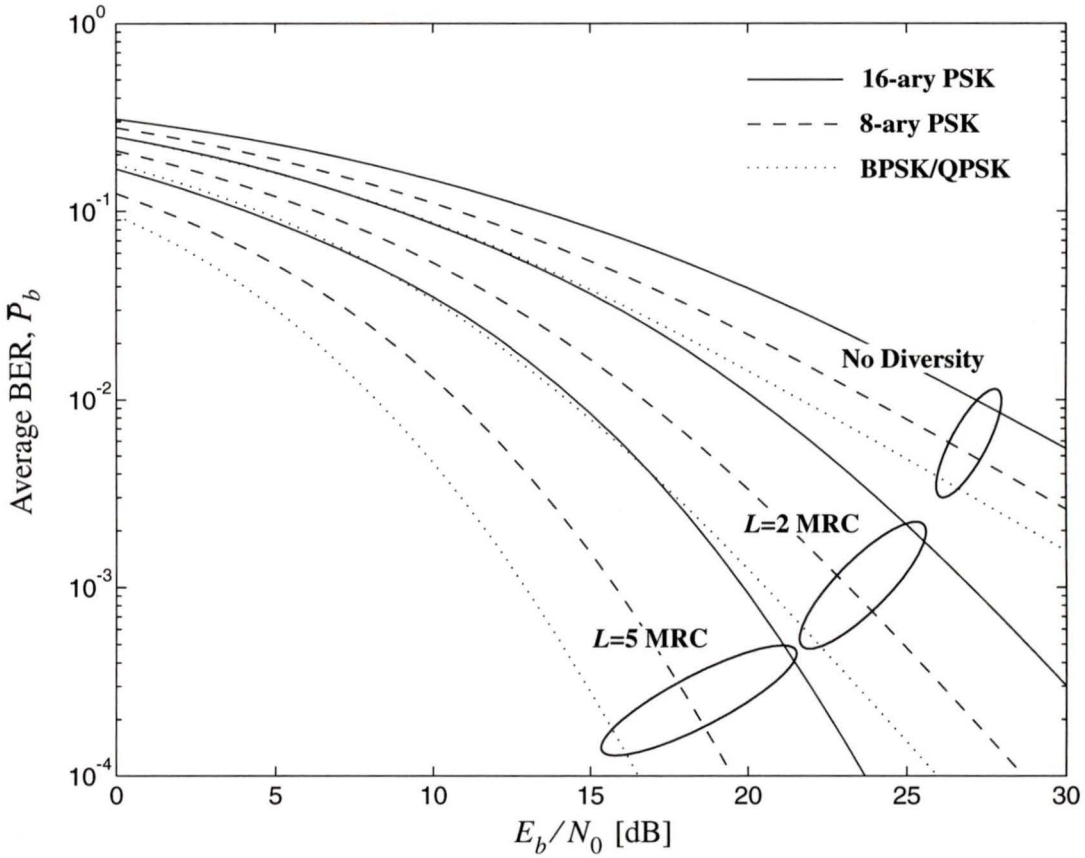

Figure 4.3 Average bit error rate of M-ary PSK ($M = \{2, 4, 8, 16\}$) with MRC micro-diversity ($L = \{1, 2, 5\}$) in the Munich city environment.

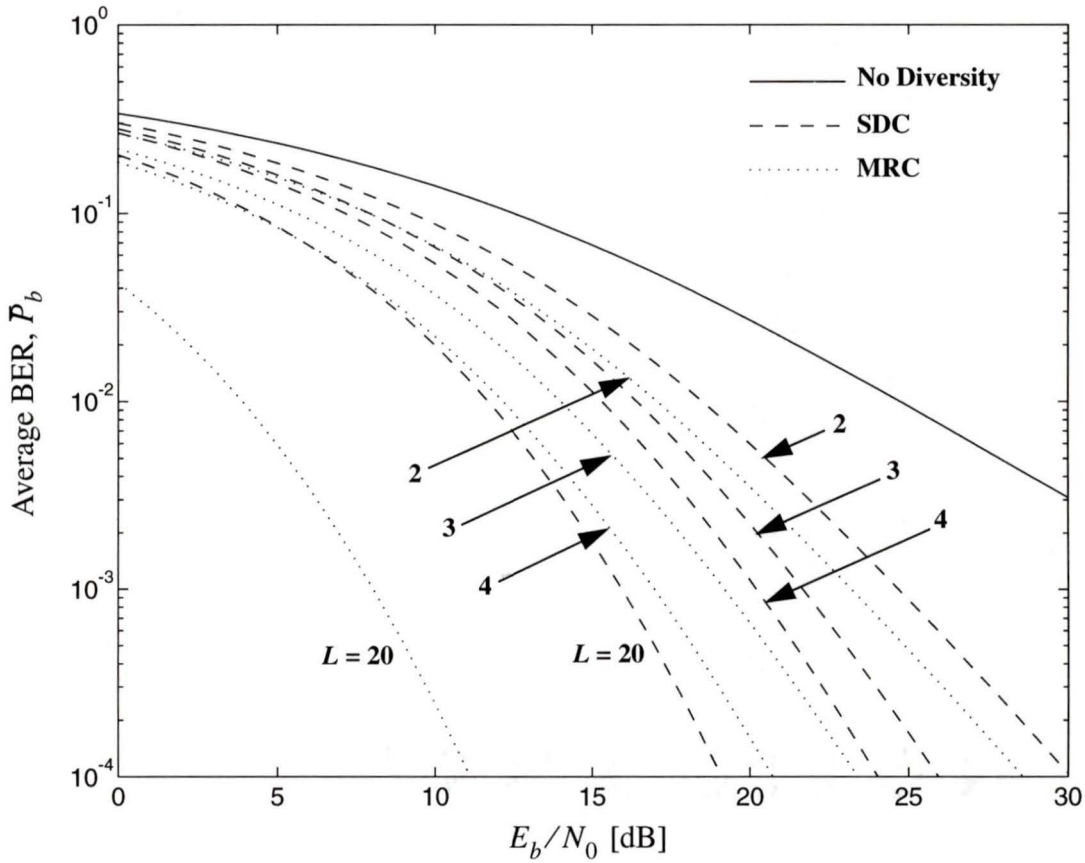

Figure 4.4 Average bit error rate of 4-ary DPSK (differential QPSK) with L-branch micro-diversity in the Munich city environment.

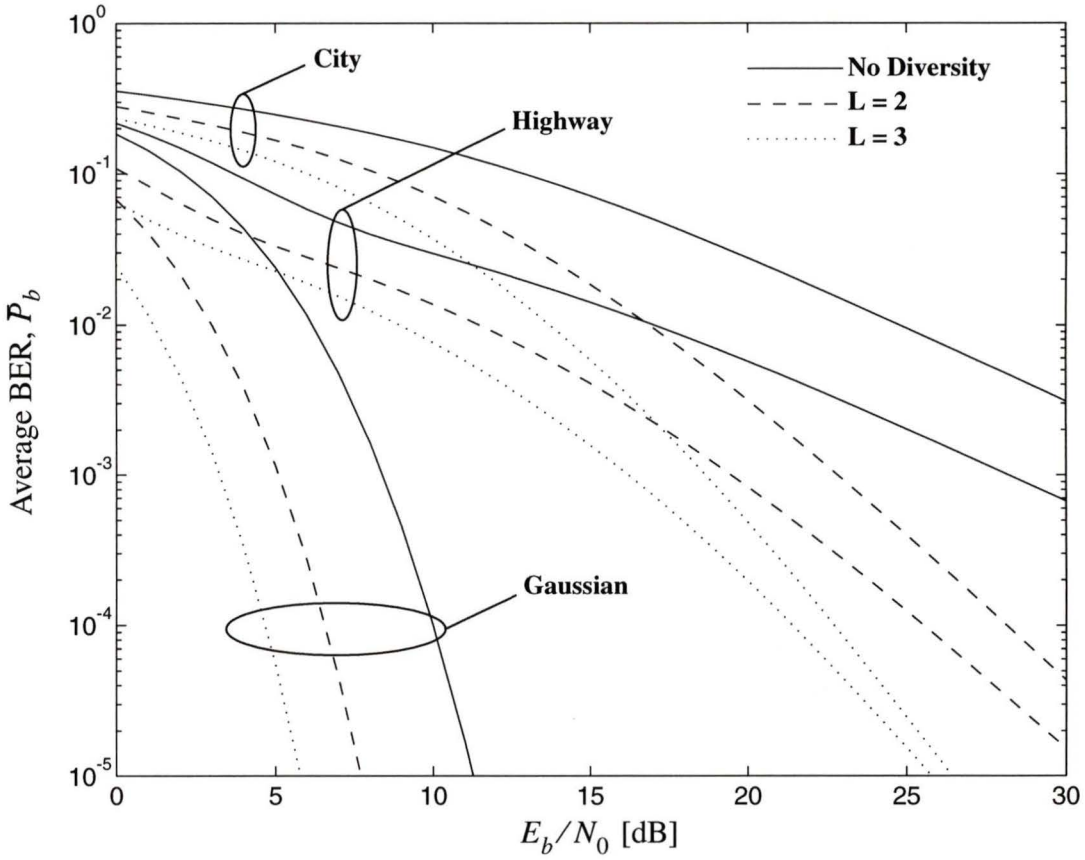

Figure 4.5 Average bit error rate of binary DPSK with and without micro-diversity in the city and highway environments around Munich. Performance of the Gaussian channel is provided for comparison.

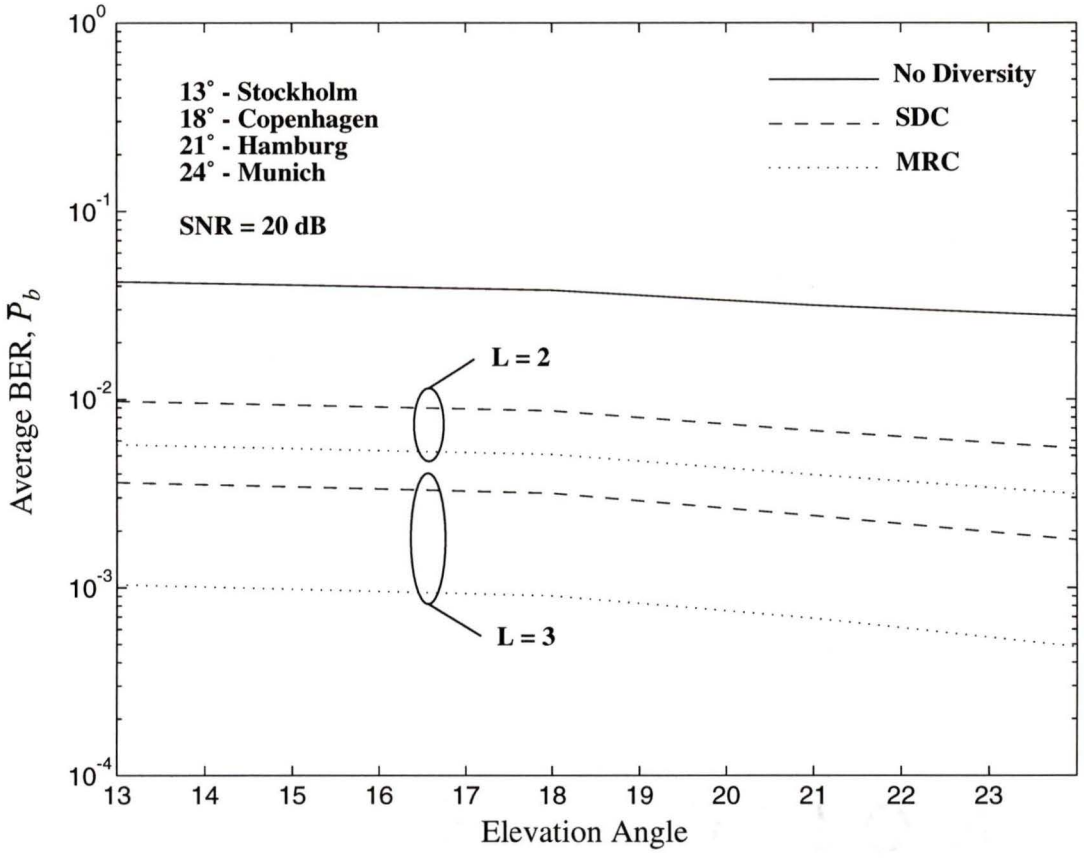

Figure 4.6 Average bit error rate of binary DPSK with micro-diversity in the city environment as a function of the elevation angle for a fixed SNR of 20 dB.

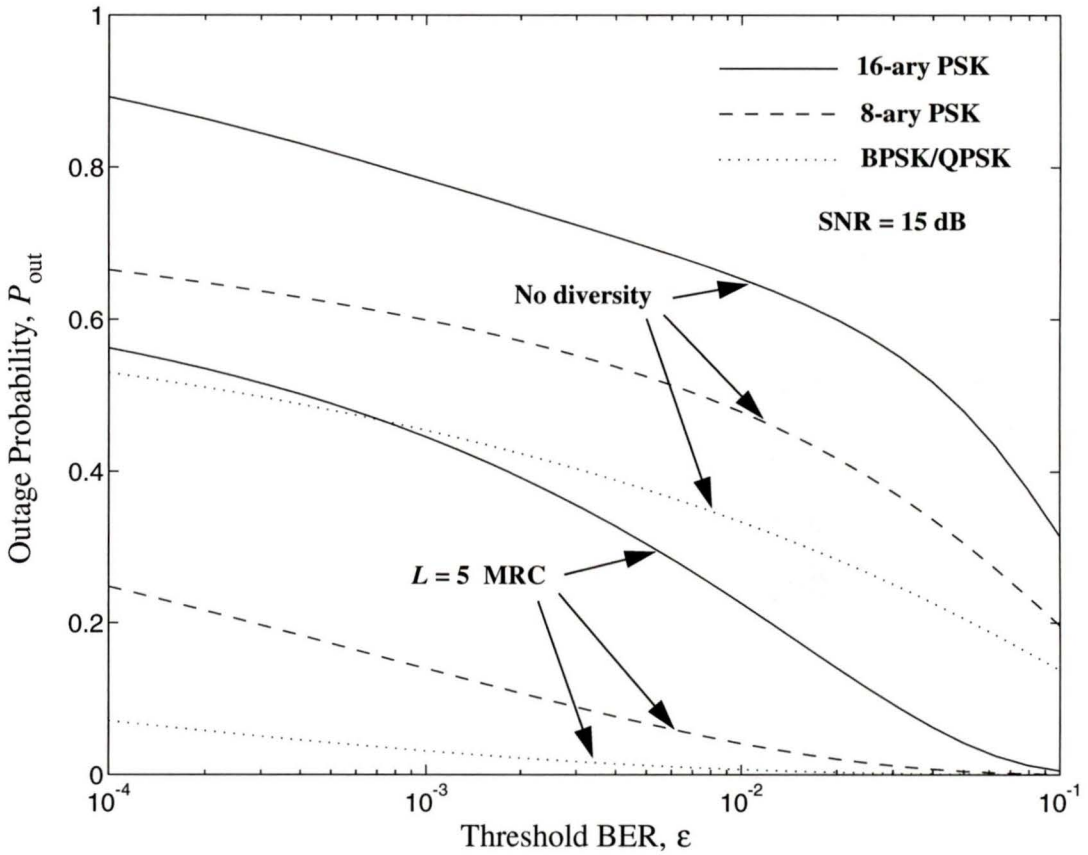

Figure 4.7 Outage probability for M-ary PSK ($M = \{2, 4, 8, 16\}$) with MRC micro-diversity ($L = \{1, 5\}$) in the Munich city environment.

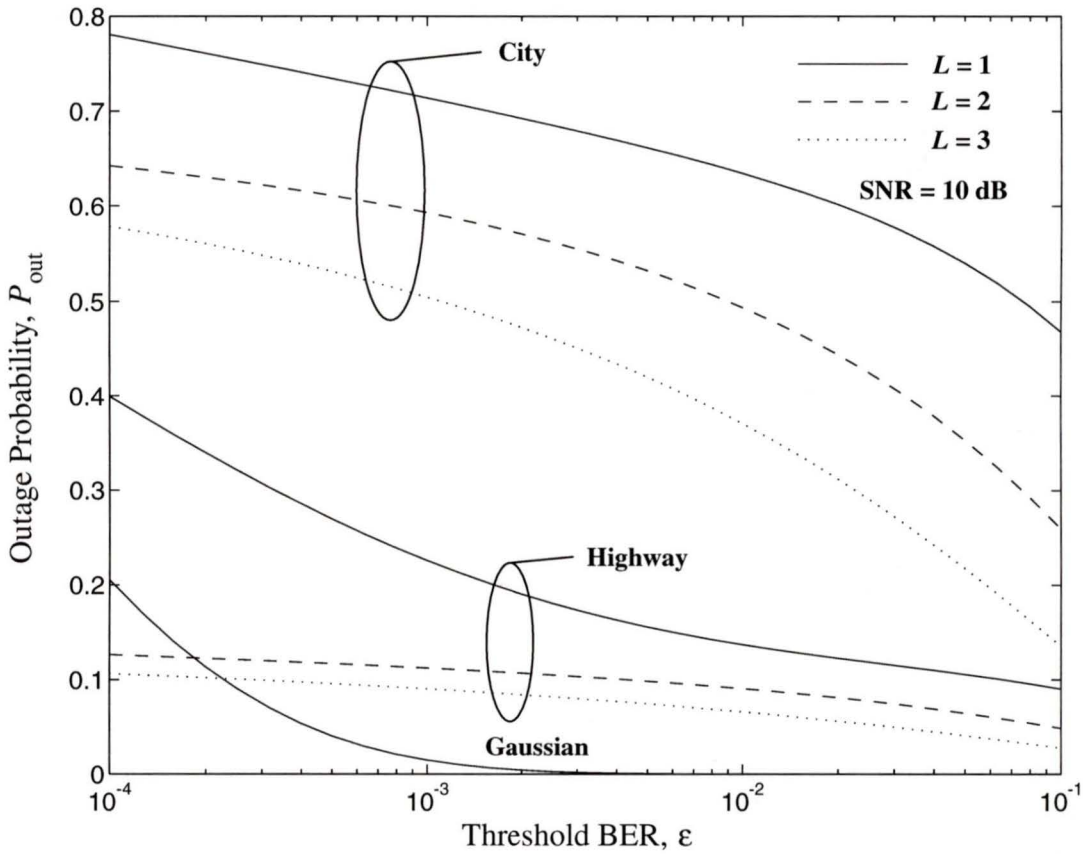

Figure 4.8 Outage probability for DPSK with MRC micro-diversity ($L = \{1, 2, 3\}$) for the city and highway environments around Munich. The performance of Gaussian (without diversity) is provided for comparison.

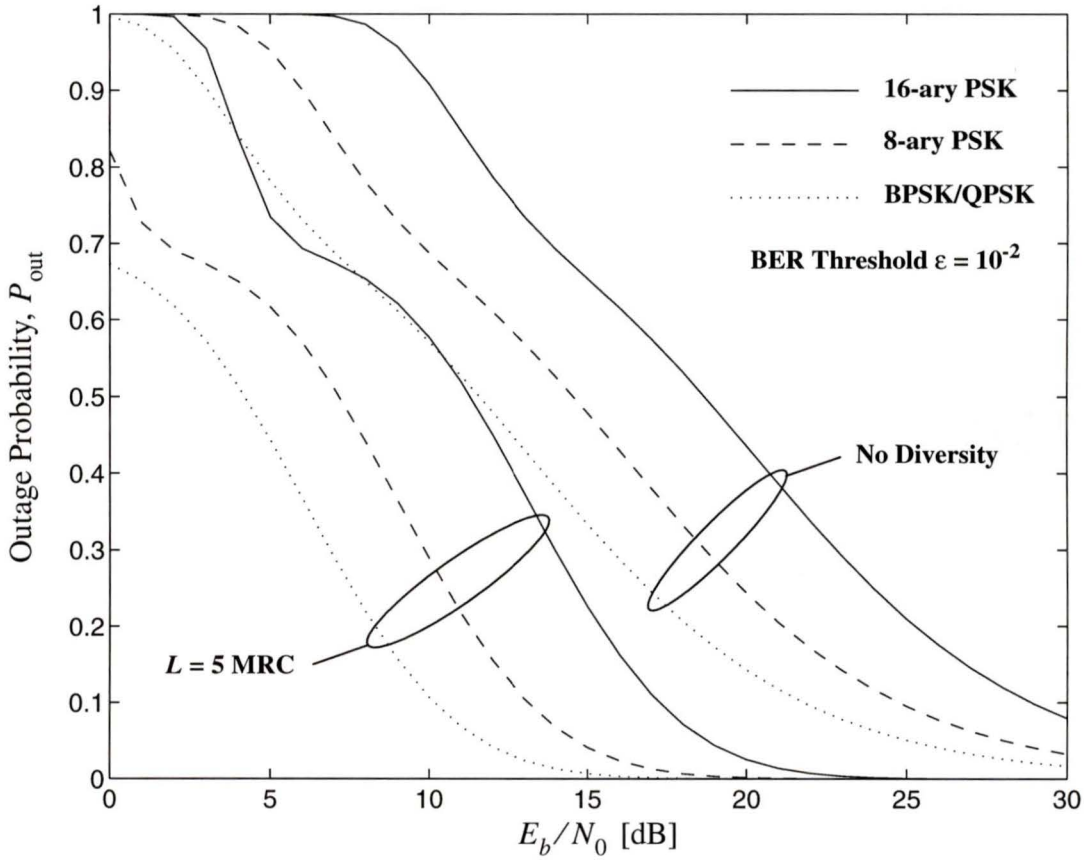

Figure 4.9 Outage probability for M-ary PSK with and without $L = 5$ branch MRC micro-diversity for Munich city as a function of the SNR. The threshold BER ε is fixed to 10^{-2}.

Chapter 5

Adaptive Error Control Coding

A second technique for combating fading in a time correlated channel is adaptive error control coding. Error control coding (ECC) is used to combat the effects of noise and interference by detecting and correcting errors introduced by a noisy channel. This is performed by the systematic addition of coding overhead. As coding overhead reduces data throughput and increases interference to other users, the goal of the code designer is to minimize the amount of coding overhead employed while still maintaining the integrity of the data. Defining the code rate as the ratio of information symbols to total symbols transmitted, a rate adaptive code adjusts the amount of coding overhead transmitted in order to compensate for changing data integrity requirements and channel conditions.

Several motivations exist for adaptive coding schemes. In systems with fixed code rates, the amount of coding overhead is selected such that, when transmitting in the worst channel conditions (or when transmitting the most error sensitive data), the error control code is still capable of providing the required quality of service. This amount of overhead however, proves wasteful during periods where the channel is not in its worst state. An adaptive scheme eliminates this waste by providing only the overhead required for the prevailing data requirements and channel conditions. An alternative for fixed rate codes is to reduce the coding overhead at the cost of outages where the transmission quality is less than what is required. Again, adaptive error control compensates to the channel and thus ensures outages occur less frequently. Finally, the adaptive error control code provides greater flexibility for mobile subscriber by allowing them to select the grade of service desired and thus be billed accordingly.

In this chapter, a very powerful, flexible and highly adaptive error control scheme is presented. Leading up to this, the required background theory in error control coding is provided. A more thorough discussion may be found in most introductory texts on error

control coding (i.e. see [33], [34]).

Several constraints are placed on the code design [37]. In order to maintain compatibility with the proposed asynchronous transfer mode (ATM) and the proposed integrated wireless access network (IWAN) [35], [36], the code must operate on data packets rather than on a continuous data stream. Secondly, the code must provide a wide range of bit error rates (from 10^{-2} for voice down to 10^{-9} for data) and must account for various delay requirements. Furthermore, the encoder and decoder must be designed independent of data type thus allowing a single encoder/decoder pair to service all data types. Another requirement dictates that the code adapts in real-time and with minimal delay to ensure its effectiveness in fading channels. Finally, reasonable implementation complexity is required.

The two primary strategies for error control coding are forward error correction (FEC) and automatic repeat request (ARQ). FEC attempts to detect, locate and correct errors in a received message. ARQ attempts to detect errors and, if present, ARQ requests a re-transmission. To capitalize on the advantages of each, FEC and ARQ can be combined to form a third strategy, hybrid ARQ (HARQ). The proposed code uses HARQ.

A block diagram of the communication system is shown in Figure 5.1. The ECC encoder divides the incoming data sequence from the data source into message blocks of k information symbols each, where a symbol can assume any value from a finite set of discrete values[1]. The encoder transforms each message into a code word of n discrete symbols, where $n \geq k$. This encoded word is passed to the modulator and transmitted over the noisy channel. At the receiver, the unreliable word is demodulated and passed to the ECC decoder. If the demodulated word contains errors, the ECC decoder attempts to detect and correct these errors before passing the decoded message to the data sink.

The proposed code consists of a rate adaptive concatenated FEC code combined with type-II HARQ and code combining. The individual components of the code will be described first followed by a description of the complete adaptive code.

1. For example, a bit is a symbol from a finite set with 2 possible discrete values, 0 or 1.

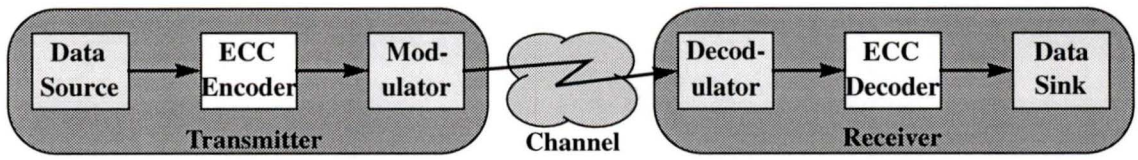

Figure 5.1 Block diagram of communication system under study.

5.1 Concatenated FEC Code

A rate adaptive concatenated code is suggested for FEC. The inner code is a punctured convolutional code and the outer code is a punctured Reed-Solomon code. These two codes have been selected for several reasons. Both are excellent burst error correction codes (a requirement for the fading channel dominated by bursty errors). Furthermore, the maximum distance separability property of the Reed-Solomon code and the utilization of the maximum likelihood Viterbi decoder ensures that both codes provide optimum error correction. In addition, as both convolutional and Reed-Solomon codes have been applied extensively[2], implementation is not of significant concern. Finally, very little additional complexity is required to make these codes adaptive.

5.1.1 Punctured Convolutional Code

Convolutional codes form one class of FEC codes and are distinguished from other codes by the historical information encoded into each code word. For each k-bit input block, the (n, k, m) convolutional code produces one n-bit code word which is a linear combination of the present input block and the previous m input blocks. The ratio of input bits to output bits is defined as the code rate, $r = k/n$. Another useful definition, the constraint length is defined as $K = m + 1$ and represents the number of input blocks required to produce one code word [33], [34]. Thus, the (n, k, m) convolutional code can be equivalently described as a rate k/n, constraint length K convolutional code.

Of special interest here is the rate $1/2$, constraint length K, $3 < K < 9$, convolutional code from which all other codes are generated through puncturing. Figure 5.2a illustrates the encoder for the rate $1/2$, constraint length 3 code. The generator

2. Convolutional codes are commonly applied to deep-space, satellite and digital wireless communications. Reed-Solomon codes are commonly used in deep-space communications and in compact disc storage.

sequences for this code are, in octal notation, $\{5, 7\}$ [3]. The corresponding trellis diagram, shown in Figure 5.2b, traces a path through the encoder states for all possible input sequences of length D bits and provides the corresponding output bits. After all D bits have been input, an additional $K-1 = 2$ input zeros are required to return the trellis to the zero state (required for decoding). Given the generator sequences of the other constraint length codes of interest (see Table 5.1), the corresponding encoder and trellis diagrams can be derived.

Constraint Length, K						
3	**4**	**5**	**6**	**7**	**8**	**9**
$\{5, 7\}$	$\{15, 17\}$	$\{23, 35\}$	$\{53, 75\}$	$\{133, 171\}$	$\{247, 371\}$	$\{561, 753\}$

Table 5.1 Generator sequences of the best rate $1/2$ convolutional codes (octal) [34].

Puncturing is one technique by which the code rate (and thus error correction capability) of a code can be modified. After encoding using a standard code[4], the puncturing operation deletes selected bit coordinates from the output code word prior to transmission, thus resulting in a partial loss of information. After transmission and prior to decoding, dummy bits are inserted into the previously punctured bit coordinates. Decoding is performed using the standard decoder which attempts to restore the punctured information as well as correct any errors induced by the noisy channel.

In [38] [39], the puncture maps for a rate $(n-1)/n$ punctured convolutional code $(2 < n < 17)$ based on the best rate $1/2$ codes have been found through computer search. These are listed in Table 5.2 for constraint length 7 codes (a complete list for $3 \le K \le 9$ can be found in [39]). Figure 5.3 illustrates the puncturing operation for a rate $5/6$ convolutional code. Using the standard rate $1/2$ encoder, five data bits are encoded to produce ten output bits. Four bits are deleted and the resultant six bit code word is transmitted. At the receiver, dummy bits (zeros) are inserted in the deleted bit coordinates to once again obtain a ten bit code word which can be decoded with the rate $1/2$ decoder. The decoder outputs the decoded five bit message.

---

3. Derived from the convolutional encoder where the feedforward taps are represented as '0' for no connection and '1' for connection.

4. Here, a standard code refers to a non-punctured code rather than a code set through standardization.

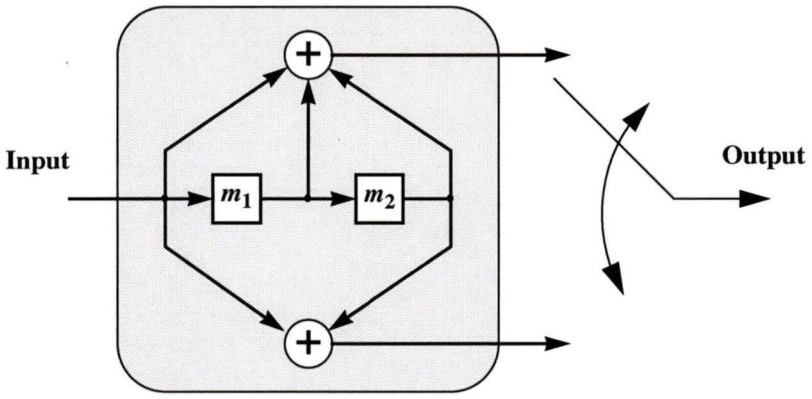

(a) Rate 1/2, constraint length 3, convolutional encoder

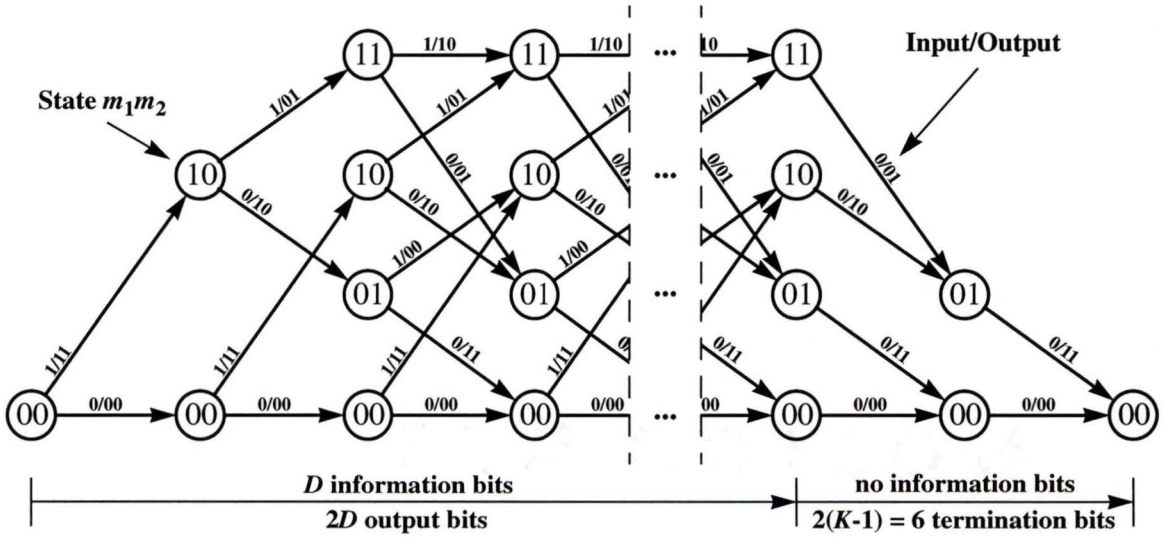

(b) Corresponding trellis diagram

Figure 5.2 Rate 1/2 convolutional encoder and trellis diagram.

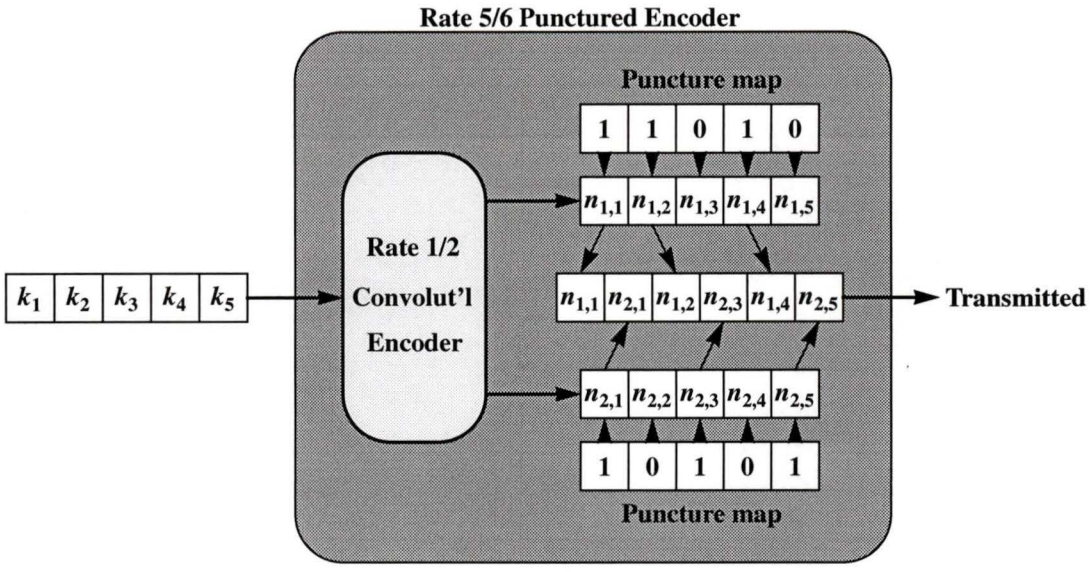

(a) Encoder

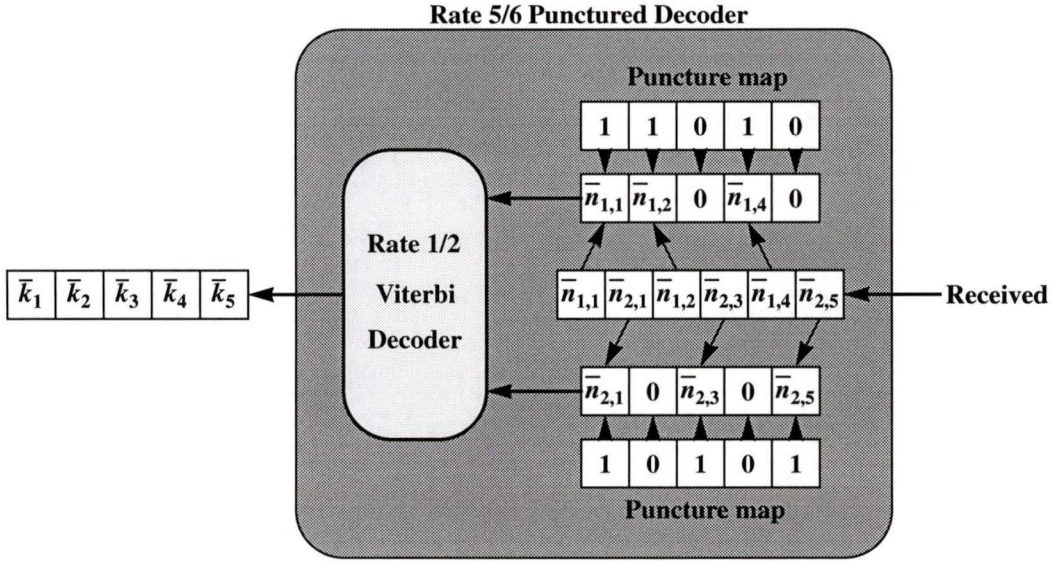

(b) Decoder

Figure 5.3 Rate 5/6, $K = 7$, punctured convolutional encoder and decoder.

Code	Deleting Map[a]	Code	Deleting Map
1/2	(1, 1)	9/10	(756, 421)
2/3	(3, 2)	10/11	(1667, 1110)
3/4	(6, 5)	11/12	(3676, 2101)
4/5	(17, 10)	12/13	(7765, 1012)
5/6	(32, 25)	13/14	(15017, 12760)
6/7	(72, 45)	14/15	(32666, 25111)
7/8	(172, 105)	15/16	(71322, 46455)
8/9	(354, 213)	16/17	(152205, 125572)

Table 5.2 Puncture maps for rate $(n\text{-}1)/n$, constraint length 7 convolutional codes [39].

a. In octal notation, where '0' indicates deleting bit position.

Decoding is performed using a rate $1/2$ Viterbi decoder. Based on the trellis diagram (see Figure 5.2), the Viterbi decoder compares the received code word with every possible path through the trellis and selects that path which is most likely to be correct (i.e. that path which differs the least from the transmitted path). This is performed by assigning a metric to each branch for all paths indicating the degree of similarity between the received code word and the output at that branch. Summing the metrics of all branches in each possible path through the trellis, the path with the greatest total metric is selected as the most probable path.

The demodulator assigns bit metrics to each received bit. For hard-decision decoding, the metrics are simply -1 if a '0' is demodulated or $+1$ if a '1' is demodulated. For punctured bits, the neutral value 0 is assigned. A significant gain in performance (upwards of 2 dB in signal power [33]) can be achieved if, besides indicating if a '0' or '1' is demodulated, additional bits are used to indicate the level of confidence in the bit decision. This is referred to as soft-decision decoding and is illustrated in Figure 5.4 for 3-bit quantization. Each branch metric is computed by summing the bit metrics corresponding to each of the branch's output bits. For example, if $\{001, 011\}$ is received, the metric for the branch with output, say $\{1, 0\}$, would be $-3 + 7 = 4$.

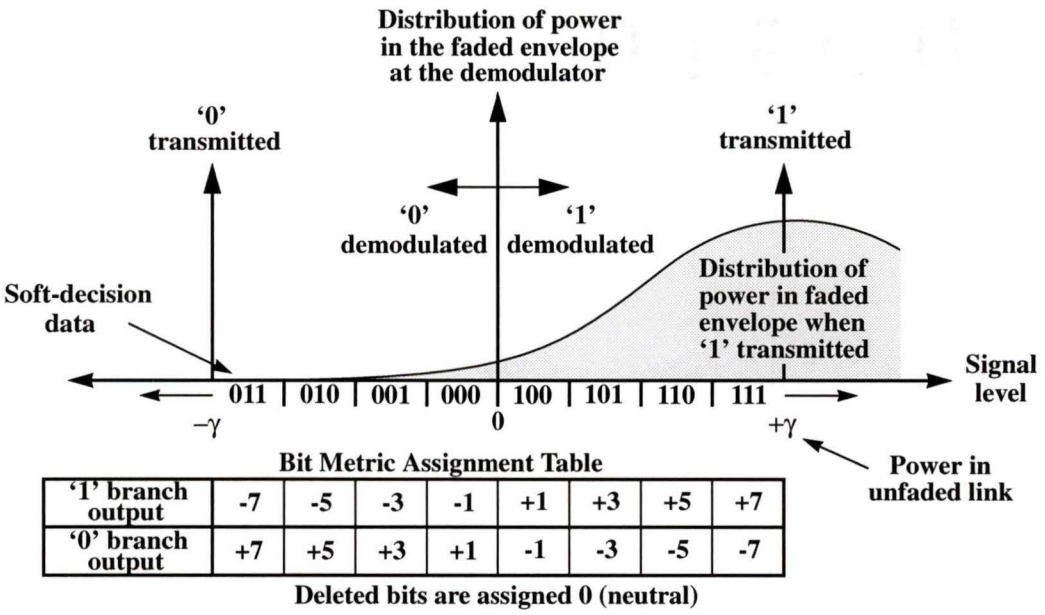

Figure 5.4 Metric assignment for 3-bit quantization.

5.1.2 Punctured Reed-Solomon code

Reed-Solomon codes belong to the class of codes referred to as linear block codes and, unlike the convolutional codes, do not have memory. For the general (n, k) linear block code, each unique k-symbol input block is mapped to one unique n-symbol code word. Reed-Solomon codes are distinguished from other block codes by the method in which these code words are assigned (refer to [33]).

The minimum number of symbols by which *any* two code words differ is defined as the minimum Hamming distance of the code, $d_{\min}$. For linear block codes, $d_{\min}$ is upper bounded by the Singleton bound:

$$d_{\min} \leq n - k + 1 . \tag{5.1}$$

Those codes achieving equality in Eq (5.1) are optimal in the sense that they provide "maximum distance" between code words and are thus referred to as maximum distance separable (MDS) codes. Reed-Solomon codes are MDS codes.

At the decoder, error correction is performed by replacing each received word with the code word which differs by the least number of symbols. For any linear block code,

the maximum number of symbol errors which are guaranteed correctable is [33]

$$t = \left\lfloor \frac{d_{min} - 1}{2} \right\rfloor \tag{5.2}$$

where $\lfloor x \rfloor$ denotes the largest integer not exceeding x. This is intuitive since for any number of errors less than or equal to t, the received word is closest in Hamming distance to the correct word according to the definition of $d_{\min}$.

The basic parameters of Reed-Solomon codes are defined as follows [33]:

$$\begin{aligned} n &= 2^m - 1 \\ n - k &= 2t \end{aligned} \tag{5.3}$$

where $m \geq 3$ is the number of bits per symbol. To maintain compatibility with the proposed ATM packet-based protocol, the value $k = 53$ is assumed.

Consider now the $(255, k)$ Reed-Solomon code with byte sized (8 bit) symbols. Through puncturing, this code can be modified to obtain a generalized $(n', 53)$ code with byte sized symbols where $255 \leq n' \leq 53$. The puncturing operation is performed by deleting $255 - n'$ symbol coordinates from the $(255, 53)$ code. Notice that by removing one symbol from the code, the minimum distance of the code can be reduced by at most one. Thus, according to Eq (5.1), the resulting set of punctured code words must also be MDS [45]. This property holds true for all punctured Reed-Solomon codes regardless of symbol size.

5.1.3 Concatenated Code

The method of concatenating two shorter codes to form a longer (and thus more powerful) code was first proposed by Forney [46] as a means of avoiding the complexity typically required in the implementation of single long codes.

A block diagram of the concatenated code is shown in Figure 5.5. Since the convolutional code with maximum likelihood Viterbi decoding makes the best possible estimate of the transmitted message, it is used as the inner code. Since the Reed-Solomon code is only effective when the noise is below some threshold (which ensures the number of errors is less than one-half the code's minimum distance), it is used as the outer code. A second motivation for this pair of concatenated codes is that an inner convolutional code may re-shape the random channel errors to bursty channel errors suitable for symbol cor-

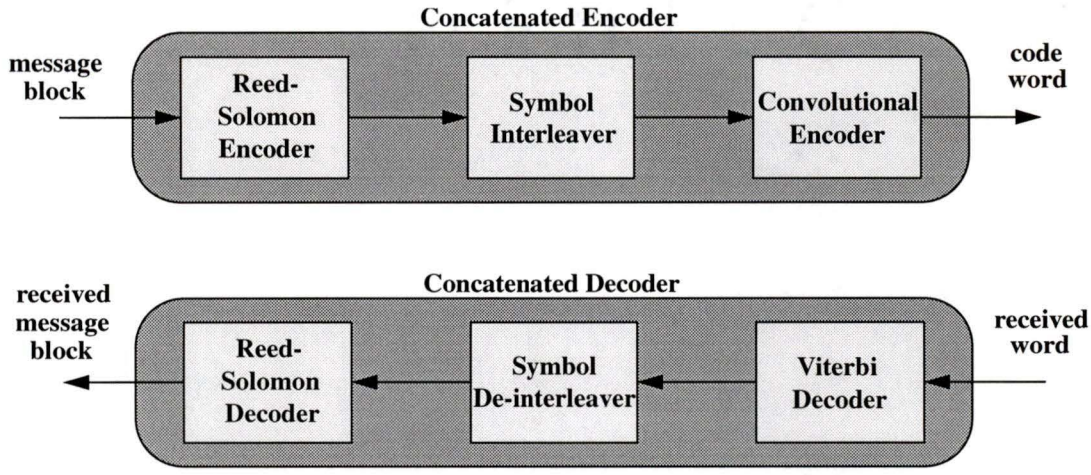

Figure 5.5 Block diagram of the concatenated code.

recting Reed-Solomon codes. Thus, the convolutional code performs an initial attempt at error correction by correcting some or all of the errors and the Reed-Solomon code attempts to correct any of the remaining errors.

Due to the bursty nature of errors from the output of the Viterbi decoder, interleaving between the two codes is required [41][42]. Interleaving reduces the correlation between adjacent symbols through time diversity. At the encoder, the interleaver arranges the incoming symbols into λ rows and reads them out in columns. The effect of this operation is to separate previously adjacent symbol coordinates by λ positions. Thus, during transmission, an error burst does not destroy adjacent code symbols but rather spreads these errors across multiple code words [43]. Prior to decoding, de-interleaving restores the original order of the code words.

Using the punctured convolutional and Reed-Solomon codes previously described, the code rate of the concatenated code can range from $\frac{1}{2} \cdot \frac{53}{255} \approx \frac{1}{10}$ to unity (in the case of no coding) with 1632 intermediary code rates and a resolution of less than $\frac{1}{132} \approx 0.0076$. This resolution far exceeds the requirements of most, if not all applications, but does illustrate the excellent potential of this code for adaptive rate coding.

5.2 Hybrid ARQ

A second technique for correcting errors is ARQ (see [33], [47]). ARQ uses linear block codes to detect errors in transmitted packets and, if present, requests a re-transmission of

the erroneous packets. Since the probability of undetected error is much less than the probability of an error in error correction, ARQ offers a much greater data reliability over FEC. However, in poor channel conditions, the average number of re-transmissions required may become significantly large in which case the channel throughput[5] will approach zero. A solution is hybrid ARQ (HARQ).

HARQ combines FEC and ARQ in order to reduce the average number of re-transmissions while still maintaining a high data reliability. This typically requires two error control codes: an FEC code which corrects the most common errors and an error detection code to verify if the packet was corrected. If after FEC, no errors are detected, the transmitter sends a positive acknowledgment (ACK) to the transmitter and the decoded data is passed to the data sink. If errors are detected, a re-transmission request is issued in the form of a negative acknowledgment (NACK).

Two techniques exist for increasing the throughput of the HARQ scheme in noisy channels: type-II HARQ and code combining. The underlying premise of both techniques is the combining of previously unsuccessful transmissions with the present transmission in order to increase the probability of correct decoding at the FEC stage. Both techniques are presented here.

5.2.1 Type-II Hybrid ARQ

Two types of HARQ protocols exist, namely type-I and type-II. In type-I HARQ, each packet is encoded for both error detection and correction. If, at the receiver, errors are detected after error correction, the packet is discarded and a re-transmission request is issued. The transmitter responds by sending the same packet as was originally sent. This protocol is inherently sub-optimal in that the discarded packets still contain information, albeit insufficient to perform error correction.

Type-II HARQ provides a solution through the use of an (n, k) FEC code which can be decomposed into ν (n', k) individual codes (where $k \leq n' \leq n/\nu$). Figure 5.6 illustrates FEC encoder and decoder operation for the type-II HARQ protocol. At the transmitter, the packet is encoded using the full (n, k) code; however, only the first n' symbols are transmitted initially. At the receiver, error correction followed by error detec-

5. Here, the throughput is defined as the ratio of the number of information symbols (i.e. not including coding overhead) to the total transmitted symbols in the first transmission and all subsequent re-transmissions.

tion is performed on the packet. If no errors are detected, the decoded data is passed to the data sink and an ACK is sent to the transmitter. If errors are detected, the erroneous packet is buffered and a NACK is returned. Upon receipt of the NACK, the transmitter sends the second set of n' symbols. The receiver performs error correction and detection on this second packet and, if no errors are detected, the decoded data is passed to the data sink. If errors are detected, the first and second packets are concatenated forming a new packet with a reduced code rate equal to $k/(2n')$. If after performing error correction and detection on the concatenated packet, no errors are detected, the decoded data is passed to the data sink. If errors are detected, a NACK is sent to the transmitter and the process repeats for the next n' code symbols. If errors persist still after the $(\nu - 1)$ -th re-transmission (i.e. after the complete code word has been transmitted), the transmitter re-sends the first n' code symbols. If after error correction, errors are yet detected, the receiver replaces the first packet in the concatenated packet with the new packet and error detection and correction are attempted again. This process of discarding previous packets in favor of new packets continues until errors are no longer detected.

Besides being decomposable, the FEC code used for type-II HARQ must possess strong separability and strong invertability [47]. An FEC code is separable if the information and parity symbol coordinates in the code words can be separated. A code is strongly separable if any k code word coordinates can be used for the information symbols. An FEC code is invertible if the parity check symbols of the code word can be used by themselves to uniquely determine the information symbols through an inversion process. A code is strongly invertible if any k symbols from the code word can be used to recover the information symbols. The MDS punctured Reed-Solomon codes are both strongly separable, strongly invertible and can be decomposed through puncturing [45].

As an example, consider the $(255, 53)$ Reed-Solomon code. Puncturing this code, a $(252, 53)$ code is obtained which can be decomposed into four $(63, 53)$ codes through a second puncturing operation (recall that the particular bits which are punctured are irrelevant). Thus, each decomposed code can correct up to 5 symbol errors and when concatenated can correct 36, 68 and 99 symbol errors given the first, second and third re-transmissions respectively. For all subsequent re-transmissions (if required) 99 symbol errors may be corrected.

5.2.2 Code Combining

Code combining is a maximum-likelihood decoding (MLD) approach for combining an

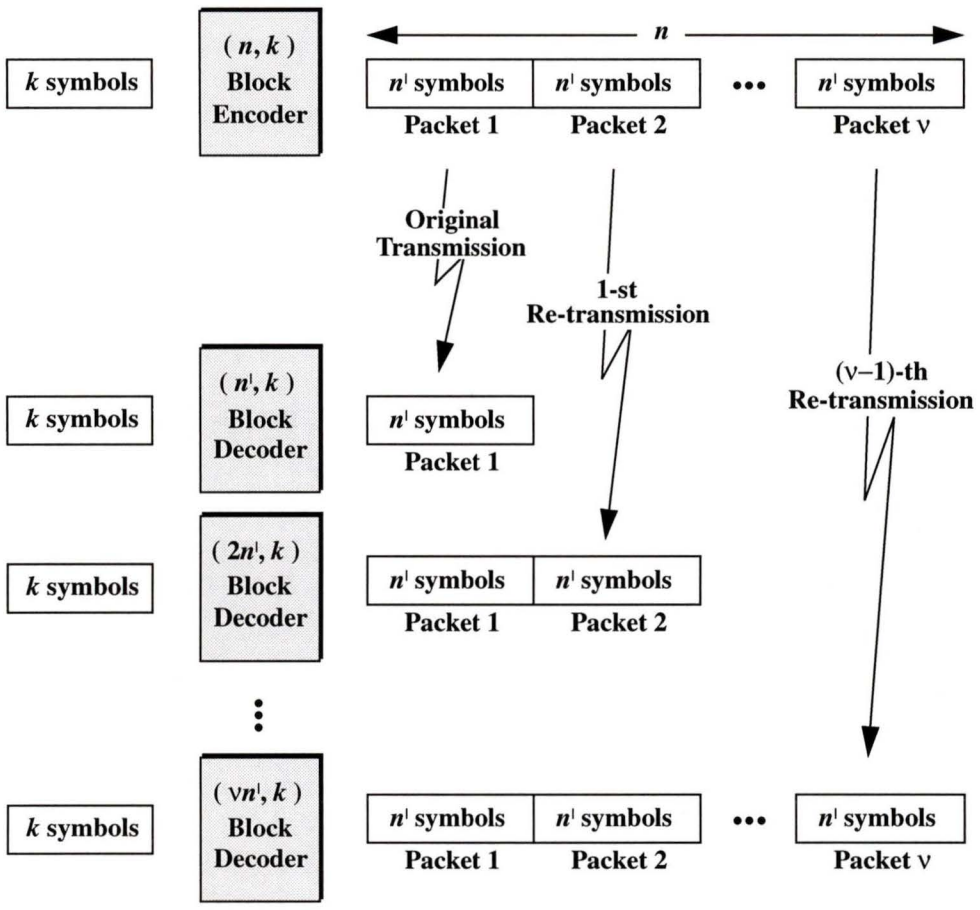

Figure 5.6 Functional diagram of the type II hybrid ARQ scheme.

arbitrary number of unreliable packets to obtain a lower rate, and thus more powerful, error-correcting code [48]. Code combining is designed to work in very noisy environments and is capable of maintaining practical communications over all channels provided the channel error rate is below one-half.

Code combining utilizes channel estimation in order weight each received packet by an estimate of its reliability (effectively performing soft-decision on the packets). After each transmission, the received packet is weighted according to the estimated state of the channel during the packet's transmission and summed to the previously transmitted packets. The resulting combined packet is then decoded using a standard error correction and detection FEC code.

As the combining produces soft-decision bits (as well as can operate on soft-decision bits), soft-decision decoders are especially favorable. For this reason, convolutional

codes employing soft-decision Viterbi decoders (such as the punctured convolutional codes previously presented) are ideal for code combining.

5.3 Proposed Rate Adaptive Code Scheme

The proposed error control coding scheme combines the rate adaptive concatenated FEC code with the two HARQ strategies presented to form a very powerful, flexible and highly adaptive error control scheme. A block diagram of this scheme is presented in Figure 5.7.

FEC is performed using the rate adaptive concatenated code previously presented. A second interleaving process, added at the channel, helps alleviate the effects of the time correlated channel. The data source indicates the BER and delay requirements of the data to be transmitted and the channel estimator provides an estimate of the current channel conditions. The code adaptor utilizes this information in order to determine the required code rate for the concatenated code. The control channel ensures that both the FEC encoder and decoder operate using the same code parameters. The design and optimization of the code adaptor's protocol for selecting code rates is beyond the scope of this thesis.

Type-II HARQ in conjunction with code combining is proposed for delay insensitive data types. FEC is performed by the concatenated code where the inner code is the punctured convolutional code and the outer code is the punctured Reed-Solomon code. An important advantage of using the Reed-Solomon code is its simultaneous error correction and detection capabilities, which unlike for other block codes, does not impinge on the error correction capabilities of the code[6]. In [49], it is shown that for a t symbol correcting Reed-Solomon code, the probability of a decoder error (i.e. occurs when a packet containing errors is released to the data sink) is

$$\text{Prob}\,[\text{Undetected Errors}] < \frac{1}{t!}. \tag{5.4}$$

Assuming the Reed-Solomon code is decomposed into ν packets and ν unsuccessful transmission attempts have been made, rather than discarding the first packet in lieu of the $(\nu + 1)$ -th packet, code combining is employed (and similarly for any other re-trans-

6. Generally, a linear block code with minimum distance, $d_{\min}$, is restricted to correcting λ or fewer errors while simultaneously detecting l $(l > \lambda)$ while maintaining $d_{\min} > \lambda + l$ [33].

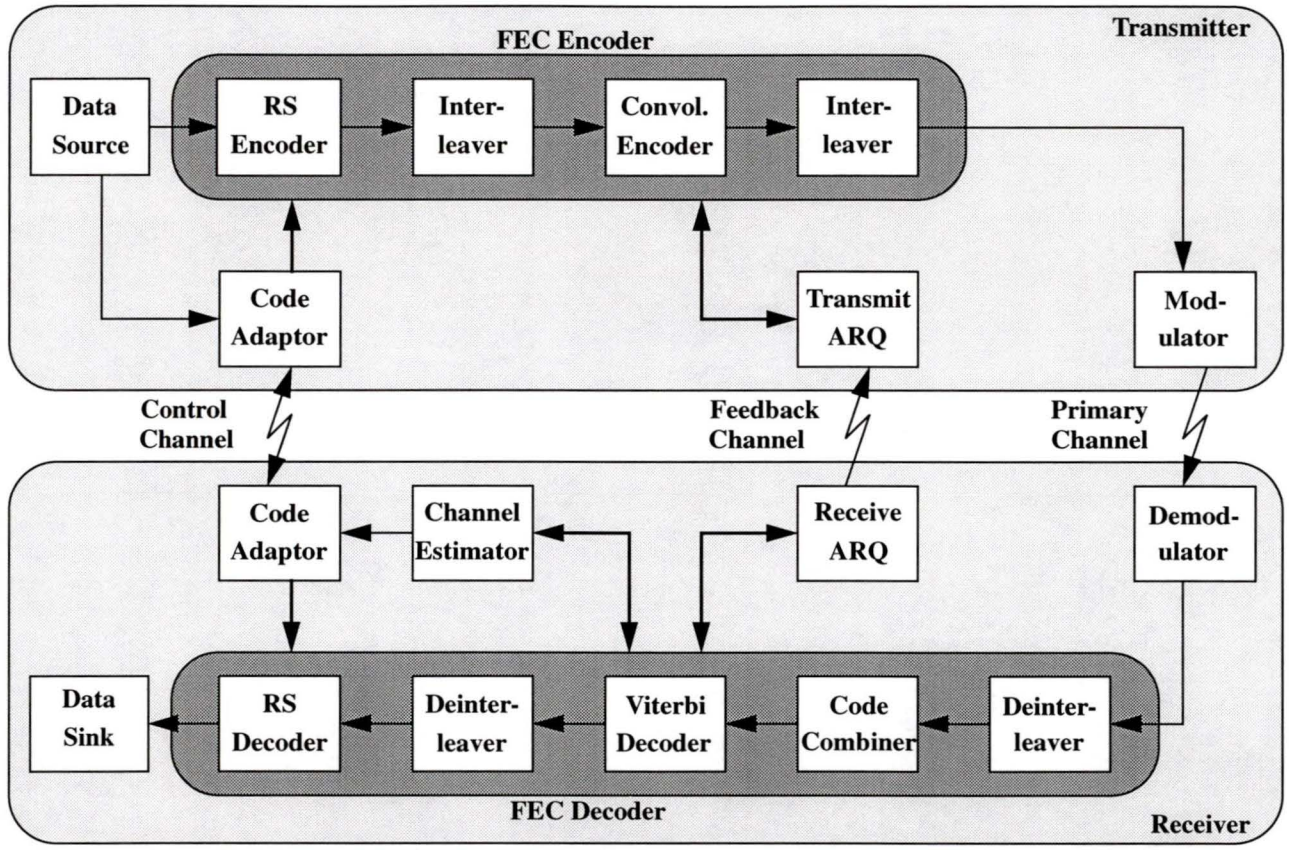

Figure 5.7 Block diagram of proposed adaptive error control scheme.

mitted packets). Weighting and summing the repeated packets is performed by the code combiner using the channel information supplied by the channel estimator. The transmit and receive ARQ blocks perform buffering and control the ARQ process. A feedback channel is used by the receiver to communicate ACKs and NACKs back to the transmitter.

Figure 5.8 illustrates the packet size at each stage of the proposed code. This assumes a punctured and decomposed Reed-Solomon code (resulting in ν (n, k) codes) employing m-bit symbols and a rate $(N-1)/N$, constraint length K convolutional code. The channel interleaver has depth λ_{in} and the code interleaver has depth λ_{out}.

The designed code rate is simply the product of the code rates of the individual codes:

$$r_{\text{d}} = \frac{k}{n}\left(\frac{N-1}{N}\right). \tag{5.5}$$

However, tracing the packet sizes through the code (see Figure 5.7), it becomes apparent that the actual code rate will be less than the designed code rate due to (a) possible mismatched bits per block at the interleavers and (b) additional overhead required to return the trellis to the all zero state. Thus, the actual code rate is

$$r_{\text{a}} = \frac{\lambda_{\text{out}}\,(k \times 2^m)}{\left\lceil \left(\left\lceil \frac{\lambda_{\text{out}}\,(n \times 2^m)}{N-1} \right\rceil N + 2\,(K-1) \right) / \lambda_{\text{in}} \right\rceil \lambda_{\text{in}}}, \tag{5.6}$$

where $\lceil x \rceil$ denotes the smallest integer not less than x. As this additional overhead does not contribute to increased error correction performance, the code parameters must be selected such that r_{a} is not significantly less than r_{d}.

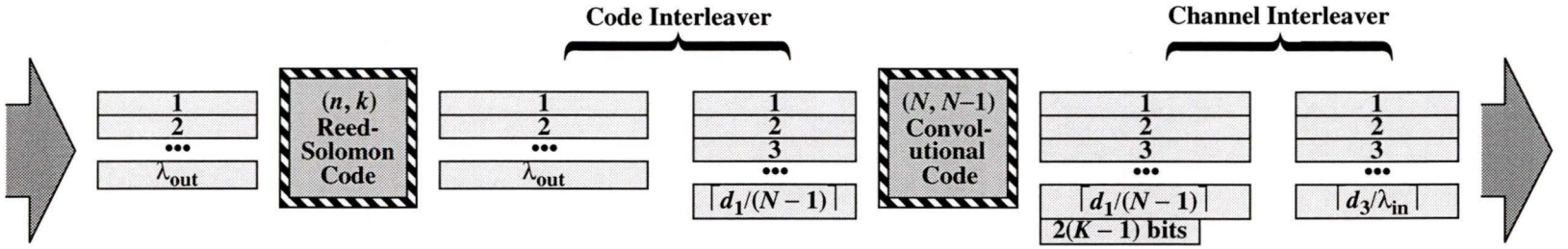

Bits per packet:				
$k \times 2^m$	$n \times 2^m$	$N-1$	N	λ_{in}
Packets per block:				
λ_{out}	λ_{out}	$\lceil d_1/(N-1) \rceil$	$\lceil d_1/(N-1) \rceil$	$\lceil d_3/\lambda_{in} \rceil$
Bits per block:				
$d_0 = \lambda_{out}(k \times 2^m)$	$d_1 = \lambda_{out}(n \times 2^m)$	$d_2 = \lceil d_1/(N-1) \rceil \times (N-1)$	$d_3 = \lceil d_1/(N-1) \rceil \times N + 2(K-1)$	$d_4 = \lceil d_3/\lambda_{in} \rceil \times \lambda_{in}$

Figure 5.8 Intermediary packet and block sizes throughout the concatenated encoder and decoder.

Chapter 6

BER Performance Analysis of the Proposed Coding Scheme

In this chapter, a BER performance analysis is performed on the FEC portion of the adaptive error control code presented in Chapter 5. This analysis is not only crucial in measuring the effects of the adaptive FEC code in the fading environment but also provides the basis for future work in designing the ARQ and code adaptation protocols.

Simulation is chosen to evaluate the codes for several reasons. First, the existing bounds on the performance tend to be tight only at lower bit error rates. This is especially evident for concatenated codes where a loose error bound on the inner code further reduces the accuracy of the bounds of the outer code. Secondly, in the fading channel, average channel statistics cannot be utilized in determining error performance due to the time correlation (i.e. the received power is not necessarily constant over the duration of one transmitted code word). Finally, the shadowed Rician channel statistics are sufficiently complicated to make analytical expressions intractable.

Simulation software employing Monte Carlo trials has been developed for the concatenated code. Unfortunately, for bit error rates less than 10^{-5}, the time required to perform such simulations becomes prohibitively long. However, simulating to 10^{-5} in most cases is sufficient in establishing the general trends of the curves, thus allowing extrapolation to estimate performance at lower bit error rates.

For this analysis, BSPK modulation is assumed. This however, does not limit the generality of the results since the performance gains of the codes relative to each other remain constant independent of the modulation scheme (assuming bbinary symbols). In all cases, the BER is determined with respect to the average energy per information bit in

the unfaded link and thus, the actual energy per *transmitted* symbol in the unfaded link is

$$\frac{E_s}{N_0} = \frac{1}{r_a} \times \frac{E_b}{N_0} \tag{6.1}$$

where r_a is the actual code rate defined by Eq. (5.6). This ensures that the same power is expended in transmitting one data packet regardless of the particular code and code rate employed. This provides for fair grounds for comparison between the various codes.

6.1 Rate Adaptive Convolutional Code

In Section 5.1.1, a rate adaptive convolutional code based on the rate $(N-1)/N$ punctured convolutional code was presented. For this analysis, a constraint length 7 code with 7-bit quantization for soft-decision Viterbi decoding is assumed.

For the non-fading Gaussian channel, an analytical bound on the BER exists. Assuming BPSK modulation and infinite quantization, the BER at the output of the Viterbi decoder is [34]

$$P_b(\gamma) = \sum_{i=d_{\text{free}}}^{\infty} C_i Q\left(\sqrt{2 r_a i \gamma}\right) \tag{6.2}$$

where d_{free} is the minimum free distance of the convolutional code[1], C_i is the number of bits in error for the adversaries (incorrect paths) of Hamming distance i from the correct path and r_a is the actual code rate given as

$$r_a = \frac{N-1}{N+2(K-1)} \tag{6.3}$$

for the convolutional code when used alone. The weights C_i for the punctured codes considered here are obtained through computer search and have been tabulated in [40], [44]. Figure 6.1 illustrates both the analytical and simulated BER curves for the rate $1/2$, $3/4$, $7/8$ and $16/17$ codes. These show strong agreement between theory and simulation. The slight discrepancy between theory and the simulated points is due to truncation of the series in Eq. (6.2) (particularly evident for the rate $1/2$ code where only the first 6 terms were used).

---

1. The minimum free distance is equal to the minimum Hamming distance between any two paths in the trellis.

Figure 6.1 illustrates the significant improvements which can be achieved, especially for higher signal to noise ratios when coding is employed. In fact, even for the least powerful code, the rate $16/17$ code, an improvement of 2 dB in SNR at a BER of 10^{-4} is possible. However, for lower SNR's, the coded performance is less than that of the uncoded channel due to the higher channel error rate and coding overhead.

Bounds for the BER performance of convolutional codes in the time-varying Rician channel are derived in [50]; however, these are only useful only for predicting the performance in the two extremes, for no time correlation and for infinite time correlation (simulation was required for the cases between the two extremes). Here, simulation is also used to determine the performance of the punctured codes over the correlated Rayleigh fading channel (worst case Rician). Figure 6.2 shows the results for the rate $1/2$ and $7/8$ codes for several values of f_D, the normalized Doppler frequency. The normalized Doppler frequencies $f_D = 0.01$, 0.001 and 0.0001 correspond to 760, 76 and 7.6 kilometers per hour respectively, assuming a 64 kilobit per second data rate and 900 MHz carrier frequency. For severe correlation (i.e. $f_D = 0.01$), the BER performance is worse than that of the uncoded case. Furthermore, as the time correlation increases, the spread in SNR between the rate $1/2$ and $7/8$ codes decreases. From this figure, it becomes evident that in order to achieve a reasonable BER, interleaving or diversity is required to remove some of the time correlation from the channel.

Of interest is the BER performance over the shadowed Rician channel. Three channel types are considered: the good channel representing the lightly shadowed channel with a strong line of sight, the bad channel representing the heavily shadowed channel with no line of sight, and a typical channel which falls between the two. The parameters for each channel type are listed in Table 6.1. Simulated BER curves for these channel environments are shown in Figure 6.3 for several code rates. Sufficient interleaving is assumed to remove all time correlation. The need for a stronger code (possibly the concatenated code) is evident especially due to the poor performance in the bad channel state. Regardless, for all channel states, a BER less than 10^{-4} is achievable given an SNR of 7 dB, 16 dB and 28 dB for the good, typical and bad channels respectively.

6.2 Rate Adaptive Reed-Solomon Code

The BER performance for the punctured Reed-Solomon code is determined here for the $(n, 53)$, 8-bit symbol code. Where simulation is required, rather than simulating the full

	Good	Typical	Bad
Rice Factor	5	2	0
Standard Deviation of Shadowing [dB]	3	8	12

Table 6.1. Parameters for the good, typical and bad channel model.

Reed-Solomon decoder, a quicker alternate method is employed. Given that the Reed-Solomon code can correct exactly t or less symbol errors, only those code words containing more than t errors need be considered for decoding. However, rather than actually performing the decoding operation, a tight bound on the BER can be derived by exploiting the properties of the Reed Solomon code. For those code words containing more than t errors, the decoder attempts to correct at most t symbols and thus in doing so may corrupt at most t additional symbols above those that were already corrupted during transmission. This results in a decoding error; however, the probability of an undetected decoding error is less than $1/t!$. Therefore, assuming that one-half of the bits in a corrupted symbol are wrong, a tight upper bound on the error rate can be derived:

$$\bar{P}_b \leq \frac{b_e + p_e \frac{tm}{2t!}}{b_t} = \frac{b_e}{b_t} + \frac{p_e m}{b_t (t-1)!} \tag{6.4}$$

where b_e is the number of bits in error in the k information symbols, p_e is the number of received words with greater than t symbol errors and b_t is the total number of information bits transmitted. Notice that for large t, the second term in Eq. (6.4) becomes negligible. Therefore using this bound, it is sufficient to simulate the channel and demodulation process and then determine b_e, p_e from the resulting packet.

This bound can be tested against the conventional error bounds for the Gaussian channel. The symbol error rate at the input to the Reed-Solomon decoder is [34]

$$P_s = 1 - (1-p)^m \tag{6.5}$$

where p is the channel error rate given in Table 4.2 for BPSK. The bit error rate at the output of the Reed-Solomon decoder is approximated as [3]

$$P_b = \frac{2^{m-1}}{2^m - 1} \sum_{i=t+1}^{n} i \binom{n}{i} P_s^i (1-P_s)^{n-i}. \tag{6.6}$$

In Figure 6.4, the BER curves obtained through simulation using the bound given by

Eq. (6.4) are compared to those obtained from the analytical bound given by Eq. (6.6). The code lengths considered are $n = 63, 85, 127$ and 255 which, for $k = 53$, results in approximate code rates of $4/5$, $3/5$, $2/5$ and $1/5$ respectively. Notice that at high SNR, the simulated bound is one-quarter the theoretical bound. This is due to the fact that the theoretical bound in Eq. (6.6) assumes that if an information symbol is in error, one-half the bits are in error. However, for higher SNR and the Gaussian channel, it is more probable that only one bit is in error. Thus for $m = 8$, the theoretical bound assumes that 4 bits are in error whereas, most probably only one bit is in error and thus explains the factor of four difference between the two bounds. At lower SNR, the probability of more than one bit error per symbol error increases and thus the difference between the two curves decreases.

Notice that the performance of the lower rate codes (in particular the rate $1/5$ code) does not outperform the higher rate codes until the BER is very small. This is due to the increased packet length and thus lower energy per transmitted symbol. It appears that for the range of BER's of concern, the higher rate codes are more efficient. Regardless, the BER improvement due to coding is substantial for BER's less than 10^{-4}.

Figure 6.5 illustrates the performance of the punctured code over the good, typical and bad channel conditions listed in Table 6.1. Again, at higher BER's, the higher rate codes outperform the lower rate codes. However, as the channel gets progressively worse, the performance difference between the rate $1/5$ and the higher rate codes decreases. Finally, comparing the performance of these Reed-Solomon codes to the convolutional codes in Figure 6.3 for lower SNR's, the convolutional codes with higher code rates outperform the Reed-Solomon codes with lower code rates. This helps substantiate the choice of order in the concatenated FEC code (i.e. the convolutional code is the inner code and the Reed-Solomon code is the outer code).

Consider for a moment the type-II HARQ scheme using the decomposed and punctured Reed-Solomon code. Recall that the original transmission and all subsequent retransmissions use the same packet size and thus share the same code rate. As a result, when re-transmitted packets are appended to the original packet the result is to effectively increase the energy per information bit. For this reason, it is instructive to consider the BER performance when the energy per transmitted symbol is constant and the energy per information bit varies with the code rate. This is illustrated in Figure 6.6 for the typical shadowed Rician channel. As expected, the SNR improvement for the decreasing

SNR is quite substantial which indicates that type-II HARQ will be quite effective in the fading channel.

6.3 Concatenated FEC Code

In this section, the performance of the concatenated code is presented for the Gaussian and shadowed Rician channels. Again the constraint length 7 soft-decision Viterbi decoding with 7-bit quantization is assumed for the convolutional code and a $(n, 53)$ Reed-Solomon code with 8-bit symbols is used for the outer code. Infinite channel interleaving is assumed and no code interleaving is employed.

Figure 6.7 illustrates the BER performance of the concatenated code in the Gaussian channel. In all cases, for the range of BER's simulated, the lower rate convolutional codes outperformed the higher rate convolutional codes however, the higher rate Reed-Solomon codes outperformed the lower rate Reed-Solomon codes (especially for the rate $1/5$ code). However, observing the slopes of the curves, it is anticipated that for lower BER's, the lower rate Reed-Solomon codes will eventually outperform the higher rate codes. Comparing these curves to those for the convolutional code alone (see Figure 6.1), significant gains are seen for the concatenated code employing the rate $1/2$ convolutional code for BER's less than 10^{-4} and for the rate $7/8$ codes, for BER's less than 10^{-6}. Notice that the effect of concatenating the codes is to increase the steepness of the slope of the curves.

Finally, in Figure 6.8, the BER performance of the concatenated code for the various shadowed Rician environments is shown (see Table 6.1). Again the effects of the convolutional code's code rate seems to dominate. Furthermore, the higher rate Reed-Solomon codes again outperform the lower rate codes but to a much lesser degree than for the Gaussian channel. In fact, as the channel degrades, the lower rate codes become much more effective with respect to the higher rate codes. Finally, the spread between the rate $1/2$ and $7/8$ convolutional codes increases as the channel degrades which in an adaptive code provides a greater range of adaptation.

In conclusion, it is apparent that for lower BER's, the concatenated code provides a moderate gain in performance above that of the convolutional code alone. Much larger gains are anticipated when the adaptive code also employs type-II HARQ.

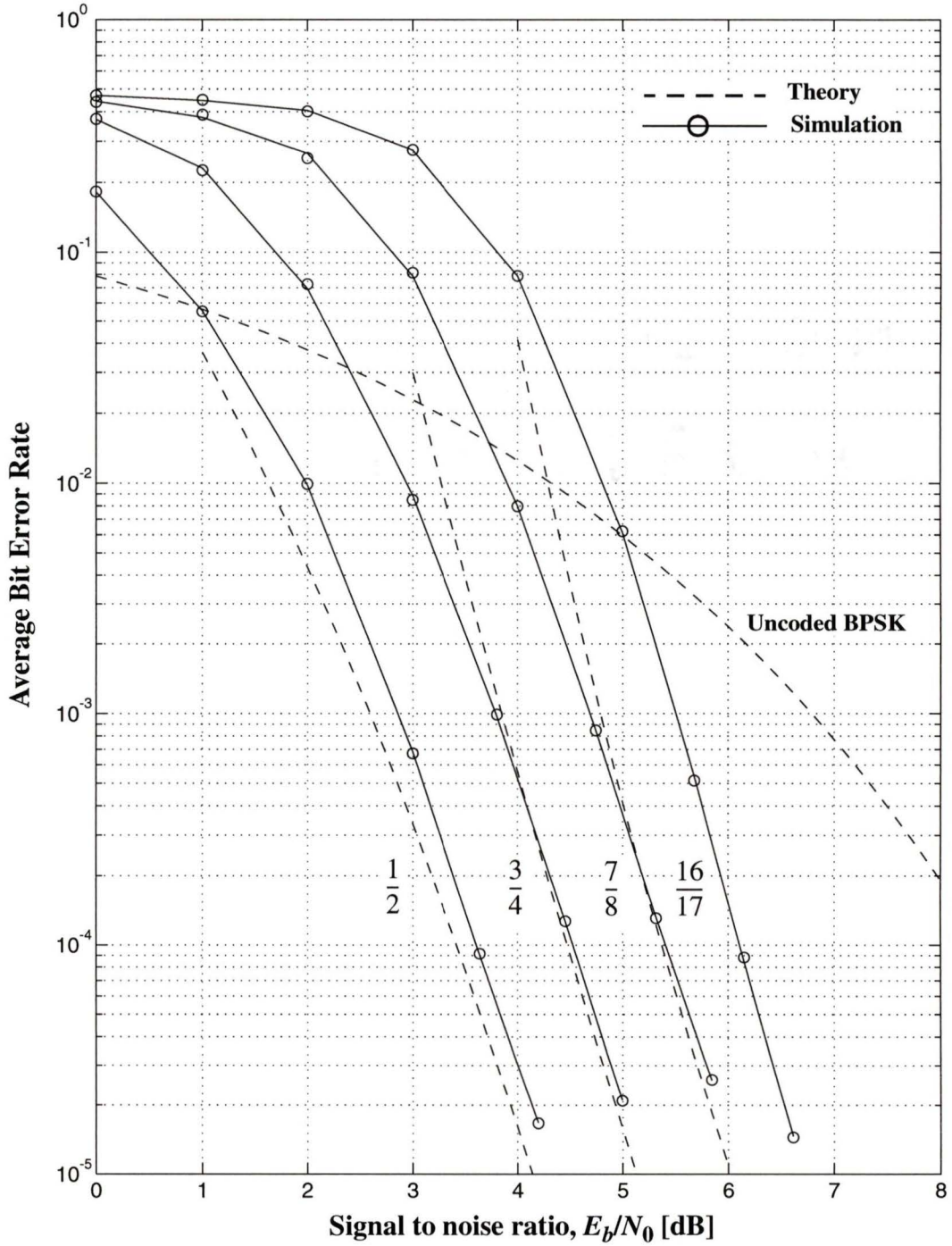

Figure 6.1 BER curves for the constraint length 7 punctured convolutional codes in the Gaussian channel.

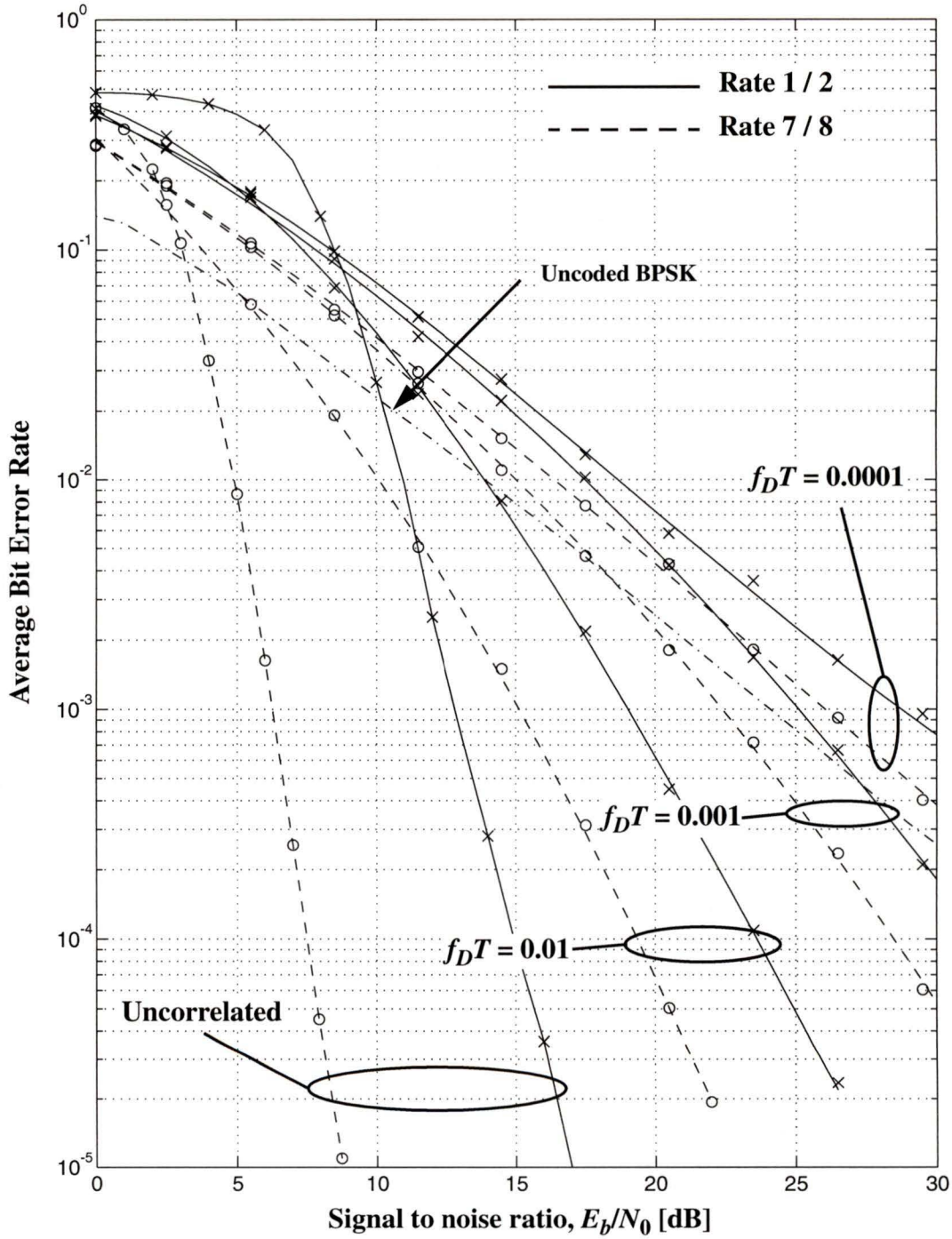

Figure 6.2 BER curves for the convolutional codes in a time correlated Rayleigh fading channel.

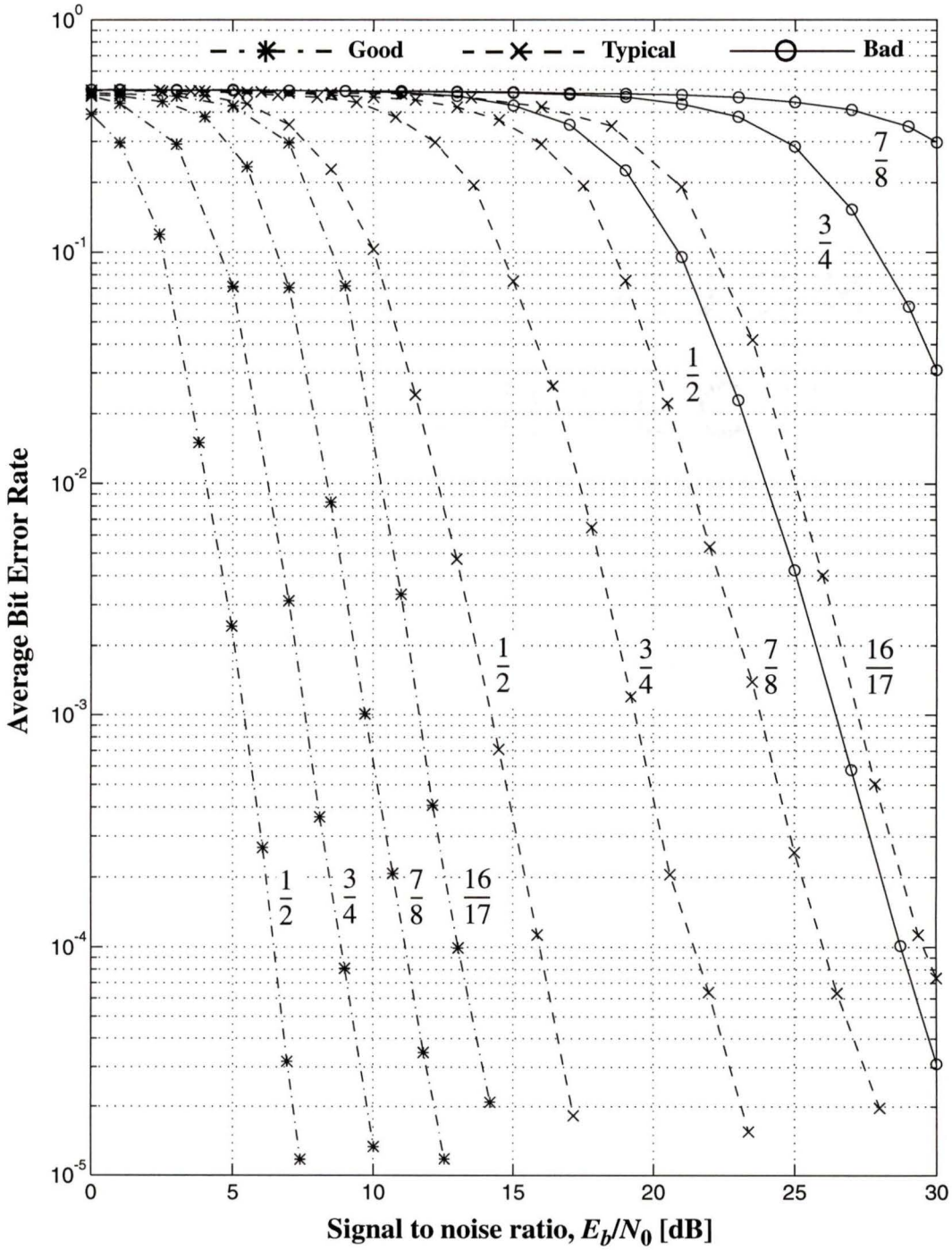

Figure 6.3 BER curves of the punctured convolutional code for various shadowed Rician fading channel conditions.

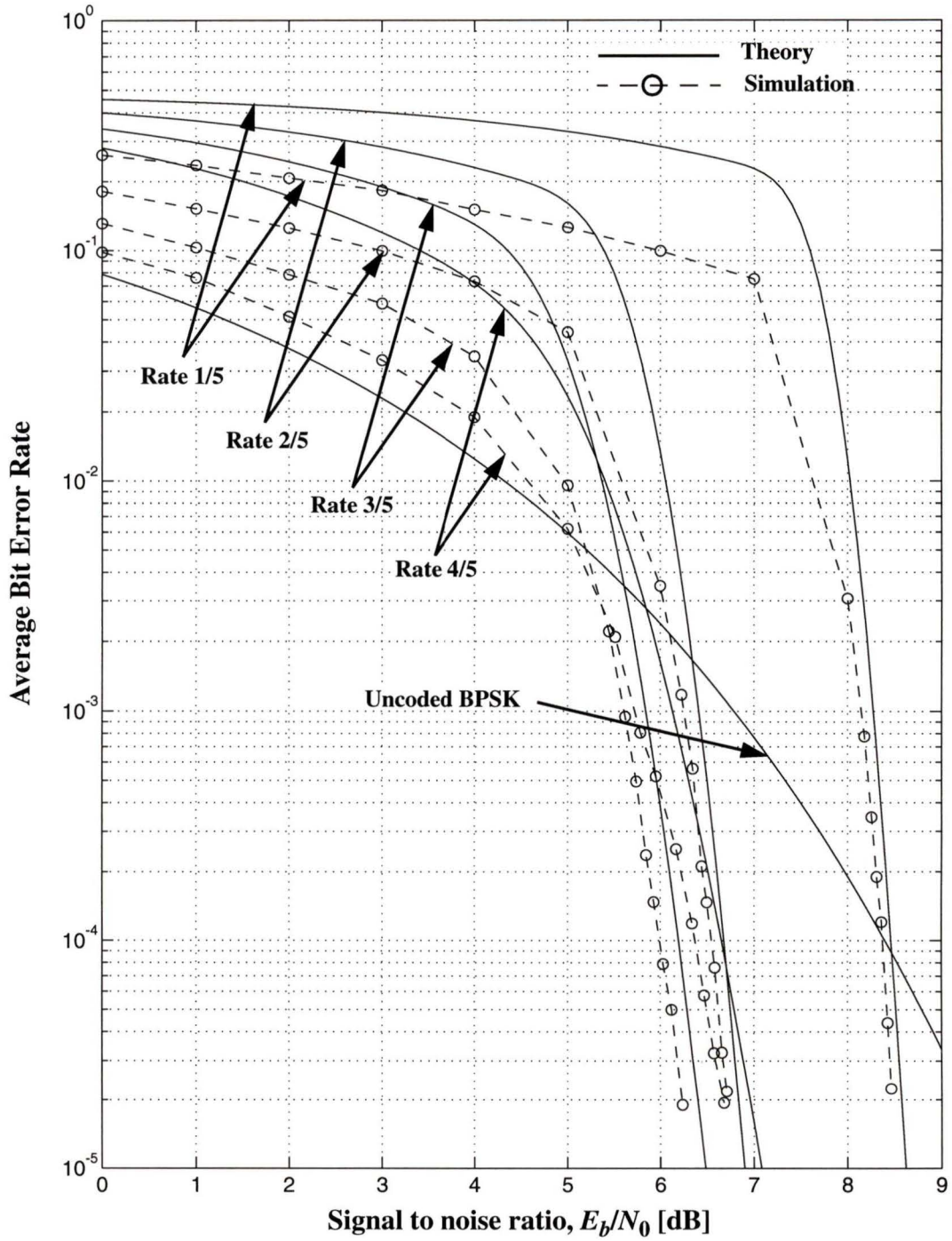

Figure 6.4 BER curves for the punctured Reed-Solomon codes in the Gaussian channel.

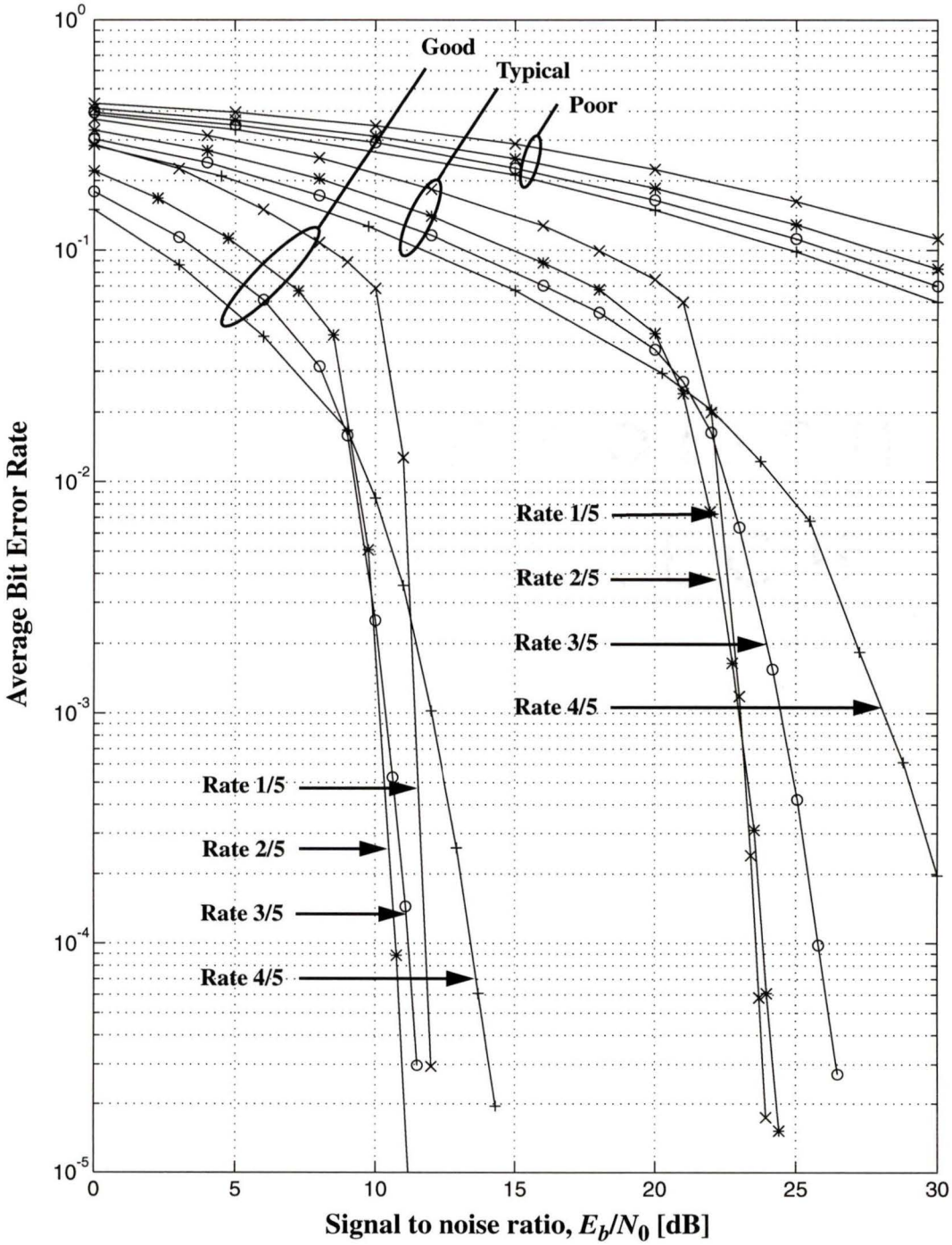

Figure 6.5 BER curves of the punctured Reed-Solomon codes for various shadowed Rician fading channel conditions.

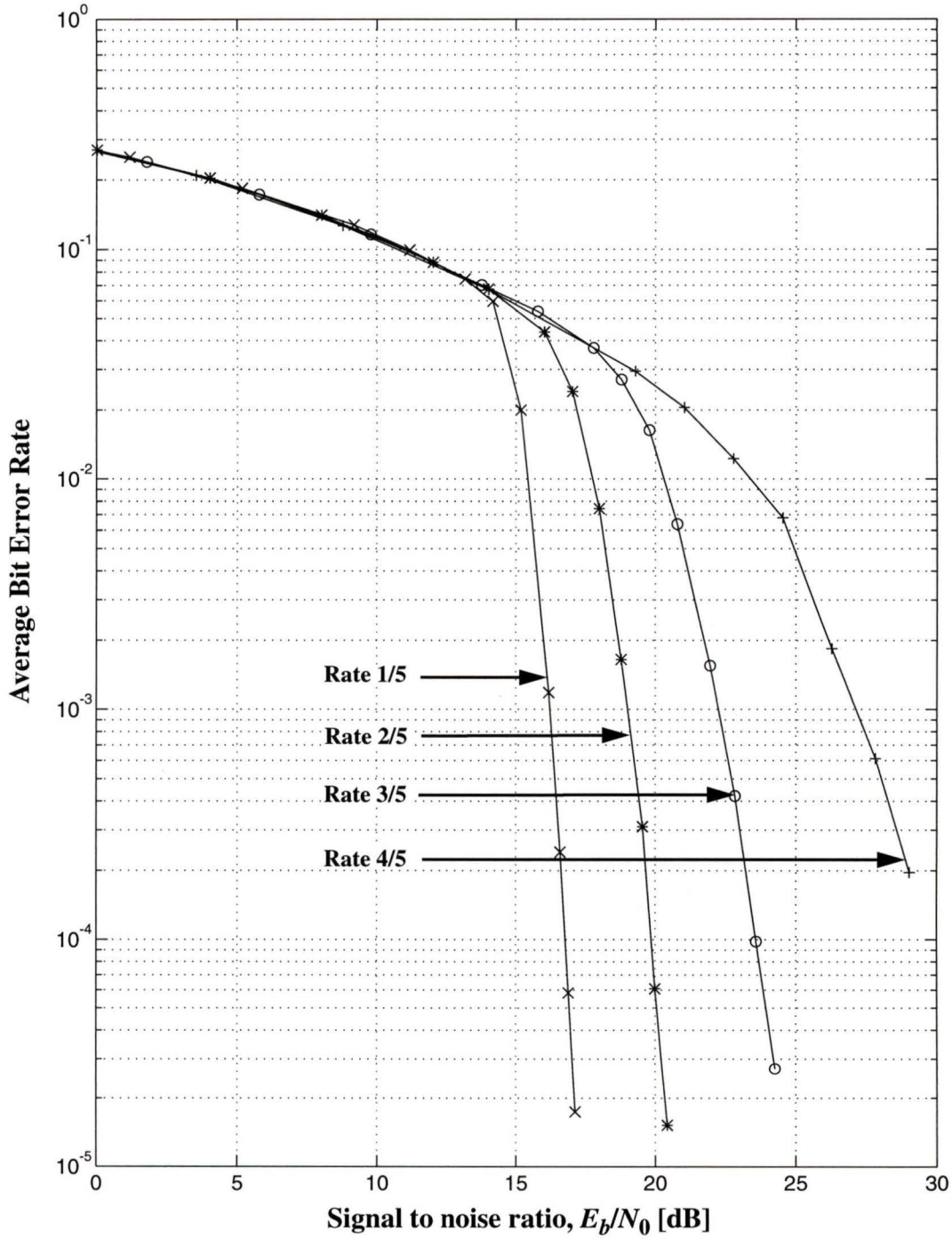

Figure 6.6 BER curves of the punctured Reed-Solomon codes assuming a fixed energy per transmitted symbol in the typical Rician fading channel.

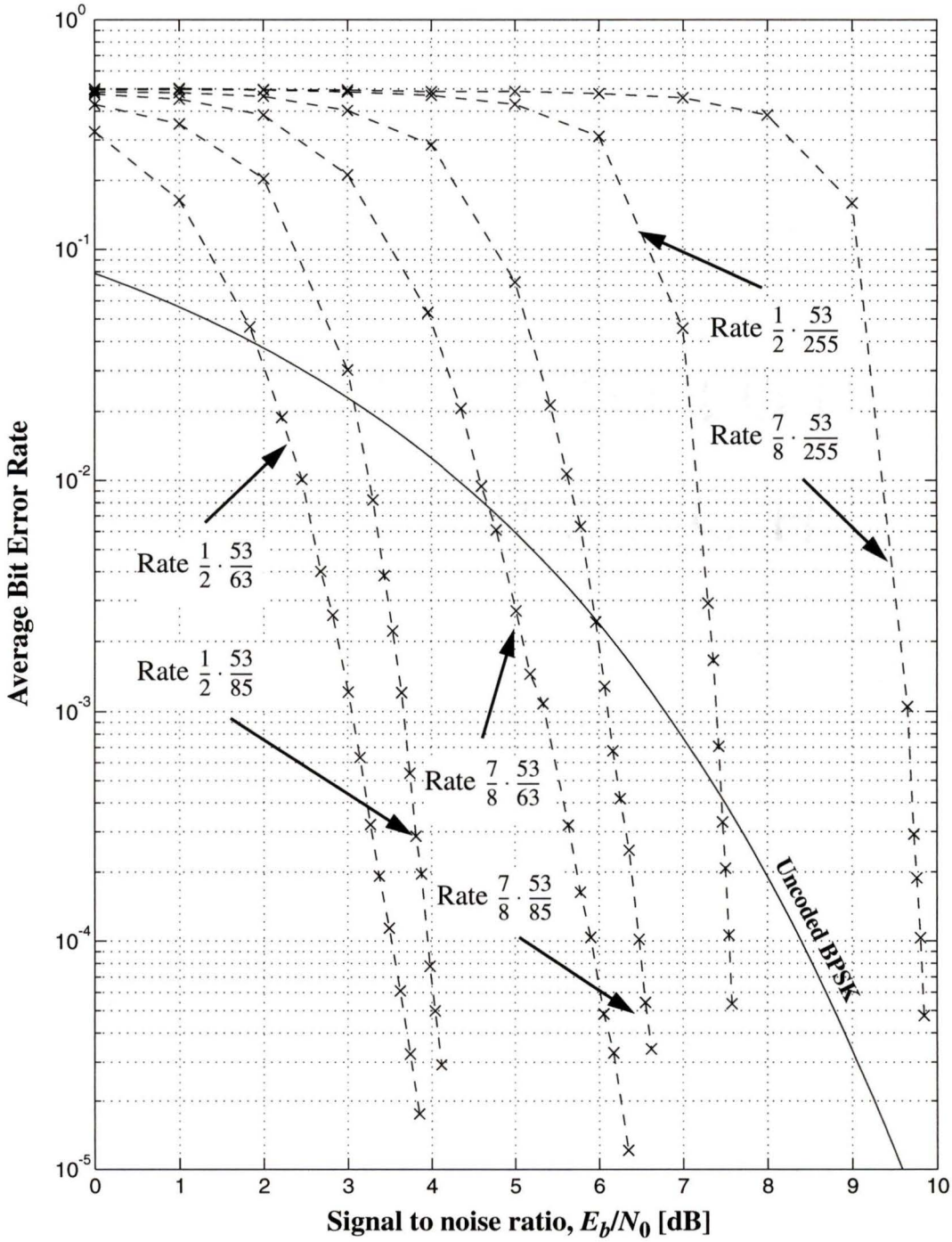

Figure 6.7 BER curves for the concatenated code in the Gaussian environment.

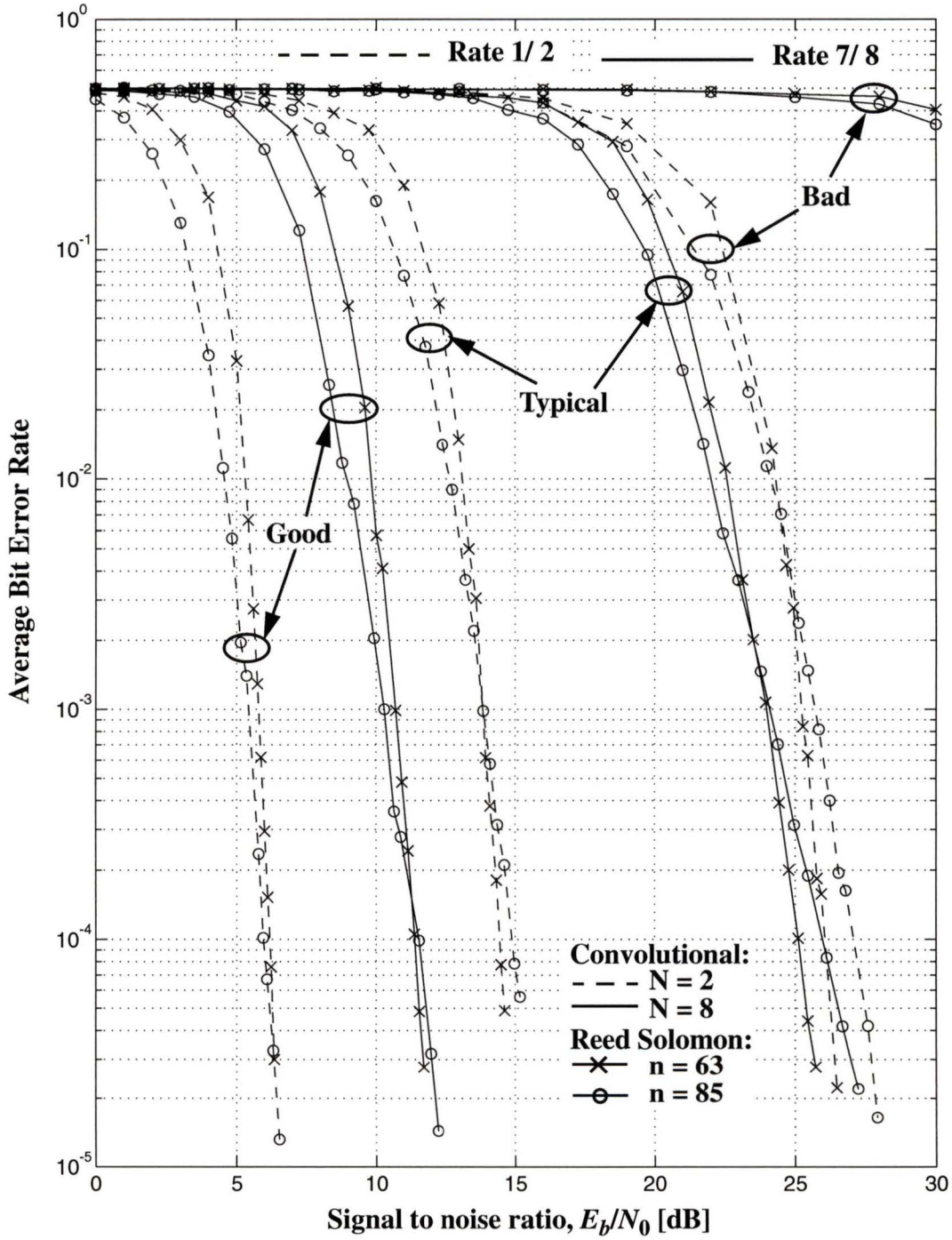

Figure 6.8 BER curves for the concatenated code in various shadowed Rician fading channel conditions.

Chapter 7

Conclusion

This thesis focuses on two techniques for improving the quality of service over the wireless network: diversity reception and adaptive error control coding. For both techniques, examples are provided to help quantify the performance improvements achievable.

To aid in the analysis, a detailed description of the mobile channel (assuming both terrestrial and satellite base stations) is provided. For the land mobile terrestrial channel, a shadowed Rician channel model is used, which provides the flexibility to model most mobile environments ranging in size from picocells up to macrocells. For the land mobile satellite channel, a time-shared Rician/Suzuki distribution is used for which the parameters are obtained from actual channel measurements. A channel simulator incorporating both channel models is presented.

For diversity reception, analytical expressions well suited to numerical analysis for the average BER and outage probability are presented for both terrestrial and satellite channels. Besides several common modulation schemes, both coherent and non-coherent M-ary phase shift keying are considered. For diversity, both microscopic (i.e. multiple mobile antennas) and macroscopic (i.e. multiple base stations) diversity are analyzed. Finally, these analytical expressions incorporate both selection diversity combining (for micro- and macro-diversity) and maximal ratio combining (for micro-diversity). These expressions are very powerful in that they are functions of the MGF and CDF of the fading channels and can thus be easily adapted to any channel model provided the MGF and CDF are known.

A numerical analysis for the satellite channel with MRC and SDC micro-diversity is performed. Using measured channel parameters, BER and outage probability curves are plotted for various channel environments. Without diversity reception, the BER per-

formance of M-ary PSK for $M > 4$ is sufficiently poor that the more bandwidth efficient modulation schemes can not be utilized. However, it is shown that diversity reception (especially MRC) provides significant improvements in both the BER and outage probability. In fact, using 2-branch MRC diversity, 16-ary PSK out performs BPSK without diversity. Furthermore, increasing the number of diversity branches reduces the dependency of the fading environment on the BER and outage probability. Finally, the satellite elevation angle is found to have little effect on the BER performance.

For adaptive error control coding, a very powerful, flexible and highly adaptive error control code is proposed. The overall code uses a type-II HARQ strategy (where ARQ is utilized only if the delay constraints of the particular traffic permit). The FEC portion of the code is performed using a concatenated code consisting of a punctured convolutional inner code and a punctured Reed-Solomon outer code. The maximum distance separability property of the Reed-Solomon code and the utilization of the maximum likelihood Viterbi decoder ensures that both codes provide optimum error correction. Furthermore, both codes are extensively used in practice and thus implementation is not of significant concern. HARQ is employed through the decomposition of the Reed-Solomon code into smaller code words and by combining the combining of repeated packets (weighted according to the channel conditions during transmission) at the input to the Viterbi decoder. Finally, error detection (for ARQ) is provided by the Reed-Solomon decoder. The greatest advantage of this proposed code is its adaptability (with code rates from $1/10$ to unity and over 1600 intermediary values) and the ease of implementation.

Examples of the BER performance of the convolutional code, the Reed-Solomon code and the two codes concatenated are provided using simulation. Several general trends were observed. At high BER's (10^{-2} and higher), the higher rate codes out perform the lower rate codes and both are generally outperformed by the uncoded case. For the Reed-Solomon code, the higher rate codes outperform the lower rate codes except when the BER is small. The concatenated code provides substantial improvements in BER and also provided a great range of SNR for which the adaptive code can operate. Finally, the application of type-II HARQ offers great potential for further performance improvements.

7.1 Suggestions for Further Work

The following are interesting topics which may be pursued for future work.

1. Diversity combining techniques:
    - Extension of the analytical expressions for the GMSK modulation scheme, for switched diversity combining and for the Nakagami fading channel model.
    - Application of maximal ratio combining to macroscopic diversity.
    - Further analysis of the Hermitian and Laguerre remainder terms in attempt to provide a tighter bound on the remainder terms.
2. Adaptive error control:
    - Further analysis of the BER performance in the fading channel including effects of code and channel interleaving.
    - Investigation of channel estimation techniques and development of a protocol for adapting the code.
    - Outage probability, throughput analysis and delay profile of the proposed code for the designed adaptation protocol.
    - Investigation of the inter-relationship between adaptive error control and power control.

Bibliography

[1] H. Suzuki, "A statistical model for urban radio propegation," *IEEE Trans. Commun.,* vol. COM-25, pp. 673-680, July 1977.

[2] W. C. Jakes, *Microwave Mobile Communications,* American Telephone and Telegraph Company, 1974 (Reissued by IEEE Press, Piscataway, NJ, 1993).

[3] J. G. Proakis, *Digital Communications,* McGraw-Hill, New York, NY, 1989.

[4] H. L. Bertoni, W. Honcharenko, L. R. Maciel, H. H. Xia, "UHF propagation prediction for wireless personal communications," *Proc. IEEE,* vol. 82, pp. 1333-1359, Sept. 1994.

[5] S. H. Jamali, Tho Le-Ngoc, *Coded Modulation Techniques for Fading Channels,* Kluwer Academic Press, Boston, MA, 1994.

[6] G. E. Corazza, C. Ferrarelli, F. Vatalaro, "A rice-lognormal terrestrial and satellite channel model," *Proc. IEEE Int. Conf. on Universal Personal Communications,* pp. 155-159, 1994.

[7] R. Steele, *Mobile Radio Communications,* Pentach Press Ltd., London, England, 1992.

[8] C. Tellambura, V. K. Bhargava, "Performance of binary modulations for a Rician-fading and shadowing channel," Not yet submitted for publication, 1994.

[9] M. Nakagami, "The *m*-distribution — A general formula of intensity distribution of fading," in *Statistical Methods in Radio Wave Propagation,* W. C. Hoffman, Ed., Pergamon, London, England, 1960.

[10] C. Loo, "A statistical model for a land mobile satellite link," IEEE Trans. Veh. Technol., vol. VT-34, pp. 122-127, Aug. 1985.

[11] C. Loo, N. Secord, "Computer models for fading channels with applications to digital transmission," IEEE Trans. Veh. Technol., VT-40, pp. 700-707, Nov. 1991.

[12] E. Lutz, D. Cygan, M. Dippold, F. Dolainsky, and W. Papke, "The land mobile satellite communication channel — Recordings, statistics and channel model," *IEEE Trans. Veh. Technol.,* vol. VT-40, pp. 375-386, May 1991.

[13] D. Cygan, "Analytical evaluation of average bit error rate for the land mobile satellite channel", *Int. J. Satell. Commun.,* vol. 7, pp. 99-102, Apr. 1989.

[14] J. S. Bendat, A. G. Piersol, *Random Data — Analysis and Measurement Procedures,* 2nd Ed., John Wiley & Sons, New York, NY, 1986.

[15] W. C. Y. Lee, *Mobile Communications Design Fundamentals,* 2nd Ed., John Wiley & Sons, Inc., New York, NY, 1993.

[16] C. W. Helstrom, *Elements of Signal Detection and Estimation*, Prentice-Hall, Englewood Cliffs, New Jersey, 1995.

[17] J.-P. Linnartz, *Narrowband Land-mobile Radio Networks*, Artech House, Boston, MA, 1993.

[18] M. Abramowitz and I. Stegun, *Handbook of Mathematical Functions,* National Bureau of Standards, Washington, DC, 1972.

[19] C. Tellambura, A. J. Mueller, V. K. Bhargava, "Analysis of *M*-ary phase shift keying with diversity reception for land mobile satellite channels," Accepted for publication in the *IEEE Trans. Veh. Tech.*, 1995.

[20] A. Salmasi, "An overview of code division multiple access (CDMA) applied to the design of personal communications networks," in *Third Generation Wireless Information Networks,* Sanjiv Nanda, Ed., David J. Goodman, Ed., Kluwer Academic Publishers, Boston, MA, 1992.

[21] P. J. McLane, P. H. Wittke, P.K.-M. Ho and C. Loo, "PSK and DPSK Trellis Codes for Fast Fading, Shadowed Mobile Satellite Communication Channels," *IEEE Trans. Commun.,* vol. 36, pp. 1242-1246, Nov. 1988.

[22] R. Pichna, R. Kerr, Q. Wang, V. K. Bhargava, I. F. Blake, "CDMA cellular network analysis software," *Final Report* prepared for the Department of Communications under contract #36-001-2-3560/01-ST, Ottawa, ON, 1993.

[23] R. Kuc, *Introduction to Digital Signal Processing,* McGraw-Hill Book Company, New York, NY, 1988.

[24] C. Tellambura, A. J. Mueller, V. K. Bhargava, "BER and outage probability for the land mobile satellite channel with maximal ratio combining," *Electronic Letters*, Vol. 31, No. 8, pp 606-608, Apr. 13, 1995.

[25] A. Turkmani, "Performance evaluation of a composite microscopic and macroscopic diveristy system," *IEE Proc.-I,* vol. 138, pp. 15-20, Feb. 1991.

[26] F. G. Stremler, *Introduction to Commmunication Systems*, Third Ed., Addison-Wesley Publishing Company, Inc., New York, 1990.

[27] S. Haykin, *An Introduction to Analog and Digital Communications*, John Wiley & Sons, New York, 1989.

[28] I. S. Gradshteyn, I.M. Ryzhik, A. Jeffery Ed., *Tables of Integrals, Series, and Products,* 5th Edition, Academic Press, Inc., Boston, 1994.

[29] C. K. Pauw and D. L. Schilling, "Probability of Error for *M*-ary PSK and DPSK on a Rayleigh Fading Channel," *IEEE Trans. Commun.*, vol. COM-36, pp. 755-756, June 1988.

[30] R. F. Pawula, S. O. Rice and J. H. Roberts, "Distribution of the phase angle between two vectors perturbed by Gaussian noise," *IEEE Trans. Commun.*, vol. COM-30, pp. 1828-1841, Aug. 1982.

[31] Staff of Research and Education, *Handbook of Mathematical, Scientific, and Engineering: Formulas, Tables, Functions, Graphs, Transforms,*" Research and Education Association, Piscataway, New Jersey, 1989.

[32] W. C. Lindsey, "Error probabilities for Rician fading multichannel reception of binary and N-ary signals," *IEEE Trans. Info. Theory*, vol. IT-10, pp. 339-350, Oct. 1969.

[33] S. Lin and D. J. Costello, Jr., *Error Control Coding: Fundamentals and Applications*, Prentice-Hall, Inc., New Jersy, 1983.

[34] G. C. Clark, Jr. and J. B. Cain, *Error Correction Coding for Digital Communications*, Plenum Press, New York, 1981.

[35] J. Zou, R. Pichna, Q. Wang and V. K. Bhargava, "Efficient methods for high rate data transmission in mobile and personal communications," *Proc. of Mexicon '94*, Puebla, Mexico, pp. 140-145, Feb. 1994.

[36] P. Mermelstein, A. Jalali and H. Leib, "Integrated services on wireless multiple access networks," *Proc. of ICC '93*, pp. 863-867, 1993.

[37] A. J. Mueller, V. K. Bhargava and Q. Wang, "Design and analysis of a rate adaptive concatenated code for the cellular channel," presented at the Canadian Workshop on Information Theory, Lac Delage, Canada, May 1995.

[38] Y. Yasuda, Y. Hirata, K. Nakamura and S. Otani, "Development of variable-rate Viterbi decoder and its performance characteristics," *Conference Proceedings of the 6th International Conference on Digital Satellite Communications*, Phoenix, Arizona, pp. 24-31, Sept. 1983.

[39] Y. Yasuda, K. Kashiki and Y. Hirata, "High-rate punctured convolutional codes for soft decision Viterbi decoding," *IEEE Trans. Commun.*, vol COM-32, pp. 315-319, Mar. 1984.

[40] D. Haccoun and G. Bégin, "High-rate punctured convolutional codes for Viterbi and sequential decoding," *IEEE Trans. Commun.*, vol COM-37, pp. 1113-1125, Nov. 1989.

[41] A. Franchi and R. A. Harris, "On the burst properties of Viterbi decoding," *Proc. of ICC '93*, pp. 1086-1091, 1993.

[42] J. M. Morris, "Burst error statistics of simulated Viterbi decoded BPSK on fading and scintillating channels", *IEEE Trans. Commun.*, vol COM-40, pp. 34-41, Jan. 1992.

[43] M. Vogel, *A Performance Analysis of Interleaving,* M.A.Sc. Thesis, University of Victoria, British Columbia, Canada, 1993.

[44] G. Bégin, D. Haccoun and C. Paquin, "Further results on high-rate punctured convolutional codes for Viterbi decoding," *IEEE Trans. Commun.*, vol COM-38, pp. 1922-1928, Nov. 1990.

[45] S. B. Wicker, M. J. Bartz, "Type-II Hybrid-ARQ protocols using punctured MDS codes," *IEEE Trans. Commun.*, vol COM-42, pp. 1431-1440, Feb./Mar./Apr. 1994.

[46] G.D. Forney, Jr., *Concatenated Codes*, MIT Press, Cambridge, Mass., 1966.

[47] S. Lin, D. l J. Costello, Jr. and M. J. Miller, "Automatic-repeat-request error-control schemes," *IEEE Commun. Mag.*, vol. 22, pp. 5-16, Dec. 1984.

[48] D. Chase, "Code combining — a maximum-likellyhood decoding approach for combining an arbitrary number of noisy packets," *IEEE Trans. Commun.*, vol COM-33, pp. 385-393, May 1985.

[49] R. J. McEliece and L. Swanson, "On the decoder error probability for Reed-Solomon codes," *IEEE Trans. Inf. Theory*, vol. IT-32, pp. 701-703, Sept. 1986

[50] J. W. Modestino, S.-Y. Mui, "Convolutional code performance in the Rician fading channel," *IEEE Trans. Commun.*, vol. COM-24, pp. 592-606, June. 1976.

Appendix A

Hermitian and Laguerre Integration Remainder Term

In this appendix, a quasi-analytic approach to the error analysis for both the Hermitian and Laguerre integration methods is presented. An alternative method for Hermitian integration, namely Simpson's integration is also presented. Simpson's integration may be used to verify the accuracy of the Hermitian integration when the bound on the Hermitian integration error term is not sufficiently tight. As the mathematics becomes quite difficult, only the micro-scopic diversity cases are considered at this time (i.e. $M = 1$). It should be noted that although Hermitian integration is typically used in co-channel interference analysis [17], to the knowledge of the author, no work on error analysis has been performed.

Here, the error analysis for Hermitian integration will be performed for the basic function

$$m_{\text{Suzuki}}^{(\text{MRC!})} = \frac{1}{\sqrt{\pi}} \sum_{i=1}^{n} w_i \left[\frac{1}{1 + z\mu e^{\sqrt{2}\sigma x_i}} \right]^L + R_n \tag{A.1}$$

where x_i and w_i are the i-th abscissa and weight respectively of the n-th order Hermite polynomial and R_n is the remainder term of interest. Most functions using Hermitian integration in Chapters 2 and 3 are extensions of Eq. (A.1).

Similarly for Laguerre integration, the function of interest is Eq. (3.6)

$$m_{\text{Rice}}^{(\text{SDC})}(z) = \sum_{i=1}^{n} \omega_i \left[1 - Q\left(\sqrt{2K}, \sqrt{2(1+K)(\chi_i / z)} \right) \right]^L + R_n \tag{A.2}$$

where χ_i and ω_i are the i-th abscissa and weight respectively of the n-th order Laguerre polynomial and R_n is the remainder term. All functions in Chapters 2 and 3 employing Laguerre integration are extensions of Eq. (A.2).

A.1 Hermitian Integration

For Hermitian integration, the remainder term is defined as [18]

$$|R_n| \leq \frac{n!\sqrt{\pi}}{(2n)!2^n}\left(\max_{-\infty<\zeta<\infty}\left|f^{2n}(\zeta)\right|\right) \tag{A.3}$$

where, for this application, $f(x)$ is given as (see Eq. (A.2))

$$f(x) = \frac{1}{\sqrt{\pi}}\frac{1}{(1+z\mu e^{\sqrt{2}\sigma x})^L}. \tag{A.4}$$

To simplify the evaluation of Eq. (A.3), let $e^{\delta} = z\mu$. Thus, $f(x)$ in Eq. (A.4) can be re-written as a function of $\sqrt{2}\sigma x + \delta$. Note that the effect of the δ term is to shift the origin of the function but not its shape, and thus has no effect on the derivative of $f(x)$. Furthermore, the $\sqrt{2}\sigma x$ term implies that the n th derivative has a factor of $(\sqrt{2}\sigma)^n$. By this argument, the remainder term becomes

$$|R_n| \leq \frac{n!\sigma^{2n}}{(2n)!}\left(\max_{-\infty<\zeta<\infty}\left|f_1^{2n}(\zeta)\right|\right) \tag{A.5}$$

where, now

$$f_1(x) = \frac{1}{(1+e^x)^L} \tag{A.6}$$

which does not depend on z or μ. Now define a new function $\phi(n, L)$ such that

$$|R_n| \leq \phi(n, L)\,\sigma^{2n} \tag{A.7}$$

where

$$\phi(n, L) \equiv \frac{n!}{(2n)!}\left(\max_{-\infty<\zeta<\infty}\left|f_1^{2n}(\zeta)\right|\right). \tag{A.8}$$

Using a mathematical evaluation package such as *Maple*, Eq. (A.8) can be evaluated for the n and L of interest. Table A.1 provides some results. Using this table, an upper bound can be estimated for a given σ. For $\sigma < 4.3$ dB and $L = 1$,

$R_{10} \leq 2.4\times10^{-4}$ which is sufficient. For larger σ, the bound on the error term is not sufficiently tight to guarantee a negligible error term. However, this is not to imply that the error term is indeed significant. In Section A.3, Simpson's integration method is introduced which can be used to verify the accuracy of Hermitian integration for larger σ.

Order	$L = 1$	$L = 2$	$L = 3$	$L = 4$
$n = 5$	7.3×10^{-4}	2.9×10^{-3}	6.4×10^{-3}	1.0×10^{-2}
$n = 10$	2.4×10^{-4}	1.5×10^{-3}	5.4×10^{-3}	1.6×10^{-2}
$n = 15$	1.0×10^{-1}	1.2×10^{-1}	1.6×10^{-1}	1.8×10^{-1}
$n = 20$	4.6×10^{6}	7.4×10^{6}	7.5×10^{6}	7.6×10^{6}
$n = 25$	6.9×10^{14}	1.1×10^{15}	1.8×10^{15}	2.2×10^{15}

Table A.1. Computed values of $\phi(n, L)$ using *Maple*.

A.2 Laguerre Integration

Similarly for the Laguerre integration, the remainder term is bounded by [18]

$$|R_n| \leq \frac{n!}{(2n)!}\left(\max_{-\infty < \zeta < \infty} |f^{2n}(\zeta)|\right) \tag{A.9}$$

where from Eq. (A.2)

$$f(x) = (1 - Q(\sqrt{2K}, \sqrt{2(1+K)x/z}))^L. \tag{A.10}$$

Recognizing that $f(x)$ can be expressed as a function of $2(1+K)x/z$, then the bound on the remainder term can be re-written as

$$|R_n| \leq \frac{n!}{(2n)!}\left(\frac{2(1+K)}{z}\right)^{2n}\left(\max_{-\infty < \zeta < \infty} |f_1^{2n}(\zeta)|\right) \tag{A.11}$$

where now

$$f_1(x) = (1 - Q(\sqrt{2K}, \sqrt{x}))^L. \tag{A.12}$$

Note that since $m(z)$ is needed for larger values of z, the error term appears negligible.

Thus if $z \gg 2(1+K)$, then this approximation becomes very accurate.

A.3 Simpson Integration

An alternative approach to the Hermitian integration is to truncate the infinite interval to a finite interval and use Simpson integration. Thus define the truncated integral as

$$M(z) = \int_a^b e^{-x^2} f(x)\,dx + R_t \tag{A.13}$$

where $a < 0$, $b > 0$, $f(x)$ is given by Eq. (A.4) and R_t is the truncation error,

$$R_t = \frac{1}{\sqrt{\pi}}\left[\int_b^{\infty} \frac{e^{-x^2}}{(1+z\mu e^{\sqrt{2}\sigma x})^L}dx + \int_{-a}^{\infty} \frac{e^{-x^2}}{(1+z\mu e^{-\sqrt{2}\sigma x})^L}dx\right]. \tag{A.14}$$

To control the total truncation error, both integrals in Eq. (A.14) must be less than some tolerance ε. Consider first the positive tail for $a < x < \infty$

$$\int_b^{\infty} \frac{e^{-x^2}}{\sqrt{\pi}(1+z\mu e^{\sqrt{2}\sigma x})^L}dx < \int_b^{\infty} \frac{e^{-x^2}}{\sqrt{\pi}(1+z\mu e^{\sqrt{2}\sigma b})^L}dx = \frac{1-\mathrm{erf}(b)}{2(1+z\mu e^{\sqrt{2}\sigma b})^L}. \tag{A.15}$$

Thus b must be selected such that

$$\frac{1-\mathrm{erf}(b)}{2(1+z\mu e^{\sqrt{2}\sigma b})^L} \le \varepsilon. \tag{A.16}$$

Note that only a crude solution is required. Similarly, for the negative tail ($-\infty < x < a$), a crude upper bound is

$$\int_{-a}^{\infty} \frac{e^{-x^2}}{\sqrt{\pi}(1+z\mu e^{-\sqrt{2}\sigma x})^L}dx < \int_{-a}^{\infty} e^{-x^2}dx = \frac{1-\mathrm{erf}(-a)}{2}. \tag{A.17}$$

Note that this limit is independent of z, σ and μ. Thus for $\varepsilon \le 2\times10^{-8}$, $a = -4$ is sufficient.

Now that it has been shown that the truncation error can be controlled by properly selecting the finite interval, $2n$ point Simpson integration can be used to estimate the finite integral. Select the coordinate sequence such that $x_0 = a$, $x_0 < x_1, \ldots, x_{2n-1}$, $x_{2n} = b$, with $x_{i+1} - x_i = h$, $i = 0, 1, \ldots, 2n-1$ where $h = (b-a)/(2n)$. Now a functional form for Eq. (A.13) becomes [18]

$$M(z) = \sum_{i=0}^{2n} \frac{w_i}{(1 + z\mu e^{\sqrt{2}\sigma b})^L} + E \tag{A.18}$$

where the weights are

$$w_i = \begin{cases} \frac{h}{3} f(x_i)\, e^{-x_i^2} & \text{for } i = 0, 2n \\ \frac{4h}{3} f(x_i)\, e^{-x_i^2} & \text{for } i = 1, 3, \ldots, 2n-1 \\ \frac{2h}{3} f(x_i)\, e^{-x_i^2} & \text{for } i = 2, 4, \ldots, 2n-2 \end{cases} . \tag{A.19}$$

The error term E is then limited by [18]

$$|E| \le \frac{(b-a)^5}{2880n^4} \left(\max_{a \le \zeta \le b} |g^4(x)| \right) \tag{A.20}$$

where $g(x) = \exp(-x^2) f(x)$. Thus the error term can be made arbitrarily small by choosing a large enough n .

Appendix B

Closed Form Solutions to Equation (4.1)

In Chapter 4, the average BER was defined as

$$\bar{P}_b(\gamma) = \int_0^\infty P_b(\gamma|S)\, p(S)\, dS. \tag{B.1}$$

For a class of modulation schemes having an instantaneous BER expression of the form $a\,\mathrm{erfc}(\sqrt{bS\gamma})$ it was shown that

$$\bar{P}_b^{(1)}(\gamma) = \frac{2a}{\pi}\int_0^{\pi/2} m[b\gamma\sec^2\theta]\, d\theta \tag{B.2}$$

where $m(z)$ is the MGF of the fading channel of interest. Here, closed form expressions are derived for the channel MGFs of the form $m(z) = (1+cz)^{-1}$ and $m(z) = (1+cz)^{-L}$.

B.1 Form 1 — $m(z) = (1 + cz)^{-1}$

Substituting $m(z) = (1+cz)^{-1}$ into Eq. (B.2), using the property $\sec\theta = (\cos\theta)^{-1}$ and rearranging, the average BER can be written as

$$\bar{P}_b^{(1)}(\gamma) = \frac{2a}{\pi}\int_0^{\pi/2} \frac{1}{1+cb\gamma\sec^2\theta} d\theta = \frac{2a}{\pi}\int_0^{\pi/2}\left(1 + \frac{ab\gamma}{cb\gamma+\cos^2\theta}\right) d\theta. \tag{B.3}$$

Using the following solved integral [31]

$$\int \frac{1}{\alpha+\beta\cos^2 x} dx = \frac{1}{\sqrt{\alpha(\alpha+\beta)}}\arctan\left(\frac{\alpha\tan x}{\sqrt{\alpha(\alpha+\beta)}}\right) \qquad \alpha(\alpha+\beta) > 0 \tag{B.4}$$

a closed form expression for Eq. (B.3) can be obtained

$$\bar{P}_b^{(1)}(\gamma) = a\left(1 - \frac{1}{\sqrt{1 + 1/(cb\gamma)}}\right). \tag{B.5}$$

For the SDC, Suzuki channel case, Eq. (3.20) can be easily manipulated into the desired form to obtain (ignoring R_n)

$$\bar{P}_{b,\,\text{Suzuki}}^{(1,\,\text{SDC!})}(\gamma) = \frac{aM}{\sqrt{\pi}} \sum_{i=1}^{n} w_i \left[1 - Q\left(\sqrt{2}x_i\right)\right]^{M-1} \sum_{j=0}^{L} (-1)^j \binom{L}{j} \left[1 - \frac{1}{\sqrt{1 + 1/(a_i b\gamma)}}\right] \tag{B.6}$$

where w_i and a_i are given for Eq. (3.20).

B.2 Form 2 — $m(z) = (1 + cz)^{-L}$

It was shown in [3] that for the Rayleigh fading case with L branch MRC diversity, one can directly solve Eq. (B.1) for the BPSK case. Given that the MGF of the Rayleigh fading channel is $m(z) = (1 + cz)^{-L}$ and the instantaneous BER is $(1/2)\,\text{erfc}(\sqrt{\gamma})$, the result in [3] can be extended to obtain

$$\bar{P}_b(\gamma) = a\phi(cb\gamma, L) \tag{B.7}$$

where

$$\phi(x, L) = \left(\frac{1 - \sqrt{x/(1+x)}}{2}\right)^L \sum_{k=0}^{L-1} \binom{L-1+k}{k} \left(\frac{1 + \sqrt{x/(1+x)}}{2}\right)^k. \tag{B.8}$$

Consider now the MGFs derived in Chapter 3. Using the series expansion for the exponential term[1] and simplifying, the MGF for the MRC, Rician channel Eq. (3.13) can be written in the desired form

$$m_{\text{Rice}}^{(\text{MRC})}(z) = e^{-KL} \sum_{n=0}^{\infty} \frac{(KL)^n}{n!\,(1 + z/(1+K))^{n+L}}. \tag{B.9}$$

Thus the closed form expression for the average BER is

---

1. The series expansion for the exponential function is [18]

$$e^x = \sum_{n=0}^{\infty} \frac{x^n}{n!}$$

$$\bar{P}_{b,\,\text{Rice}}^{(1,\,\text{MRC})}(\gamma) = ae^{-KL}\sum_{n=0}^{\infty}\frac{(KL)^n}{(n)!}\phi\left(\frac{b\gamma}{1+K}, n+L\right) \tag{B.10}$$

which is a rapidly converging series[1]. Note, when $K = 0$, Eq. (B.10) resorts to the Rayleigh fading case with $P_{b,\,\text{Rayleigh}}^{(1)}(\gamma) = \phi(\gamma, L)$ [3]. In fact, Lindsey [32] derives an alternate expression for Eq. (B.10). This is a recursion formula containing a confluent hypergeometric function. Thus, Eq. (B.10) is much easier to compute.

Similarly, for the MRC, lognormally shadowed Rician MGF, Eq. (3.15) can be written as

$$\bar{P}_{b,\,\text{lnRice}}^{(1,\,\text{MRC!})}(\gamma) = \frac{aMe^{-KL}}{\sqrt{\pi}}\sum_{i=0}^{n_H} w_i\left[1-Q\left(\sqrt{2}x_i\right)\right]^{M-1}\sum_{n=0}^{\infty}\frac{(KL)^n}{(n)!}\phi\left(\frac{b\gamma}{a_i}, n+L\right) \tag{B.11}$$

where $a_i = \mu\exp\left(\sqrt{2}\sigma x_i\right)$.

Finally, since the MGF for the MRC, Suzuki channel Eq. (3.22) is already in the desired form, the average BER is (ignoring R_n)

$$\bar{P}_{b,\,\text{Suzuki}}^{(1,\,\text{MRC!})}(\gamma) = \frac{aM}{\sqrt{\pi}}\sum_{i=1}^{n} w_i\phi(a_i b\gamma, L)\left[1-Q\left(\sqrt{2}x_i\right)\right]^{M-1} . \tag{B.12}$$

Of course, when $L = 1$, these special cases can also be expressed in the more convenient form derived in Section B.1.

---

1. The following recursive property can be exploited in the computation of (B.10)

$$\phi(x, L+1) = \phi(x, L) - \left(\sqrt{\frac{x}{1+x}}\right)\left(\frac{1}{4(1+x)}\right)^L\binom{2L-1}{L} .$$

VITA

Arndt Joseph Mueller
Born September 2, 1967, Edmonton, Alberta

Educational Institutions Attended:

University of Victoria	1993 to 1995
University of Alberta	1987 to 1992

Degrees Awarded:

Bachelor of Science	University of Victoria, 1992

Honours and Awards:

B.Sc. studies

Alexander Rutherford Scholarship

Syncrude Higher Education Award

Publications:

Journal

C. Tellambura, A. J. Mueller, V. K. Bhargava, "Analysis of M-ary phase shift keying with diversity reception for land mobile satellite channels," Accepted for publication in the *IEEE Trans. Veh. Tech.*, 1995.

C. Tellambura, A. J. Mueller, V. K. Bhargava, "BER and outage probability for the land mobile satellite channel with maximal ratio combining," *Electronic Letters*, Vol. 31, No. 8, pp 606-608, Apr. 13, 1995.

Conference

A. J. Mueller, V. K. Bhargava and Q. Wang, "Design and analysis of a rate adaptive concatenated code for the cellular channel," presented at the Canadian Workshop on Information Theory, Lac Delage, Canada, May 1995.

A. J. Mueller, V. K. Bhargava and Q. Wang, "Code Rate Optimization for Coded Packet CDMA Cellular Networks," *Proc. of International Conference on Universal Personal Communications*, San Diego, CA, pp. 320-324, Sept. 27 - Oct. 1, 1994.

Partial Copyright License

I hereby grant the right to lend my thesis (or dissertation) to users of the University of Victoria Library, and to make single copies only for such users or in response to a request from the Library of any other university, or similar institution, on its behalf or for one of its users. I further agree that permission for extensive copying of this thesis for scholarly purposes may be granted by me or a member of the University designated by me. It is understood that copying or publication of this thesis for financial gain shall not be allowed without my written permission.

Title of Thesis/Dissertation: **Issues in Diversity and Adaptive Error Control Coding for Wireless Communications**

Autho[redacted]
(Signature)

ARNDT JOSEPH MUELLER

September 26, 1995
(Date)